

Abstract

MCCULLEN, SETH DYLAN. Development, Characterization, and Function of Electrospun Nanocomposites for Tissue Engineering. (Under guidance of Dr. Russell E. Gorga and Dr. Elizabeth G. Lobo.)

Nanocomposites for tissue engineering scaffolds were fabricated by the electrospinning process. Multi-walled carbon nanotubes were incorporated into the electrospun scaffolds, and validated through microscopy analysis to be dispersed and aligned inside the polymeric nanofibers. Mechanical and electrical properties were determined for electrospun polymer/MWNT systems and the electrical conductance was optimized at a loading level of 1 wt%. Cell studies showed that adipose-derived human mesenchymal stem cells (hMSCs) were able to adhere and proliferate for two weeks in culture on the scaffold. DNA quantification indicated that hMSCs grown on the nanocomposite scaffold yielded a higher number of cells. Microscopy indicated that the cells grown on the novel material were aligned and formed a confluent construct. This work has demonstrated the feasibility and efficacy of developing novel nanocomposite materials for use as tissue engineering scaffolds.

**Development, Characterization, and Function of Electrospun Nanocomposites for
Tissue Engineering**

by

Seth Dylan McCullen

**A thesis submitted to the Graduate Faculty of North Carolina State University and
University of North Carolina at Chapel Hill in partial fulfillment of the requirements
for the Degree of Master of Science**

**TEXTILE ENGINEERING
BIOMEDICAL ENGINEERING
Raleigh, North Carolina**

2006

Approved By:

Dr. Russell E. Gorga, Co-Chair (TE)

Dr. Elizabeth G. Lobo, Co-Chair (BME)

Dr. Wendy E. Krause, Committee Member (TE)

Dr. Nancy A. Monteiro-Riviere, Committee Member (BME)

Biography

Seth Dylan McCullen was born on March 3, 1982 to Hugh and Martha McCullen. He is the oldest of four children with two brothers Chad and Christian and one sister, Meredith. During his childhood Seth was involved in soccer, football, his church youth group, and the Boy Scouts of America where he obtained the rank of Eagle Scout. In June 2000 Seth graduated from Clayton High School, and upon graduation, he accepted the Pearl Balthis Dixon Scholarship at the College of Textiles, North Carolina State University. While at N.C. State, Seth enjoyed playing club Rugby for most of his collegiate career. He graduated in December 2004 with a B.S. in Textile Engineering. Upon graduation he enrolled into the graduate programs for Textile and Biomedical Engineering. After, Seth obtains his master's degree he plans on gaining industrial experience before pursuing his PhD in Biomedical Engineering.

Acknowledgements

This work has been developed and supported by many individuals. I would like to thank my committee for all of their ideas and acceptance of this project. I would like to thank Dr. Gorga for his energy, positive outlook, and being available to discuss research and other matters. I hope we remain friends throughout our careers. I would like to thank Dr. Loboa for her drive, ambition, and constant motivation throughout the project. I would like to thank Dr. Krause for her insightful knowledge and practical ideas on everything. I would like to thank Dr. Monteiro-Riviere for her analysis of transmission electron micrographs and meeting with me throughout my research. I would like to express my sincere thanks to Dr. Clarke and her entire research team for all of their assistance and their pivotal role of the conductance measurements for this work. I would like to thank Dr. Bernacki for teaching me tissue culture techniques and for all her work during this project. I would like to thank Mr. Al Inman for all his technical assistance with the transmission electron microscope. Finally, I would like to thank Dr. Rust, for his support and guidance from the transition from undergraduate to graduate and beyond.

Next I would like to thank all my fellow researchers including Hailey Queen, Denice Young, Rebecca Klossner, Kelly Stano, Jonathan Pasley, Alan Kinlaw, Carla Haslauer, Ariel Hanson, Ben Moody, Derrick Stevens, Wesley Roberts, Satyajeet Ojha, Andy Coughlin and Johnny Cash. Finally, I would like to thank Ashley Tharrington for making me want more.

Table of Contents

List of Tables.....	vi
List of Figures.....	vii
Chapter 1.....	1
Introduction.....	1
1.1 General Introduction.....	1
1.2 Relevance.....	6
1.3 Overall Objective.....	8
1.4 References.....	9
Chapter 2.....	11
Literature Review.....	11
2.1 Introduction.....	11
2.2 Nanocomposite Materials.....	11
2.3 Tissue Engineering.....	15
2.31 Scaffold Fabrication.....	21
2.32 Nanocomposite Scaffolds.....	23
2.33 Stem cells in Tissue Engineering.....	25
2.4 Functional Tissue Engineering.....	26
2.5 References.....	29
Chapter 3.....	34
Research Objectives.....	34
3.1 Research Objectives.....	34
Chapter 4.....	38
Morphological, electrical, and mechanical characterization of electrospun nanofiber mats containing multi-walled carbon nanotubes.....	38
4.1 Abstract.....	38
4.2 Introduction.....	39
4.3 Experimental.....	42
4.4 Results and Discussion.....	47
4.5 Conclusions.....	60
4.6 Acknowledgements.....	61
4.7 References.....	61
Chapter 5.....	67
Development of electrospun poly (L-D-lactic acid) fibers containing multi-walled carbon nanotubes for tissue engineering scaffolds and optimization of fiber morphology.....	67
5.2 Introduction.....	68
5.3 Materials and Methods.....	72
5.31. Fabrication.....	72
5.32 Materials.....	72
5.33 Characterization.....	73
5.33.1 Scanning Electron Microscopy.....	73
5.33.2 Transmission Electron Microscopy.....	73
5.33.3 Fourier Transform Infrared Spectroscopy.....	74
5.33.4 Statistical Analysis.....	74
5.4 Results and Discussion.....	75
5.41 Effect of Polymer Concentration.....	75

5.42 Effect of Flow Rate.....	77
5.43 Effects of Voltage	78
5.44 Effect of Working Distance	79
5.45 Effect of Solvent System	79
5.46 Effect of MWNT Addition.....	80
5.5 Conclusions.....	89
5.6 Acknowledgements.....	90
5.7 References.....	90
Chapter 6.....	94
Electrospun conductive nanocomposites with adipose-derived human mesenchymal stem cells for tissue engineering applications	94
6.1 Abstract.....	94
6.1 Introduction.....	95
6.3 Materials and Methods.....	99
6.31 Materials	99
6.32 Electrospinning Solution Preparation	99
6.33 Electrospinning Apparatus.....	100
6.34 Electrospun Scaffold Characterization	101
6.35 Human Mesenchymal Stem Cell Isolation and Expansion.....	102
6.36 Cell Seeding	103
6.4 Results.....	104
6.41 Scaffold Characterization.....	104
6.42 Cell/Scaffold Interaction.....	108
6.5 Discussion	112
6.51 Scaffold Characterization.....	112
6.52 Human MSC/Scaffold Interaction	115
6.6 Conclusions.....	116
6.7 Acknowledgements.....	116
6.8 References.....	117
Chapter 7.....	121
Conclusions.....	121
7.1 Conclusions.....	121
Chapter 8.....	122
Future Work	122
8.1 Future Directions	122

List of Tables

Table 1.1 Outline of the number of procedures per number of patients occurring per year for the United States.....	3
Table 4.1 Parameters for the three conductance models. * G_m was held at the conductance limit of our system. G_n , G_m , a' and c' are the conductance equivalents of the conductivity quantities given the text.....	59
Table 4.2 Modulus and tensile strength as a function of nanotube concentration.....	60
Table 5.1 Design of Experiment for electrospinning of PLDLA with MWNTs.....	75
Table 5.2 Estimated chain entanglements per chain based on weight average molecular weight, entanglement molecular weight, and polymer concentration.....	77
Table 5.3 Electrospinning parameters and fiber diameters for PLDLA and MWNT/PLDLA nanofibers. All solutions were in the solvent system of Chloroform and DMF at a ratio of 3:1 respectively and at a flow rate of 1 mL/min.....	82

Lists of Figures

Figure 1.1 Diagram of the tissue engineering method and the three required components.....	3
Figure 2.1 Image of a single-walled carbon nanotube and multi-walled carbon nanotube.....	12
Figure 2.2 Twist structure of carbon nanotubes and the indicative conductive behavior.....	13
Figure 2.3 Design Scheme I for soft tissue scaffold displaying the relationship between mechanical integrity and degradation.....	18
Figure 2.4 Design Scheme II for hard tissue scaffold displaying the relationship between mechanical integrity and degradation.....	19
Figure 2.5 Diagram of electrospinning with labeled entities.....	22
Figure 2.6 Picture of actual electrospinning setup.....	23
Figure 2.7 Diagram of Yasuda’s Hypothesis depicting that applied electrical currents can produce an adaptive response in bone tissue.....	27
Figure 4.1 Schematic of the electrospinning apparatus used to produce the nanocomposite samples. Each component is labeled.	44
Figure 4.2 Flow curve plot of viscosity vs. shear rate for MWNT/PEO solutions.....	48
Figure 4.3 : SEM of aligned and random nanofibers (1 wt % MWNT in 4 wt % PEO). Images were captured at 10,000X. The scale bar is 1 μm	50
Figure 4.4 a-f: SEM images of electrospun nanocomposites. 4.4a-b images of 3 wt% PEO, 4.4c-d images of 4 wt% PEO, 4.4e-f images of 4 wt% PEO with 1 wt% MWNT. By increasing the polymer concentration by 1%, we were able to produce uniform nanofibers. Images a, c, and e have scale bars of 1 μm , where images b, d, and f have scale bars of 100 nm.....	51
Figure 4.5a TEM image of 2 wt % MWNT in 4 wt% PEO nanofibers showing dispersion and alignment along the axis of the fiber and b TEM image of 2 wt% MWNT in 4 wt% PEO sample. This image captures four multi-walled carbon nanotubes within several nanofibers bonded together.....	52

Figure 4.6 Electrical conductance vs. MWNT concentration in 4 wt% PEO or alternatively, versus the measured volume fraction of MWNT. With increasing MWNT concentration, the conductance demonstrates a percolation threshold for the random mats. The three fits are described in the text, with fit parameters presented in Table 1.....	56
Figure 5.1a-c SEM Images of electrospun PLDLA at varying concentrations.....	76
Figure 5.2a-c SEM images of electrospun 20 wt% PLDLA at varying voltages.....	79
Figure 5.3a-b SEM images of electrospun 20 wt% PLDLA with different solvent systems.....	80
Figure 5.4 SEM images of a) electrospun 20 wt% PLDLA and b) 1wt% MWNT/ 20% PLDLA.....	81
Figure 5.5 Distribution of fiber diameters for electrospun PLDLA.....	83
Figure 5.6 Distribution of fiber diameters for electrospun MWNT/PLDLA.....	83
Figure 5.7 Bivariate plot of electrospun PLDLA fiber diameter by MWNT concentration.....	84
Figure 5.8 TEM image of electrospun MWNT/PLDLA. The arrows indicate the MWNT.....	86
Figure 5.9 Contour Plot for Electrospun PLDLA fiber diameters.....	87
Figure 5.10 Contour plot for Electrospun MWNT/PLDLA fiber diameters	88
Figure 5.11 Absorbance spectrum for PLDLA from FTIR.....	89
Figure 5.12 Absorbance spectrum for PLDLA and the individual solvents (chloroform and DMF) from FTIR.....	90
Figure 6.1 Labeled schematic of the electrospinning apparatus used to produce the nanocomposite samples.....	101
Figure 6.2 SEM image of electrospun PLA, containing a) 1 wt% MWNTs and b) 0 wt% MWNTs.....	105
Figure 6.3 TEM images of electrospun nanocomposite, a: showing MWNT alignment along fiber axis and b: showing MWNT aggregation.....	106
Figure 6.4 Plot of the Young's modulus of the electrospun fibrous mats by MWNT wt %; (n = 10), Error Bars = Std Error Mean.....	107

Figure 6.5 Conductance plot for mats spun from varying MWNT wt% in 20 wt% PLA solution. The error on each point is exceeded by the point size. At both 0.375 and 1 wt% two samples are represented. The mat conductance, G , is fit after (Fournier 1997) with $\log(G) = \log(G_f) + [\log(G_m) - \log(G_f)]/z$ where G_m and G_f are the matrix (polymer) and final composite (maximum) conductance, p is the wt%, and p_c the critical weight percentage for conductance. The parameter b determines the slope of the curve across the percolation threshold. We find $G_m = 2 \times 10^{-15}$ S (indistinguishable from the limit of conductance in our system), $G_f = 9 \times 10^{-5}$ S, $b = 53$, and $p_c = 0.32\%$108

Figure 6.6 Live/Dead images of hMSCs on electrospun PLA without MWNTs (a,b) and with MWNTs (1 wt %) (c,d) where green = live and red = dead (indicated by arrows).....110

Figure 6.7 Number of hMSCs present throughout the course of the experiment on the electrospun tissue scaffolds with and without MWNTs. ($n = 3$, three scaffolds / time point, three samples / scaffold) (Error bars = Standard Error Mean), where star indicates significance p -value < 0.05111

Figure 6.8 SEM image of hMSCs at Day 14, completely confluent on the surface of the electrospun PLA with MWNTs.....112

Figure 6.9 SEM image at Day 14 of hMSCs integration into the electrospun nanocomposite scaffold. Arrows indicate hMSC with processes into scaffold.....113

Chapter 1

Introduction

1.1 General Introduction

Advances in the fields of medicine and engineering have awakened the need and desire to engineer human tissues, catalyzed by the demand for replacement organs. To date, there has not been an absolute success in the development of full-functioning organs created *in vitro*. Hence, better solutions have been under development and are reaching a turning point in society by attracting awareness from all fields of science.

Tissue engineering is an emerging field with the goal of replacing diseased or malfunctioning tissues and organs. Therefore, scientists have been working in multi-disciplinary teams that are progressing toward solutions to regenerate organs outside of the human body, for transplantation into multiple recipients.

Langer defines tissue engineering as “an interdisciplinary field that applies the principles of engineering and life sciences toward the development of biological substitutes that restore, maintain, or improve tissue function.”¹ The term “tissue engineering” was manifested in 1987 by Professor Y.C. Fung at the University of California at San Diego; thus this field is relatively new.¹ Table 1.1 displays the number of hospital procedures performed per year in the United States. These numbers include patients seeking treatment from genetic disorders, traumatic accidents, and other causes of organ loss or malfunction, and are merely a glimpse of the wave of potential organ treatment and organ replacement that is likely to occur as the population of the “baby-boomer” generation approaches old age. These figures are also

indicative that better solutions must be developed if society is to make significant advances in any one of these procedure types.

Table 1.1 : Outline of the number of procedures per number of patients occurring per year for the United States.¹

Procedure	Indication or patients/yr
<i>Skin</i>	
Burns(*)	2,150,000
Pressure sores	1,500,000
Venous stasis ulcers	500,000
Diabetic ulcers	600,000
Neuromuscular disorder	200,000
Spinal cord and nerves	40,000
<i>Bone</i>	
Joint replacement	558,200
Bone graft	275,000
Internal fixation	480,000
Facial reconstruction	30,000
<i>Cartilage</i>	
Patella resurfacing	216,000
Chondromalacia patellae	103,400
Meniscal repair	250,000

Table 1.1 Continued	
Arthritis (knee)	149,900
Arthritis (hip)	219,300
Fingers and small joints	179,000
Osteochondritis dissecans	14,500
Tendon repair	33,000
Ligament repair	90,000
<i>Blood vessels</i>	
Heart	754,000
Large and small vessels	606,000
<i>Liver</i>	
Metabolic disorders	5,000
Liver cirrhosis	175,000
Liver cancer	25,000
Pancreas (diabetes)	728,000
Intestine	100,000
Kidney	600,000
Bladder	57,200
Ureter	30,000
Urethra	51,900
Hernia	290,000
Breast	261,000

Table 1.1 Continued	
Blood transfusion	18,000,000
Dental	10,000,000

Tissue engineering is a unique and contemporary field where scientists are trying to recreate functional tissues and organs. Tissue engineering contains three entities: cells, growth hormones, and a scaffold as viewed schematically in Figure 1.1.

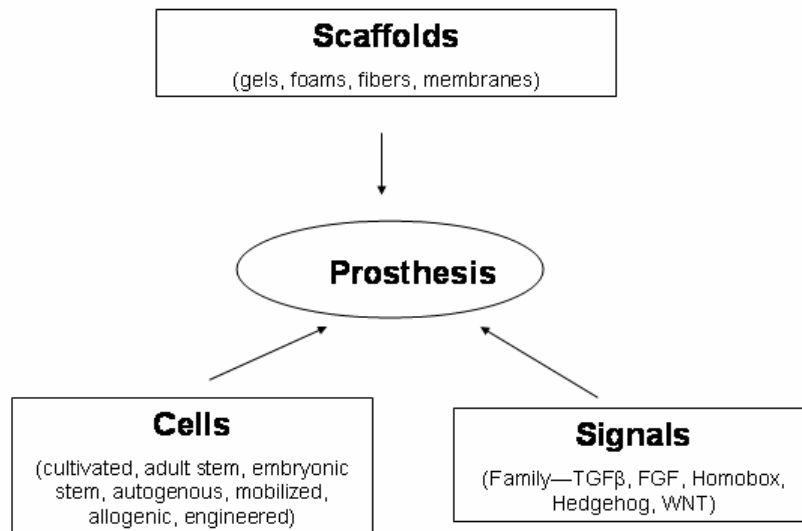


Figure 1.1 : Diagram of the tissue engineering method and the three required components.¹

The main idea in tissue engineering is to seed a scaffold with a specific cell line and influence growth and development through application of specific signaling agents including hormones, proteins, growth media, and environmental stimuli. The research plan for these three entities can be classified into six main phases²:

I: Fabrication of the bioresorbable scaffold

- II: Seeding of cell populations into the polymeric scaffold in a static culture dish
- III: Growth of premature tissue in a dynamic environment
- IV: Growth of mature tissue in a physiologic environment
- V: Surgical transplantation
- VI: Tissue-engineered transplant assimilation/remodeling

The scaffold is of high interest since it is the physical carrier that allows the arrangement of cells onto a construct and is where the cells are able to arrange into anatomically correct structures, where they can form functional units. The scaffold is the three-dimensional finite space that structurally supports the cells of interest and allows the cells to proliferate and differentiate by being able to undergo mass transfer. The scaffold must be able to degrade and be resorbed at a controlled rate at the same time as the specific tissue cells seeded into the three-dimensional construct attach, spread, and increase in quantity and quality. Selecting and designing the biomaterial for a scaffold is the most critical aspect of tissue engineering due to the material's properties having the most profound effect on the success of the tissue engineering method by dictating biocompatibility.³

The following parameters have been identified as key factors in the production of tissue scaffolds to obtain the optimum properties necessary for tissue growth. These parameters include¹:

- Biocompatibility: acceptance within the body without causing biofouling where the body attacks the implant, or the cells do not grow on the material

- Biodegradability: ability to degrade in the body into compatible by-products without causing inflammatory responses
- Mechanical integrity: ability to maintain the original structure and mechanical properties upon exposure to the body's environment, i.e. 37°C, pH 7.4, saline solution
- High porosity: ability to allow the transfer of nutrients/oxygen and removal of wastes via diffusion
- Bioactivity: ability to transform or conform depending upon the influence from the internal milieu that surrounds the scaffold seeded with cells

1.2 Relevance

Across the globe, medical doctors, healthcare providers and researchers have joined together for the “Bone and Joint Decade 2000-2010” to promote the understanding and treatment of musculoskeletal disorders through prevention, education and research.⁴ To date bone is the most transplantable organ and offers many opportunities for improving the current standards in place. Bone grafts are materials that provide support, fill voids, and enhance biologic repair of skeletal defects. The requirements for bone graft substitutes are osteoconductivity, osteogenicity, and osteoinductivity.¹ Osteoconductivity is defined where the graft supports the attachment of new osteoblasts and osteoprogenitor cells providing a porous structure through which new cells can migrate and new blood vessels can form from the host bed into the transplanted substrate. Osteoinductivity refers to the ability of a graft to induce nondifferentiated stem cells or osteoprogenitor cells to differentiate into osteoblasts. It is controlled primarily by growth factors such as bone morphogenetic proteins (BMPs).

Osteogenicity refers to the use of mesenchymal stem cells which can either be recruited from the host bed or transplanted directly on the graft.⁵

For bone grafts, approximately 500,000 cases occur annually within the United States, and continue to be an increasing trend, due to the aging population of baby boomers and high impact lifestyles that many individuals live today.⁶ The gold standard for this is the autograft where 9 out of 10 surgeries performed use this option. There are many limitations and problems associated with autografts including limited supply and infection or pain at the donor site. This standard requires two surgical sites, the first site to remove the bone graft, and the second site to implant it. The medical industry has struggled with developing an alternative strategy for autografts. Current synthetic products for bone graft substitutes are based on old technologies that utilize inert and dead materials and do not allow for the material or product to be integrated successfully within the body, to form fully functional tissue.⁴

Cell based strategies have been receiving much attention, as the goal of this method is for complete integration into the skeletal system. Current materials available for bone graft substitutes are demineralized bone matrix (DBM), calcium phosphates, collagen, calcium sulfate or Plaster of Paris, Coralline substrates, tri-calcium phosphates (TCP), and non-biological constructs.⁶ Though these products have been receiving much attention, they still do not take into account full integration within the site of transplantation. This work will highlight the development of a novel material that will allow complete integration into skeletal defects and provide a better alternative to autografting and other treatment methods.

Current trends in tissue engineering have moved towards what is known as functional tissue engineering. Functional tissue engineering uses physical stimulation to direct cell populations to produce functional tissue with anatomically correct structures. This physical stimulation can range from electric-magnetic fields, mechanical forces, ultrasonic waves, and chemical stimuli.⁷⁻⁹ The purpose of this research is to design and fabricate an electrospun nanocomposite tissue scaffold to produce an enhanced conductive scaffold for the localization and delivery of an electric field to direct human mesenchymal stem cells into osteogenesis for bone formation. Bone produces electrical potentials when mechanically stressed, and this is thought to be an essential portion of cellular events in regenerative healing.¹⁰

1.3 Overall Objective

The objective of this research is to design and engineer a novel scaffolding material with the utilization of carbon nanotubes in a composite system. The development of nano-structured materials with enhanced properties has dominated the field of material science due to the wide variety of applications, including scaffolding materials for tissue engineering.^{3,11-23} The interaction between the nano-structured composites has been of particular interest due to the possibility of generating large increases in physical properties for specific end use applications. By developing specifically tailored materials with enhanced properties, the scaffold will play a crucial role in the growth and differentiation of seeded cell populations.³ This work will highlight the development of a novel material that should allow complete integration into skeletal defects and could provide a better alternative to autografting and

other treatment methods. This strategy will make use of a composite consisting of a polymeric matrix of poly (lactic acid) (PLA) reinforced with multi-walled carbon nanotubes (MWNT). By producing a conductive scaffold and utilizing functional tissue engineering scenarios, this work aims to direct human mesenchymal stem cells into the bone cell lineage. These topics will be discussed in detail in Chapter 2.

1.4 References

1. R. Lanza, R. Langer and J. Vacanti, *Principles of Tissue Engineering*, Academic Press, Boston, 2000.
2. Hutmacher, *Biomaterials*, **21**, 2529-2543 (2000).
3. V. Thomas, D. R. Dean and Y. K. Vohra, *Current Nanoscience*, **2**, 155-177 (2006).
4. www.bonejointdecade.org
5. F. G. Lieberman and Jay, *Bone Regeneration and Repair: Biology and Clinical Applications*, Humana Press, Totowa, 2005.
6. C. Laurencin, *Bone Graft Substitutes*, ASTM International, Bridgeport, 2003.
7. M. Ochi, P. L. Wang, K. Ohura, S. Takashima, H. Kagami, Y. Hirose, T. Kaku and K. Sakaguchi, *Clinical Oral Implants Research*, **14**, 294-302 (2003).
8. J. A. Spadaro, *Bioelectromagnetics*, **18**, 193-202 (1997).
9. H. P. Wiesmann, M. Hartig, U. Stratmann, U. Meyer and U. Joos, *Biochimica Et Biophysica Acta-Molecular Cell Research*, **1538**, 28-37 (2001).
10. R. O. Becker, *Clinical Orthopaedics and Related Research*, **83**, 255-262 (1972).
11. M. Vallet-Regi, *Materialwissenschaft Und Werkstofftechnik*, **37**, 478-484 (2006).

12. N. Alobaid, H. J. Salacinski, K. M. Sales, B. Ramesh, R. Y. Kannan, G. Hamilton and A. M. Seifalian, *European Journal Of Vascular And Endovascular Surgery*, **32**, 76-83 (2006).
13. X. F. Shi, J. L. Hudson, P. P. Spicer, J. M. Tour, R. Krishnamoorti and A. G. Mikos, *Biomacromolecules*, **7**, 2237-2242 (2006).
14. E. P. S. Tan and C. T. Lim, *Composites Science And Technology*, **66**, 1102-1111 (2006).
15. R. Murugan and S. Ramakrishna, *Composites Science And Technology*, **65**, 2385-2406 (2005).
16. Y. Z. Zhang, C. T. Lim, S. Ramakrishna and Z. M. Huang, *Journal Of Materials Science-Materials In Medicine*, **16**, 933-946 (2005).
17. X. F. Shi, J. L. Hudson, P. P. Spicer, J. M. Tour, R. Krishnamoorti and A. G. Mikos, *Nanotechnology*, **16**, S531-S538 (2005).
18. M. Y. Li, M. J. Mondrinos, M. R. Gandhi, F. K. Ko, A. S. Weiss and P. I. Lelkes, *Biomaterials*, **26**, 5999-6008 (2005).
19. M. El Fray and A. R. Boccaccini, *Materials Letters*, **59**, 2300-2304 (2005).
20. V. M. Rusu, C. H. Ng, M. Wilke, B. Tiersch, P. Fratzl and M. G. Peter, *Biomaterials*, **26**, 5414-5426 (2005).
21. H. W. Kim, H. E. Kim and V. Salih, *Biomaterials*, **26**, 5221-5230 (2005).
22. S. Kalambur and S. S. H. Rizvi, *Journal Of Applied Polymer Science*, **96**, 1072-1082 (2005).
23. A. Tampieri, G. Celotti, E. Landi, M. Sandri, N. Roveri and G. Falini. in *Euro Ceramics Viii, Pts 1-3*; Trans Tech Publications Ltd, Zurich-Uetikon, 2004, p 1937-1940.

Chapter 2

Literature Review

2.1 Introduction

This chapter provides an indepth overview of a range of disciplines related to the fabrication of nanocomposite materials for functional tissue engineering scaffolds. In Section 2.2, a review of nanocomposite materials is discussed with emphasis on carbon nanotube composites. In Section 2.3 tissue engineering is discussed including development of nanocomposite scaffolds with an emphasis on carbon nanotube based scaffolds and the use of stem cell based therapies. In Section 2.4, a review on functional tissue engineering is discussed, highlighting electrical stimulation theory and application, including previous research that has demonstrated its usefulness in tissue engineering scenarios.

2.2 Nanocomposite Materials

Nanocomposites are a combination of a matrix and a filler where at least one dimension of the system is on the nanoscale being less than or equal to 100 nm. Much work has focused on the construction of nanocomposites due to the structural enhancements in physical properties, and functionality for any given composite system.¹⁻⁸ The physical enhancements result from the interaction between the filler and the matrix being near the molecular scale. Nanocomposite materials have also received interest for tissue engineering scaffolds by being able to replicate the extracellular matrix found *in vivo*.⁹

Materials that have been researched extensively in nanocomposites are carbon nanotubes. Carbon nanotubes can be envisioned as sheets of sp^2 hybridized carbon atoms rolled into a tubular structure and capped with half a fullerene on each end. Carbon nanotubes were discovered by Iijima, a Japanese microscopist in 1991.¹⁰ Carbon nanotubes differ in morphology by the number of tubes or walls that are coaxial to one another, being divided into two categories, single-walled carbon nanotubes and multi-walled carbon nanotubes as seen in Figure 2.1.

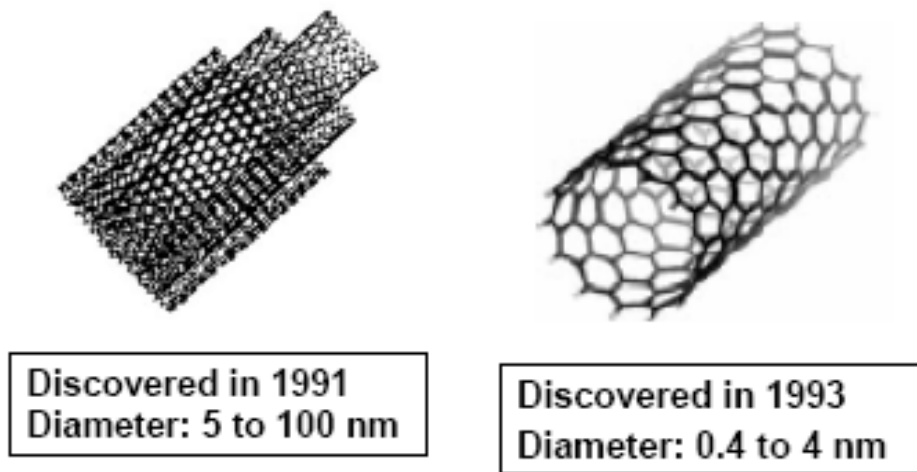


Figure 2.1: Image of a single-walled carbon nanotube and multi-walled carbon nanotube.

Another morphological feature that differs is the twist of the tube, being either armchair, zig-zag, or chiral, where the angle of twist θ is 30° , 0° , or between 0° - 30° , respectively. The differences in structure cause carbon nanotubes to have different properties and can be viewed in Figure 2.2. Armchair and zig-zag are electrical conductors, where the chiral twisted carbon nanotubes are semiconductors.

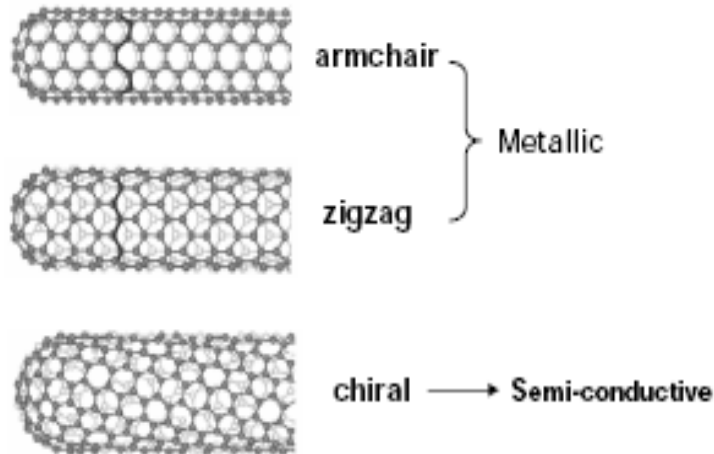


Figure 2.2: Twist structure of carbon nanotubes and the indicative conductive behavior.

Due to their aspect ratio (length/diameter) being in the thousands, these materials exhibit tremendous properties, including a tensile modulus approaching 1 TPa, a tensile strength ~ 37 GPa, and electrical conductivity of 10^6 S/m.¹¹⁻¹³ Carbon nanotubes can be produced by four main methods: arc-discharge, chemical vapor deposition, laser ablation, and high pressure carbon monoxide.¹⁴⁻¹⁶ These methods differ in the production of carbon nanotubes, by the purity level of carbon nanotube, defective geometrical shapes, size scale including diameter and length, and volume of carbon nanotubes that can be produced. For this investigation, the carbon nanotubes used were produced from chemical vapor deposition. Chemical vapor deposition produces carbon nanotubes by growing them on a silica substrate within a nitrogen environment at approximately 700°C. Iron is usually the catalyst and reacts with methane to grow the nanotubes from the surface of the substrate. The density of carbon nanotubes grown and the number of walls depends on the amount of catalyst introduced into the environment.¹⁶⁻¹⁸

Though carbon nanotubes have extraordinary physical properties, there has been a large variance in the report of the apparent properties due to their physical integration of the carbon nanotubes into the polymer matrices; specifically the dispersion and orientation of the carbon nanotubes. Due to their high surface area, carbon nanotubes tend to agglomerate and form aggregates by the interaction of the van der Waals forces between the nanotubes. To combat this, surfactants and physical stimulation can be used to break apart the aggregates and adequately disperse the tubes.^{19,20} Surfactants work by modifying the phase interfaces between two or more materials and creating a colloidal suspension by reducing the interfacial energy between the two materials and retarding phase separation by absorption of the surfactant at the surface of the materials.²¹ Typically, this has been done with carbon nanotubes suspended in a solvent.

In order to enhance the physical properties of polymer matrices, the filler must not only be dispersed but also aligned. Gorga has been able to show that when carbon nanotubes are adequately dispersed and oriented along the direction of interest large increases in physical properties can be achieved.^{2,5} Thus, a main goal of this research will be to align carbon nanotubes within electrospun nanofibers. To date, there is continued interest in the method of electrospinning for nanocomposite fabrication.^{1,3,6-8,22-24} Specifically, carbon nanotubes could be implemented for structural support and to increase the apparent conductivity of the electrospun fibers at low weight percentages due to their high aspect ratio. A theoretical model has been presented for the behavior of rod-like particles representing carbon nanotubes in electrospinning. Initially, the carbon nanotubes are randomly oriented, but due to the “sink-like” flow in a wedge-like jet they are gradually oriented mainly along the

streamlines from the flow of solution and direction of the electric field, so that aligned carbon nanotubes are drafted into the electrospun jet and become oriented. Ko has investigated the fabrication of electrospun continuous carbon nanotubes-filled nanofibers through morphological and mechanical property analysis.⁷ However, that work showed much aggregation with single-walled carbon nanotubes, and resulting poor mechanical properties. This can be attributed to the aggregated carbon nanotubes acting as stress concentrators within the electrospun matrix. For this research, a main goal is to increase the conductivity of mats of nanofibers. Past work has investigated the influence of carbon nanotubes loading and resulting conductivity.²⁵⁻²⁹ In composite systems, increased conductivity is indicative of percolation of the conducting component. For carbon nanotubes their high conductivity renders them an ideal material for conducting composites. Previous investigations have been unable to determine a percolation threshold below 0.05 wt% carbon nanotubes in electrospun fibers.²⁸ For carbon nanotubes conducting composites, the increase in conductance is attributed to a “hopping” of electrons from one conducting pathway to the next. By increasing the percentage of carbon nanotubes within a system, there is a greater likelihood that electrons will be able to continue on a conducting pathway and not terminate in the matrix of the composite. Chapter 4 will highlight the percolative behavior of carbon nanotubes in electrospun nanofiber mats.

2.3 Tissue Engineering

As discussed in Chapter 1, tissue engineering involves a triad of scaffold, cells, and signaling chemicals. This work focuses on the development and use of nanocomposites for a tissue scaffold. The purpose of the scaffold is to resemble the natural structure *in vivo* for cells to

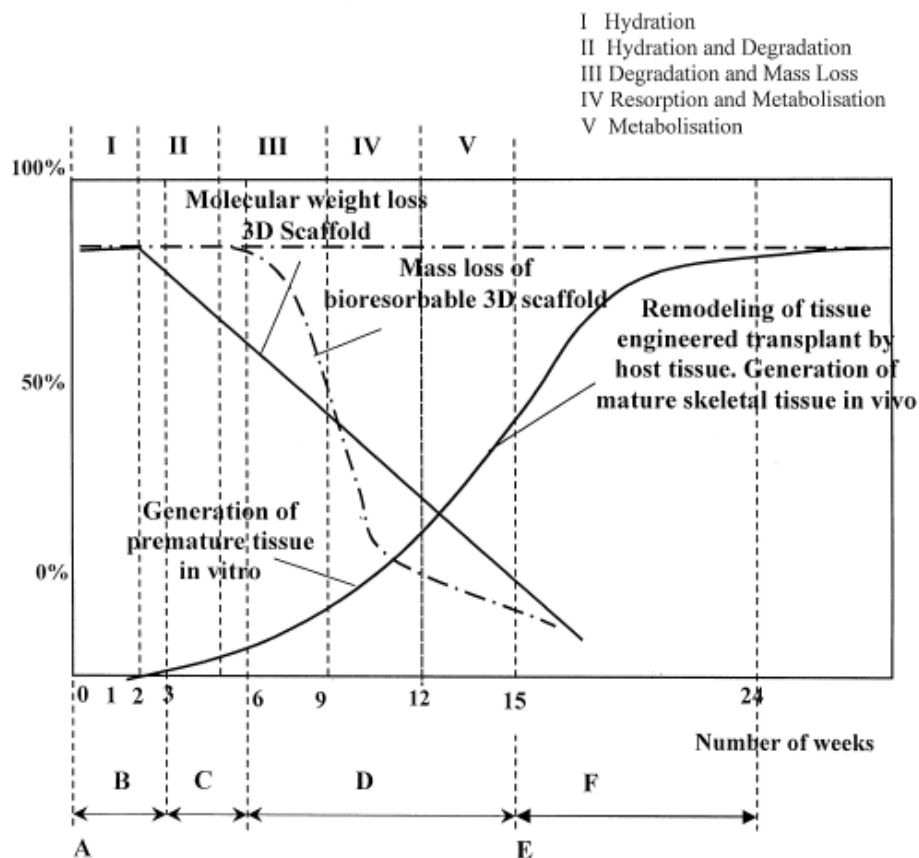
proliferate, differentiate, and maintain normal function. The scaffold itself is merely an imitation of the extracellular matrix (ECM) found within the body. The ECM is composed of proteoglycans and proteins that contain specific amino acid sequences. Proteins within the ECM are known as glycoproteins and have short chains of carbohydrate residues attached to them. Glycoproteins are amino acids covalently linked together containing both hydrophilic and hydrophobic groups. Glycoproteins have an N-terminus, where the chain ends with an amine group (NH₂), and a C-terminus, where chain ends with an carboxylic acid group (COOH).³⁰ The ECM participates in promoting cell adhesion, migration, growth, and differentiation.³⁰ It provides a framework for how the cells interact with each other and the finite space that transforms and organizes the cells into three dimensional tissues and organs. The ECM is a fibrous structure and is organized in a three-dimensional fiber network composed primarily of collagen fibers that are formed hierarchically by nanometer-scale multi fibrils, thus the dimensions of the components of a tissue-engineered scaffold should be on the same scale with those of natural ECM. The size of the ECM is on the angstrom to micro level, and thus the scaffold should be able to resemble the size of the ECM on a similar scale. Currently, many researchers are using scaffolds that are assembled on the nano-scale. These will be discussed further in the scaffold fabrication section (2.3.1).³¹⁻³³

Biocompatibility depends strictly on the material in use along with the material's chemical formula, and is influenced by other factors including biodegradability. For use within the body, the goal is to have the scaffold allow the ingrowth of cells into the substrate and breakdown through either surface or bulk erosion. If the by-products of the scaffold are not compatible with the body, by being toxic, carcinogenic, mutagenic, or causing any other type

of harmful reaction, then the body will reject the scaffold and cells will not proliferate on the scaffold. Also massive release of acidic degradation and resorption by-products results in inflammatory reactions which is a sign of rejection.^{34,35}

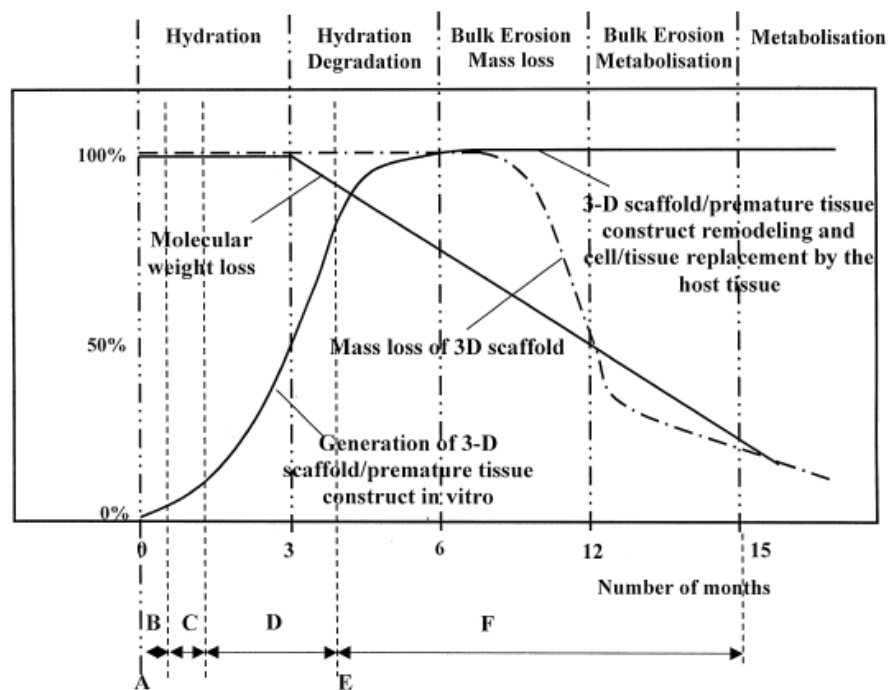
One main issue for scaffold formation is the balance of temporary mechanical function with mass transport to aid biological delivery and tissue regeneration. Mechanical integrity and high porosity or permeability are two criteria that are the most difficult to achieve, in that the very nature of each requirement contradicts the other. In some research it is suggested that the ideal porosity of the scaffold should be in the range of 80-90% which could result in a faster degradation rate of the scaffold.³⁶ Nutrient transport within the scaffold is of extreme importance and controls how the cells proliferate and differentiate. In general, tissues *in vivo* have access to vasculature that provides most of the nutrients essential for cells to functions. However, since a blood supply does not exist *in vitro*, the scaffold must be designed and engineered to be able to perform this remarkable feat of allowing mass transfer to occur via two paths, nutrient arrival to the cells and waste removal away from the cells. Thus, transport within the scaffold is mainly a function of diffusion which encompasses oxygen delivery, waste removal, nutrient arrival, protein transport, and cell migration.³⁷ The rate and capacity of transfer is based on the size, geometry, orientation, interconnectivity, branching, and surface chemistry associated with the pores and channels that are based on the material and fabrication of the material, and physical arrangement of the macroscopic material. Porosity can be dictated by having a high surface area-to-mass ratio for ensuring uniform cell delivery and tissue ingrowth.³⁶ Nutrient transport within the scaffold is of extreme importance and controls how the cells proliferate and differentiate. Transport within the

scaffold is mainly a function of diffusion which encompasses oxygen delivery, waste removal, nutrient arrival, protein transport, and cell migration. Figure 2.3 and 2.4 represent two different schemes that display two methods for the design of degradation of scaffolds within the body. The first scheme allows molecular weight loss of the scaffold as early as the second week of implantation. This method does not offer mechanical integrity and overall strength to the tissue but does allow for adequate mass transfer, and accommodates the ingrowth of tissue into the scaffold by being engineered for mass loss to occur. Thus this type of scaffold would be designed for soft tissues which do not require the structural stability of structural tissues such as bone.



Figures 2.3: Design Scheme I for soft tissue scaffold displaying the relationship between mechanical integrity and degradation.

Figure 2.4 displays a more structurally inert scaffold that offers mechanical integrity in the timeframe of months compared to the week timescale of scheme 1 (Figure 2.3). When viewing the diagram the molecular weight loss starts to occur around month 3. The main mechanism for this is that scheme 2 (Figure 2.4) requires a more crystalline polymer in order to limit the amount of water that diffuses into the amorphous regions. It is in the amorphous regions that hydrolysis can take place. This process usually occurs in reduction in molecular weight in amorphous regions with little mass loss, further molecular weight decrease followed by mass loss, and finally total hydrolysis to soluble materials which is the degradation of the crystalline regions of the polymer scaffold.



Figures 2.4: Design Scheme II for hard tissue scaffold displaying the relationship between mechanical integrity and degradation.³⁸

Mechanical integrity is required in order for the tissue scaffold to resemble the natural ECM and be able to provide structural stability. This is achieved mainly through the material's chemical constitution, depending on the type of backbone groups that it contains. The arrangement of crystalline and amorphous regions also play crucial roles, as the amount of amorphous regions is what dictates the means of degradation. This is due to the amorphous regions allowing water to infiltrate the polymer and cause hydrolysis through direct and secondary bonding of the water molecules to the fibers and to each other. The overall mechanism for degradation and loss in mechanical integrity was discussed in the schemes for the design of the scaffolds. Mechanical integrity is also dependent upon the geometrical aspects of the scaffold itself and will be further elaborated in fabrication methods. Another important aspect when considering synthetic polymeric materials for scaffold use is to know the glass transition temperature (T_g) and the melting temperature (T_m) of the polymer. The T_g is the temperature at which the amorphous regions of the polymer are able to move freely and rotate about the molecular chain axis. The T_m is the temperature at which the crystalline regions of the polymer become disordered or total disorder is reached in the system³⁹. If the polymer's glass transition temperature is around the body's temperature of 37°C, then the polymer will be able to undergo degradation. If the glass transition is much higher than this temperature, the polymer will not degrade as readily due to the amorphous regions of the polymer not being able to rotate freely and being in a glassy state. If the polymer's melting temperature is close to the temperature of the body's core temperature of 37°C it will not be able to be used due to it having no mechanical integrity or stability.³⁷

2.31 Scaffold Fabrication

The fabrication technique for the creation of the scaffold is also of prime importance for this work by understanding and developing processes that are able to reproduce what only nature has been able to achieve. These formation processes of polymers include particulate-leaching, casting of thin films, phase separation of polymer blends, CAD fabrication programs, and electrospinning. Particulate-leaching is a process where salt particles are finely ground and mixed with a polymer solution that is cast into a mold⁴⁰. After evaporation of the solvent, the salt crystals are leached away using water to form pores of the scaffold. The pore size can be controlled by numerous parameters including the size of the salt crystals and the porosity of the salt/polymer ratio.⁴⁰ Another fabrication method is phase separation where a homogenous multi-component system separates under thermodynamically unstable conditions and separates into different phases based on the order of free energy.³⁷ Finally, casting of thin films can produce uneven thicknesses and CAD fabrication requires expensive industrial machinery for production.

When reviewing these methods none are able to achieve uniform architecture on the nanometer scale. Also, there is a lack of precise control of the three-dimensional pore architecture⁴⁰. However, a novel method that has been receiving much interest is electrospinning. Electrospinning is similar to general spinning technologies except that it does not use mechanical forces to drive the polymer out of a spinneret. Electrospinning requires three elements: a syringe with metallic needle, high voltage source, and a grounded collector as viewed in Figure 2.5 and 2.6. Electrospinning utilizes the high voltage source to create an electric field between the metallic needle and collector, the solution is fed through

the syringe needle to form a droplet, and the electric field overcomes the droplet's surface tension.

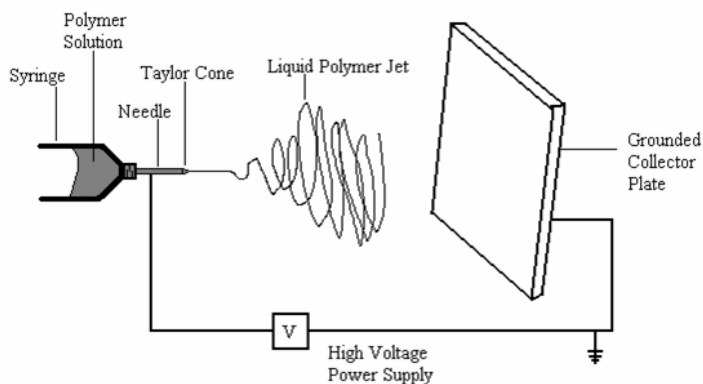


Figure 2.5: Diagram of electrospinning with labeled entities.

This is performed by connecting the high voltage source to the metallic needle. The degree to which the potential is drawn can create a “whipping” effect. As the polymer exits the capillary or tip, it is still in the form of the polymer dissolved in solution. As the polymer flows to the tip of the syringe needle, it forms a droplet, which requires a critical voltage, to overcome the surface tension of the polymer solution and form a cone known as a Taylor cone⁴¹⁻⁴⁴. The Taylor cone is where there is a high concentration of charges on the polymer and then forms a rapid whipping instability. A Taylor cone should be present during the stable and whipping phases. The cone is very similar to the cone achieved during extrusion of a polymer. However, in electrospinning the cone can be visible at the tip of the capillary or it is able to migrate to inside the capillary so all that is visible is a whipping stream⁴⁴. Once whipping is achieved, the polymer is collected as a random filament on the grounded collector. The interstices where the polymer fiber overlaps with another layer will fuse when there is residual solution. This method forms a very porous scaffold with a very high surface

area to volume ratio, improving diffusional properties. High porosity allows for adequate diffusion to and from the cells and provides ample space for cell growth, as well as sufficient surface area on the nanofibers for attachment and adhesion. This set-up for electrospinning is quite straightforward is a popular method for creating tissue scaffolds due to size of the fibers formed being on the nano scale.



Figure 2.6: Picture of actual electrospinning setup.

2.32 Nanocomposite Scaffolds

Currently, researchers have created composite materials for scaffold formation which incorporate two or more materials. Some of these materials consist of minerals for bone tissue engineering including calcium, hydroxyapatite, phosphate, or combinations of different polymers, such as poly (lactic acid) and poly (ϵ -caprolactone), collagen and poly (ϵ -caprolactone), and many other different combinations. Other work has focused on doping the polymer scaffolds with specific growth hormones or adhesion sequences to influence how cells attach to the scaffold and cause the scaffold to become a drug delivery vehicle. The principle utilized is that as the polymer degrades by common erosion methods, the encapsulated drug will be released.

Recent studies have investigated the use of carbon nanotubes as scaffolds for tissue engineering in both neat systems and in conjunction with biocompatible polymers.^{29,45,46} Chen et. al was able to graft oligomers of poly (L-lactic acid) (PLLA) to the surface of the *MWNT*; however, the grafting was not uniform and left much of the *MWNT* surface bare.⁴⁵ Zhang et al. prepared nanocomposite PLLA/*MWNT* scaffolds by solution casting. This fabrication method created uniform films but left *MWNT* exposed on the surface. Zhang et al. demonstrated that fibroblasts were able to grow to 80% confluency when in the presence of carbon nanotubes. Work by MacDonald incorporated carbon nanotubes into a collagen gel and noted that smooth muscle cells were able to remain viable in the composite scaffold for up to one week.⁴⁶ Though carbon nanotubes have such promising physical properties, their use in biomedical applications, specifically tissue engineering, has been obscured due to concerns of cytotoxicity. This issue has been investigated by various researchers with differing results depending on the purity of the carbon nanotubes and the method of production.⁴⁷ A collaborative study by Smart et al., noted that the main causes for possible toxicity were due to the surface area / volume ratio, retention time of carbon nanotubes within a tissue, and any residues of chemical within the carbon nanotubes.⁴⁷ Smart et al. also noted that the main deterrents for a comparative standard for carbon nanotubes toxicity is due to the issue of dosage, size scale and distribution of the carbon nanotubes, and dispersal of the carbon nanotubes.⁴⁷ Thus, a comprehensive understanding of carbon nanotubes interactions with cells is imperative. Monteiro-Riviere has investigated the cytotoxicity of carbon nanotubes with human keratinocytes and determined that, at increasing doses of carbon nanotubes, the cells responded with an increase of the inflammatory cytokine

interlukin-8 (IL-8).^{19,48} However, the carbon nanotubes were in solution and not incorporated into a nanocomposite configuration. For this study, carbon nanotubes will be incorporated into electrospun nanofibers with a biocompatible polymer acting as an interface between the seeded cells and the carbon nanotubes.

2.33 Stem cells in Tissue Engineering

When determining what type of cell line to use for tissue engineering, much work has concentrated on the use of stem cells. Stem cells are defined as undifferentiated cells that can proliferate and have the capacity to both self-renew and differentiate to one or more types of specialized cells. Stem cells are cells in the body that have the potential to differentiate into a variety of tissues, depending on chemical and physical stimuli. Stem cells are located within the stroma of the bone, or bone marrow, and other types of tissue including adipose.⁴⁹ Stem cells are relatively undifferentiated and do not possess functional specializations of the progeny. Also, they offer an inexhaustible cell source for tissue engineering. During traumatic injuries occurring to bone, stem cells migrate to the site where they begin undergoing differentiation to aid in the healing process. Thus, when considering that tissue engineering is geared towards restoring function of diseased, damaged, or malfunctioning tissue, it is apparent why they should be implemented. Human stem cells have brought much controversy in the past years due to the ethical issues surrounding the use of embryonic stem cells. However, a sanctioned source for stem cells is from adult tissue reservoirs. Adult-derived human stem cells are of great interest due to the relative ease of isolating and storing them for future use through cryopreservation. A specific type of stem cell known as mesenchymal stem cells have been used in multiple tissue engineering scenarios, to grow tissues including bone, cartilage, blood vessels, and skin. Mesenchymal

stem cells were originally found in the bone marrow of guinea pigs by Friedenstein in 1970 and have a fibroblastic morphology.⁵⁰ These cells were capable of differentiation into osteoblasts and adipose cells and to express smooth muscle actin.⁵⁰ Stem cells from adipose tissue have been shown to have similar differentiation potential. De Ugarte et al. has suggested that there is little difference between cells from marrow and fat in terms of yield, growth kinetics, multi-lineage differentiation capacity, and gene transduction efficiency.⁵¹

2.4 Functional Tissue Engineering

A major challenge of tissue engineering is directing the cells to establish physiological structure and function of the tissue across different hierarchical scales. Researchers tend to be moving more towards what is being labeled “functional tissue engineering” in which *in vivo* interactions are being emulated *in vitro*. These interactions include electromagnetic fields, mechanical stresses and strains, and specific chemical interactions which include arginine-glycine-aspartate (RGD) sequences for directing protein interactions and binding sequences between the cells and the scaffold. The use of mechanical and electric stimuli is receiving much attention. The goal of this study is to use mesenchymal stem cells and direct them into osteogenesis by applying an electric field with a conductive tissue scaffold. Much work has looked at the potential and application of bioelectric potentials for regenerative purposes.⁵²⁻⁵⁴ The discovery of electromechanical properties and natural biopotentials in bone by Yasuda, Fukada, Becker, Bassett, and others, led to the idea of using weak exogenous electrical currents to emulate physiological and strain-related electrical currents and thereby stimulate bone formation. The hypothesis that evolved (Figure 2.7) was that the electrical activity observed in bone was somehow the mediator of its remarkable repair and adaptive remodeling responses to mechanical loading and further, that electrical stimulus

alone could stimulate the response. Bone produces electrical potentials when mechanical stressed, and this is thought to be essential component of cellular events in regenerative healing.

"YASUDA'S HYPOTHESIS"

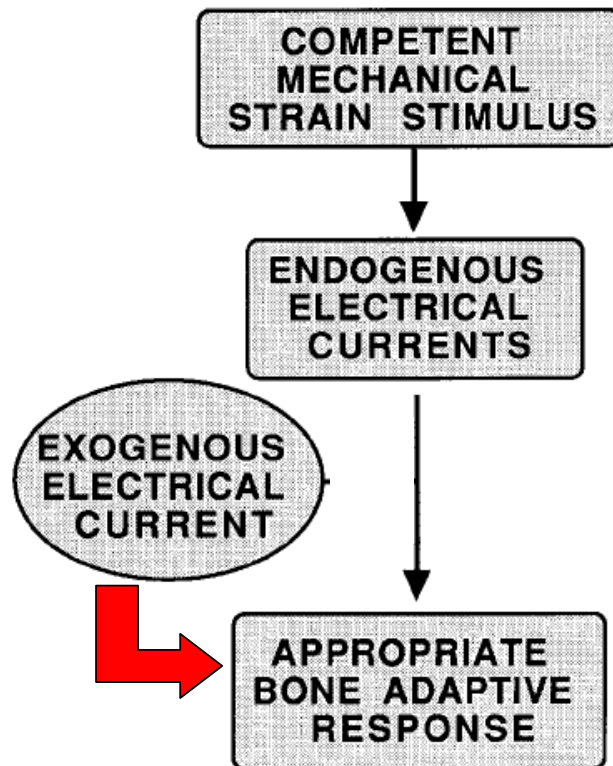


Figure 2.7: Diagram of Yasuda's Hypothesis depicting that applied electrical currents can produce an adaptive response in bone tissue.⁵⁵

These electrical potentials occur by two main components, piezoelectricity and streaming potentials. Piezoelectricity is generation of an electric potential by applying a force and changing the configuration of crystalline regions in a material. Streaming potentials are the movement of ions in fluid. Currently there are three main methods for applying an electric field or current to tissue cultures: 1) direct electrical currents, 2) capacitive coupling of electric fields, or 3) inductive coupling of electromagnetic fields.⁵⁵⁻⁵⁸ The direct method

implements an actual probe into the substrate and applies a high voltage in one specific area and is distributed throughout the substrate. By using capacitors, researchers have been able to minimize interaction with the delivery of the electric current and are better able to observe direct effects of the electric field. Capacitors can be defined as two conductors carrying charges of equal magnitude but of opposite sign, where the potential difference across the conductors or plates is known at the voltage where Capacitance (C) \equiv Charge (Q)/ Potential Difference (ΔV) or $C = Q / \Delta V$. By using a capacitor with the tissue culture, we would be able to generate an electric current through our culture, and by incorporating carbon nanotubes into our scaffold material, we would be able to create an electric field with minimum interaction with the scaffold itself, no means of removal of an electrode and no electrochemical reactions resulting from any additions to the scaffold. In order to achieve similar results without an electrode penetrating the system, large voltages need to be generated. To produce a more functional scaffold, the goal of this work is to increase the conductance of the scaffold and thereby localize the electric field within the scaffold and its access to the cells. A major inspiration for this research was work conducted by Supronowicz in 2001.⁵⁹ Their work developed a nanocomposite scaffold combining poly (lactic acid) gel with multi-walled carbon nanotubes with an electrical stimulus. Despite the great leap that research took, it opened new doors and asked fundamental questions regarding the concentration of carbon nanotubes (20 wt%), gelatinous structure of the nanocomposite, and the cytotoxicity of the carbon nanotubes. This work aims on moving forward, by using lower concentrations of carbon nanotubes for similar increases in conductance, determining cellular viability, cellular proliferation, expression of specific inflammatory cytokines, and producing a nanocomposite fibrous mat by electrospinning carbon nanotubes in

biocompatible polymer solutions. Electrospinning will afford a high degree of porosity as well as encapsulate the carbon nanotubes within polymeric nanofibers. By encapsulating the carbon nanotubes within the nanofibers, we will create a biocompatible interface, as well as a conductive tissue scaffold. These research objectives and the means for accomplishment will be discussed in detail in Chapter 3.

2.5 References

1. J. Ayutsede, M. Gandhi, S. Sukigara, H. H. Ye, C. M. Hsu, Y. Gogotsi and F. Ko, *Biomacromolecules*, **7**, 208-214 (2006).
2. W. E. Dondero and R. E. Gorga, *Journal Of Polymer Science Part B-Polymer Physics*, **44**, 864-878 (2006).
3. Dror Yael, Salalha Wael, Khalfin Rafail, Cohen Yachin, Yarin Alexander and Z. Eyal, *Langmuir*, **19**, 7012-7020 (2003).
4. M. El Fray and A. R. Boccaccini, *Materials Letters*, **59**, 2300-2304 (2005).
5. R. E. Gorga and R. E. Cohen, *Journal Of Polymer Science Part B-Polymer Physics*, **42**, 2690-2702 (2004).
6. H. Hou, *Chemical Materials*, 967-973 (2005).
7. F. Ko, Y. Gogotsi, A. Ali, N. Naguib, H. H. Ye, G. L. Yang, C. Li and P. Willis, *Advanced Materials*, **15**, 1161-+ (2003).
8. J. J. Mack, L. M. Viculis, A. Ali, R. Luoh, G. L. Yang, H. T. Hahn, F. K. Ko and R. B. Kaner, *Advanced Materials*, **17**, 77-+ (2005).
9. V. Thomas, D. R. Dean and Y. K. Vohra, *Current Nanoscience*, **2**, 155-177 (2006).
10. S. Iijima, *Science*, **354**, 56-58 (1991).

11. *Phys. Rev. Lett.*, **79**, 1297-1300 (1997).
12. *Carbon*, **33**, 925-930 (1995).
13. *Phys. Rev. Lett.*, **82** (1999).
14. C. Journet and e. al., *Nature*, **388**(1997).
15. A. Thess and e. al., *Science*, **273**(1996).
16. J. Kong and e. al., *Chem. Phys. Lett.*, **292**(1998).
17. J. Hafner and e. al., *Chem. Phys. Lett.*, **296**(1998).
18. M. Suand e. al, *Chem. Phys. Lett.*, **322** (2000).
19. N. Monteiro-Riviere, A. Inman, Y. Wang and R. Nemanich, *Nanomedicine: Nanotechnology, Biology, and Medicine 1*, 293-299 (2005).
20. V. C. Moore, M. S. Strano, E. H. Haroz, R. H. Hauge and R. E. Smalley, *Nano Letters*, **3**, 1379-1382 (2003).
21. D. Myers, *Surfactant Science and Technology*, John Wiley & Sons, Inc., Hoboken, New Jersey, 2006.
22. H. J. Gong, X. P. Yang, G. Q. Chen, T. Q. Liu, S. M. Zhang, X. L. Deng and X. Y. Hu, *Acta Polymerica Sinica*, 297-300 (2005).
23. C. Li, C. Vepari, H.-J. Jin, H. J. Kim and D. Kaplan, *Biomaterials*, **27**, 3115-3124 (2006).
24. I. D. Norris, M. M. Shaker, F. K. Koand A. G. MacDiarmid, *Synthetic Metals*, **114**, 109-114 (2000).
25. M. Grujicic, G. Cao and W. N. Roy, *Journal Of Materials Science*, **39**, 4441-4449 (2004).
26. E. Munoz, *Advanced Materials*, **17**, 1064-1067 (2005).

27. J. Sandler, M. S. P. Shaffer, T. Prasse, W. Bauhofer, K. Schulte and A. H. Windle, *Polymer*, **40**, 5967-5971 (1999).
28. Sundaray Bibekananda, Subramanian V. and N. T.S., *Applied Physics Letters*, **88**(2006).
29. D. Zhang, M. A. Kandadai, J. Cech, S. Roth and S. Curran, *Journal of Physical Chemistry B*, **110**, 12910-12915 (2006).
30. Yaszemski, *Tissue Engineering and Novel Delivery Systems*, Marcel Dekker, Inc., New York, 2004.
31. W. J. Li, R. Tuli, X. X. Huang, P. Laquerriere and R. S. Tuan, *Biomaterials*, **26**, 5158-5166 (2005).
32. E. A. Minguell JJ, Conget P, *Society for Experimental Biology and Medicine*, **226**, 507-520 (2001).
33. Venugopal, *Nanotechnology*, **16**, 2138-2142 (2005).
34. Bergsma, *Journal of Maxillofacial Surgery*, **51**, 666-670 (1993).
35. Bergsma, *Biomaterials*, **16**, 25-31 (1995).
36. Karande, *Annals of Biomedical Engineering*, **32**, 1728-1743 (2004).
37. R. Lanza, R. Langer and J. Vacanti, *Principles of Tissue Engineering*, Academic Press, Boston, 2000.
38. Hutmacher, *Biomaterials*, **21**, 2529-2543 (2000).
39. McCrum, *Principles of Polymer Engineering*, Oxford Science, Oxford, 1986.
40. Ma, *Materials Today*, 30-40 (2004).
41. E. D. Boland, G. L. Bowlin, D. G. Simpson and G. E. Wnek, *Abstracts Of Papers Of The American Chemical Society*, **222**, U344-U344 (2001).

42. E. D. Boland, J. A. Matthews, K. J. Pawlowski, D. G. Simpson, G. E. Wnekand G. L. Bowlin, *Frontiers In Bioscience*, **9**, 1422-1432 (2004).
43. E. D. Boland, D. G. Simpson, G. E. Wnekand G. L. Bowlin, *Abstracts Of Papers Of The American Chemical Society*, **226**, U436-U436 (2003).
44. Li, *Advanced Materials*, **16**(2004).
45. G.-X. Chen, H.-S. Kim, B. H. Parkand J.-S. Yoon, *Journal of Physical Chemistry B*, **109**, 22237-22243 (2005).
46. R. A. MacDonald, B. F. Laurenzi, G. Viswanathan, P. M. Ajayanand J. P. Stegemann, *Journal Of Biomedical Materials Research Part A*, **74A**, 489-496 (2005).
47. S. K. Smart, A. I. Cassady, G. Q. Luand D. J. Martin, *Carbon*, **44**, 1034-1047 (2006).
48. N. Monteiro-Riviere, *Toxicology Letters*, **155**, 377-384 (2005).
49. A. Battlerand J. Leor, *Stem Cell and Gene-Based Therapy*, Springer, London, UK, 2006.
50. N. Habib, M. Gordon, N. Levicar, L. Jiaoand G. Thomas-Black, *Stem Cell Repair and Regeneration*, Imperial College Press, London, UK, 2005.
51. D. A. De Ugarte, K. Morizono, A. Elbarbary, Z. Alfonso, P. A. Zuk, M. Zhu, J. L. Drago, P. Ashjiian, B. Thomas, P. Benhaim, I. Chen, J. Fraserand M. H. Hedrick, *Cells Tissues Organs*, **173**, 101-109 (2003).
52. R. O. Becker, *Clinical Orthopaedics and Related Research*, **83**, 255-262 (1972).
53. R. B. Borgens, J. W. Vanable Jr.and L. F. Jaffe, *Developmental Biology*, **74**, 4528-4532 (1977).
54. R. B. Borgens, J. W. Vanable Jr.and L. F. Jaffe, *Journal of Exploratory Zoology*, **200**, 403-416 (1977).

55. M. Hartig, U. Joos and H. P. Wiesmann, *European Biophysics Journal With Biophysics Letters*, **29**, 499-506 (2000).
56. M. Ochi, P. L. Wang, K. Ohura, S. Takashima, H. Kagami, Y. Hirose, T. Kaku and K. Sakaguchi, *Clinical Oral Implants Research*, **14**, 294-302 (2003).
57. J. A. Spadaro, *Bioelectromagnetics*, **18**, 193-202 (1997).
58. H. P. Wiesmann, M. Hartig, U. Stratmann, U. Meyer and U. Joos, *Biochimica Et Biophysica Acta-Molecular Cell Research*, **1538**, 28-37 (2001).
59. P. R. Supronowicz, P. M. Ajayan, K. R. Ullmann, B. P. Arulanandam, D. W. Metzger and R. Bizios, *Journal Of Biomedical Materials Research*, **59**, 499-506 (2002).

Chapter 3

Research Objectives

3.1 Research Objectives

Due to the overwhelming significance that has been placed on tissue engineering, it has become important to investigate new functional materials as scaffolds in tissue engineering scenarios. For this research, the focus will be on the fabrication of electrospun scaffolds with multi-walled carbon nanotubes, ascertaining the specific physical properties of interest, and investigating the interaction of human mesenchymal stem cells with the scaffold and the influence of electrical stimulation on human mesenchymal stem cells seeded on the scaffold. Specifically, the objectives of this research are as follows.

- (1) Fabricate multi-walled carbon nanotube / polymer composites via electrospinning and as a function of multi-walled carbon nanotubes concentration. This will be accomplished by:
 - a. determining the rheological properties of the polymer solutions and the effect of multi-walled carbon nanotube addition
 - b. analyzing the electrospun nanocomposites via scanning and transmission electron microscopy to confirm proper fiber formation and multi-walled carbon nanotube integration into the as-spun fiber.
 - c. determining any improvements in mechanical properties and electrical conductivity via tensile testing and sensitive conductivity measurements, respectively.
- (2) Fabricate multi-walled carbon nanotubes / polymer composites with a biocompatible polymer via electrospinning. This will be accomplished by:

- a. analyzing the electrospun nanocomposites via scanning and transmission electron microscopy to confirm proper fiber formation and multi-walled carbon nanotube integration into the as-spun fiber.
 - b. determining the ideal processing parameters for the electrospinning process including solution concentration, applied voltage (kV), working distance (cm), flow rate (mL/min), solvent system, and multi-walled carbon nanotubes addition using response surface methodology.
 - c. using tensile testing and sensitive conductivity measurements, for quantitating the physical properties of the scaffold.
- (3) Determine the efficacy of the electrospun tissue scaffold and compare the addition of multi-walled carbon nanotubes with human mesenchymal stem cells. This will be accomplished by:
- a. analyzing viability of the cells *in vitro* for fourteen days using a live / dead fluorescence stain with fluorescence microscopy.
 - b. analyzing proliferation of the cells by quantifying the amount of DNA present at specific time-points (days 1, 3, 7, and 14) over the course of the experiment
 - c. analyzing cellular orientation on the electrospun scaffolds via scanning electron microscopy (days 1 and 14)
- (4) Determine the use of the electrospun scaffold with multi-wall carbon nanotubes in a functional tissue engineering set-up incorporating electric field stimulation. This will be accomplished by:
- a. analyzing proliferation of the cells by quantifying the amount of DNA present at specific time-points (days 1, 7, and 14) over the course of the experiment

- b. analyzing cytokine expression of interleukin-1 β , interleukin-6, interleukin-8, and TNF- α (days 1, 7, 14)
- c. analyzing amount of calcium deposition via scanning electron microscopy using electron x-ray dispersive spectroscopy (day 21)

The first objective will focus on incorporation of multi-walled carbon nanotubes into electrospun nanofibrous mats and will be a staging ground for determining the electrical conductivity in these isotropic mats. This work will allow us to establish the optimal concentration of multi-walled carbon nanotubes for electrospun nanocomposites.

The second objective involves replicating the advancements in physical properties of electrospun fibrous mats in a biocompatible polymeric system. Response surface methodology will be utilized to establish the optimal processing parameters for the electrospinning process and investigate the physical properties of the electrospun mats using the indicated techniques.

The third objective allows for the implementation of the electrospun scaffold in a static cell culture environment with human mesenchymal stem cells. The efficacy of the electrospun scaffold will be elucidated as to what effect the multi-walled carbon nanotubes will have when in close proximity with the cells when compared to a control electrospun scaffold.

The remainder of the thesis is organized such that each subsequent chapter discusses a specific objective. Objective (1) is discussed in Chapter 4, objective (2) in Chapter 5, and objective (3) in Chapter 6. Each of these chapters has been submitted to a peer-reviewed

journal as an individual manuscript. Chapters 7 and 8 discuss the overall conclusions and future directions for this project including objective (4), respectively.

Chapter 4

Morphological, electrical, and mechanical characterization of electrospun nanofiber mats containing multi-walled carbon nanotubes

Seth D. McCullen¹, Derrick R. Stevens², Wesley A. Roberts³, Satyajeet S. Ojha⁴, Laura I. Clarke⁵, and Russell E. Gorga⁶

4.1 Abstract

This work focuses on the development of electrically-conducting porous nanocomposite structures by the incorporation of multiwalled carbon nanotubes (MWNT) into electrospun poly (ethylene oxide) (PEO) nanofibers. Electron microscopy confirmed the presence of individual aligned MWNT encapsulated within the fibers and showed fiber morphologies with diameters of 100-200 nm. Electrical conductance measurements of the random nanofiber mats showed that by increasing the concentration of MWNT, we were able to produce porous nanocomposite structures with dramatically improved electrical conductivity. Above a percolation threshold of 0.365 +/- 0.09 MWNT weight percent (wt%) in PEO the conductance increased by a factor of 10^{12} and then became approximately constant as the concentration of MWNT was further increased. Due to this percolation threshold, for a 1 wt% loading of MWNT, the conductivity is essentially maximized. Mechanical testing confirmed that the tensile strength did not change, and there was a three-fold increase in the Young's modulus when comparing a 1 wt% MWNT loading to the pure electrospun PEO.

¹Primary author and researcher, Department of Textile Engineering, Chemistry, and Science, NCSU

²Graduate student who assisted with conductance measurements, Department of Physics, NCSU

³Undergraduate student who assisted with conductance measurements, Department of Physics, NCSU

⁴Graduate student who assisted with SEM micrographs, Department of Textile Engineering, Chemistry, and Science, NCSU

⁵: Provided conductivity systems measurement and expertise, Department of Physics, NCSU

⁶Correspondence author, Department of Textile Engineering, Chemistry, and Science, NCSU

Thus the optimal MWNT concentration for PEO nanofiber mats with enhanced mechanical and electrical properties is approximately 1 wt%.

4.2 Introduction

Nanocomposites are materials that have the propensity to exhibit astonishing physical and electrical properties due to the interaction between the matrix and filler. Much work has focused on the implementation of carbon nanotubes as a filler in polymer matrices, and some success has been achieved at determining the physical properties of these systems.¹⁻⁴ The goal of this work is to create and characterize novel nanocomposites, in particular random mats of electrospun nanofibers, to be used as a model in creating functional substrates for a variety of applications ranging from electrical sensors to matrices for tissue engineering. Therefore, characterization of the overall mechanical and electrical properties of the random fibrous mat is essential to quantify the functionality of these structures. Specifically, this report focuses on the fabrication and electric and mechanical characterization of electrospun carbon nanotube/poly (ethylene oxide) (PEO) nanocomposites. Through this investigation, we will have a better representation of the nanocomposite characteristics by measuring the macroscopic nonwoven substrate, not just an individual fiber within the composite. Therefore, the properties measured here will be indicative of those of the composite in an application. A specific focus is on conductance measurements to delineate the parameters which determine the resultant conductivity of the isotropic fibrous mats, as electrical conductivity is important for both sensor and biomedical applications. Electron microscopy is utilized to determine fiber morphology and the orientation of the multi-walled carbon nanotubes (MWNT) within the fiber. A final consideration is the mechanical properties of

the system with a goal of simultaneously optimizing the mechanical and electrical properties of random fibrous mats.

Carbon nanotubes are graphitic sheets rolled into seamless tubes (*i.e.*, arrangements of carbon hexagons into tube-like fullerenes) and have diameters ranging from about a nanometer to tens of nanometers with lengths up to centimeters. Nanotubes have received much attention due to their interesting properties (high modulus and electrical/thermal conductivity) since their discovery by Iijima in 1991.^{5, 6} Since then, significant effort has gone into fabricating polymer/nanotube composites for improved strength and conductivity.⁷⁻

²² In general, for improved mechanical properties, the interaction between the filler material and polymeric matrix is the key to sustaining a compatible interface through the adhesive contact of the two materials.^{23, 24} When a conductive composite is desired, the most important parameter besides the apparent conductivity of the filler is the geometric shape; in particular, it is most advantageous to utilize fillers with an aspect ratio (length/diameter) greater than 1. Cylindrical materials such as carbon nanotubes exhibit this large aspect ratio, in the range of thousands, which alleviates the processing of the nanocomposite by assuring that only a low mass fraction is needed to obtain large increases in physical properties. Thus, carbon nanotubes are ideal candidates for nanocomposite applications and have demonstrated large increases in physical properties with relatively low mass fractions.

Here, electrospinning was used to fabricate nanocomposites constructed of carbon nanotube-polymer nanofibers. Electrospinning provides a means to construct a three dimensional matrix by creating fibers with diameters on the nano to micro scale. The fibers are created by

electrostatic repulsion and the coulombic forces due to an external electric field applied to a polymer solution.^{25,26} By applying a critical voltage between the metallic needle of a syringe filled with polymer solution and a grounded collector, a polymer jet is generated which creates fibers that can be collected at the grounded plate.^{25, 27, 28} The end result is a randomly oriented mat of fibers with a high porosity due to the high ratio of surface area to volume. This aspect of electrospun fibers is advantageous for use as a means of production for nanocomposites by generating an intimate level of interaction between the matrix and the filler due to both being on similar size scales.

Previous work on fibrous nanocomposites has highlighted the need for adequate dispersion of the filler in the matrix for enhanced mechanical properties.^{4, 21, 22} Past research has shown that dispersion and orientation of the carbon nanotubes within a nanocomposite improves physical properties.^{4, 21, 22} However, most of this work has utilized traditional polymer processing techniques such as melt-blending and coagulation spinning to name a few.⁴ Dror et al. dispersed carbon nanotubes with the additive gum arabic to create a colloidal suspension of carbon nanotubes in solution prior to electrospinning and achieved a high level of carbon nanotube orientation within the nanofibers.²⁹ Here we utilize the Dror technique to form nanofibers with ~100 nm diameters.

Researchers who have explored the interaction of carbon nanotubes in electrospun matrices have documented differing conclusions.²⁹⁻³³ This can be attributed to the polymeric system, the orientation, and the dispersion of the carbon nanotubes in the system in addition to the size scale of the carbon nanotubes, the diameter, and the length with respect to the matrix.¹

With respect to electrical properties of composite fibers, Sundaray was able to show an increase of ten orders of magnitude in conductivity between 0 weight percent (wt %) and 2 wt% carbon nanotube loading in single electrospun fiber.³³ However, this work did not display evidence of a percolation threshold between 0.05-2 wt % and the authors hypothesized that, if present, the threshold was much lower than 0.05 wt%. Through this work, our aim is to produce electrospun nanocomposites containing varying mass fractions of carbon nanotubes, to determine if the conductance of the nonwoven mat (not the individual fiber) follows a percolation model, and to report the percolation threshold via thorough conductance measurements. Again, it is essential to quantify the properties of the random fibrous mat to determine how the material behaves in bulk.

All measurements in this work were conducted on samples consisting of random nanofiber mats produced from electrospinning. By utilizing planar interdigitated electrodes onto which the mat can be directly electrospun, we can measure these extremely porous mats in their native state without concern of pinhole defects which can occur in a "sandwich" electrode configuration. In summary, we propose to optimize the parameters for the electrospinning process of PEO/carbon nanotube solutions, to determine if the conductance exhibits percolative behavior, and to measure the tensile properties of electrospun fibrous mats.

4.3 Experimental

PEO of M_w 400,000 was purchased from Scientific Polymer Products. Different wt% solutions were produced with deionized water. MWNT were supplied by Nano-Lab. The MWNT were produced by plasma enhanced chemical vapor deposition using acetylene and

ammonia with an iron catalyst and grown on a mesoporous silica substrate.³⁴ The MWNT used had a diameter of 15 +/- 5 nm and length of 5- 20 μm at 95% purity. The MWNT were dispersed using an Ultrasonic Model 2000U generator and probe operating at 25 Hz. Varying masses of MWNT were added to 50 mL deionized water and the dispersing agent gum arabic at a concentration of 3% and sonicated for one hour. The sonicated solutions of MWNT and PEO in deionized water were combined and mixed by stirring. The solution was inspected optically for up to 30 days. Solutions containing gum arabic exhibited homogenous suspensions through the 30 day period; whereas the nanotubes in solutions without gum arabic immediately fell out of suspension after sonication. The final solutions produced contained varying concentrations of MWNT from 0-3 wt % in 4 wt% PEO solution. No further processing occurred before electrospinning.

The electrospinning apparatus included a syringe pump obtained from New Era Pump Systems (Model NE 500), which operated at a flow rate of 5-55 $\mu\text{L}/\text{min}$. The high voltage power supply was obtained from Glassman (High Voltage Model # FC60R2 with a positive polarity). The operating voltage varied from 10-20 kV with an optimum electric field of 1 kV/cm. The solutions were loaded into 10 mL syringes with luer-lock connections and used in conjunction with a 4 inch 20 gauge blunt tip needle. The design of the electrospinning set-up was based on a point-plate configuration as can be seen in Figure 4.1.

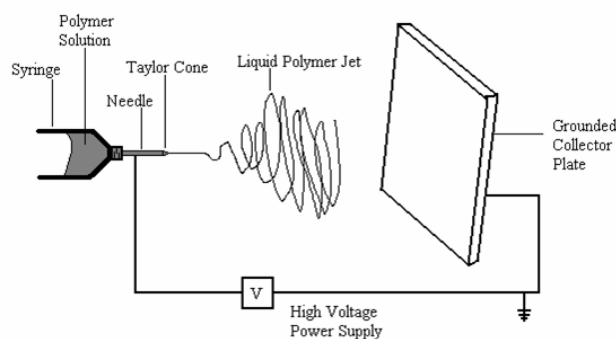


Figure 4.1: Schematic of the electrospinning apparatus used to produce the nanocomposite samples. Each component is labeled.

The fibers were collected on either a plate or a pair of aligned collector bars. The plate produced a random nonwoven array, whereas the collector bars produced oriented fibers along the same axis between the bars. The electrospun mats were deposited onto aluminum foil, which was placed over the collector plate. For scanning electron microscopy (SEM) and mechanical testing, the samples were removed from the collector. For transmission electron microscopy (TEM) and conductance testing, samples were deposited directly onto TEM grids and microelectrodes, respectively.

4.31 Electrospun Nanocomposite Characterization

Rheological measurements were performed on the MWNT/PEO solutions using a StressTech HR rheometer with Reologica Instruments and ATS Systems. These experiments were performed using a parallel plate configuration for all measurements.

For SEM, a JEOL JSM-6400 FE w/ EDS, operating at 5 kV, was used to determine fiber morphology of the electrospun samples. The electrospun samples were coated by a K-550X Sputter Coater with Au/Pd approximately 100 Å thick to reduce charging. Digital images were captured and analyzed using Scion Image™ software. TEM was performed on a JEOL 100S with samples spun directly on a Cu 400 mesh grid coated with holey thin carbon film. Micrographs were developed, digitally scanned, and were not further modified.

Electrical measurements were performed on a Keithley Model 6430 sub-femto amp remote source meter. In order to easily measure the thin, porous matrix of nanofibers, flat interdigitated electrodes on glass were utilized for conductance measurements. Each electrode consisted of twenty-six finger pairs with 1 mm long, 10 μm wide digits spaced by 10 μm, and two contact pads of approximately 1 mm² each. Conductive silver epoxy connected the contact pads to external wires. Electrodes were fabricated using lift-off standard uv-lithography on glass substrates followed by thermal evaporations of approximately 150 Å of chromium and 1150 Å of gold. Home-made triaxial cables connected the sample, which rested on a copper stage, to the remote source-meter. The sample space was evacuated to $\sim 1 \times 10^{-7}$ torr. Each electrode was measured before and after sample deposition, nominally from -10 V to 10 V with 0.1 V steps and a 15 second wait after the application of a voltage change. For highly conductive samples, the voltage range was reduced. Samples were prepared by electrospinning a solution with known concentration of multi-walled carbon nanotubes, utilizing the same preparation conditions for each sample to obtain comparable thickness. Conductance values were obtained by fitting a line to the low-voltage linear region of the current-voltage characteristic. The fringe fields from

interdigitated electrodes are known to penetrate into a film a distance roughly equivalent to the spacing between the digits. From the measured thickness of the mat as 1 - 3 μm , we expect some response from the fringing fields.³⁵ Consequently, the geometrical parameters needed to calculate the conductivity will be slightly altered. Furthermore, the extreme porosity of the nanocomposite mat makes a clear determination of the polymer density difficult. Thus, as a matter of convenience, we report conductance results only. A calibration to correct for the fringing fields is underway in our laboratory and will be reported in a future publication.

Mechanical properties were tested using an Instron Model 5544 using the Bluehill™ Version 1.00 software. Samples were prepared according to ASTM standard D4762-04. Each sample tested up to seven specimens with a sample width of 2 cm and a gauge length of 2.54 cm. The testing rate was approximately 25.4 cm/min. Samples were tested within 24 hours of fabrication.

The volume of voids in the random fibrous mats was calculated using Image J analyzer. Images obtained by SEM were scanned through Image J. Different layers of nanofibers were made distinct a using grayscale. The area (proportional to volume) of nanofibers present in one plane was then calculated and therefore void fraction was calculated in a single layer. This procedure was repeated four times for each sample for statistical purposes.

4.4 Results and Discussion

The viscosity of the spinning solution is essential for being able to produce a continuous flowing stream of polymer from the needle to the collector. Rheology measurements were performed to determine the effect on viscosity associated with an increase of MWNT and to verify whether the solutions were “spinnable”. By understanding the rheological behavior of the solution we are better able to control the processing parameters such as the flow rate. When analyzing the viscosity vs. shear rate data (as shown in Figure 4.2), the polymer solution with suspended nanotubes behaved as a classical pseudo-plastic material, exhibiting shear-thinning behavior at increasing shear rates. With the addition of MWNT to the polymer solutions, there was a slight increase in the viscosity. This can be attributed to an increased turbidity of the solution due to the presence of the MWNT.

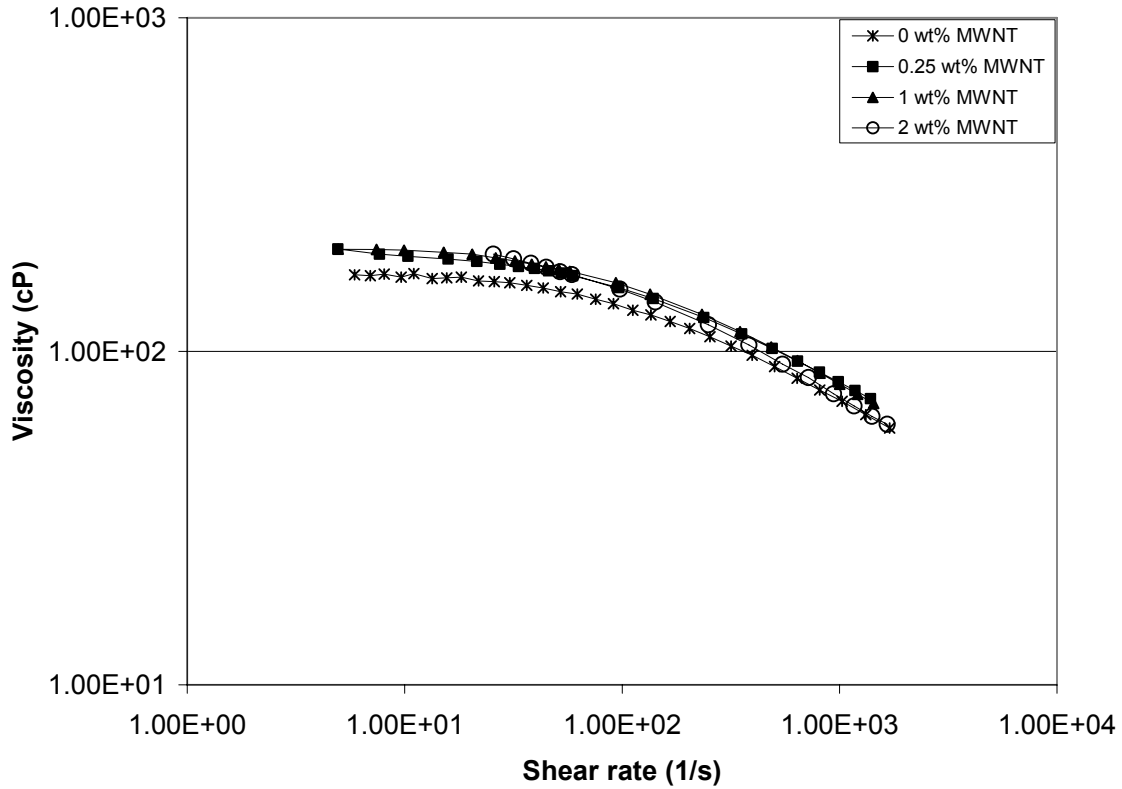
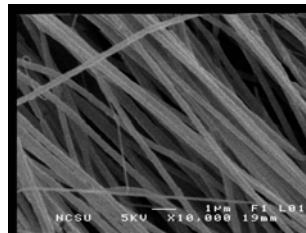


Figure 4.2: Flow curve plot of viscosity vs. shear rate for MWNT/PEO solutions.

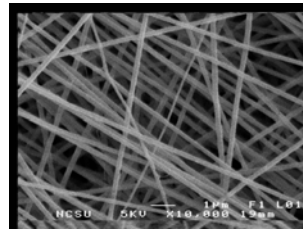
The flow of material during electrospinning is determined using the equation $Q = \Delta P/R$, where Q is the flow rate, ΔP is the pressure difference, and R is the resistance, equal to $8\eta L/\pi r^4$. For this equation L is the length of the capillary, r is the radius of the capillary, and η is the viscosity of the polymer solution. In order to determine the viscosity experienced during fiber formation, we can calculate the shear rate (Ψ) of our system with the following equation, $\Psi=4Q/\pi R^4$.³⁶ For the operational conditions, we produced a shear rate within the lower region of the viscosity plot, which depended on the flow rate from the syringe pump. The flow rate ranged from 5-55 $\mu\text{L}/\text{min}$. For this electrospinning system, the shear rate is

below 20 s^{-1} . When viewing the flow curve we can easily observe that no shear thinning is occurring at this range. The effects of interfacial bond strength, particle size, and shape distribution can be analyzed from the strain dependence of dispersions. For this system the particles in solution are the MWNT. When these particles are dispersed, each individual MWNT is separated from other MWNT and no aggregates are present. Smaller particles and stronger interfacial bonds will increase the low strain modulus of a dispersion with a given particle concentration. Forces acting on the particle in solution include gravity and random thermal (Brownian) fluctuations. In Figure 2, the viscosity plots for the different suspensions of MWNT in PEO show that the samples are within the same range, and that the MWNT do not significantly increase the viscosity of the solution. Thus, Figure 2 displays that the viscosity of PEO behaves similarly even with the addition of low mass fractions of MWNT. Also, the addition of MWNT does not change the shape of the flow curve for this polymer.

Orientation of the nanofibers can be controlled by the collector geometry. The plate collector morphology shows random orientation in all directions. Parallel bar collectors are able to align the nanofibers between the two collectors (as shown in Figure 4.3).



Aligned fibers with parallel bar collector



Random fibers with plate collector

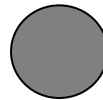
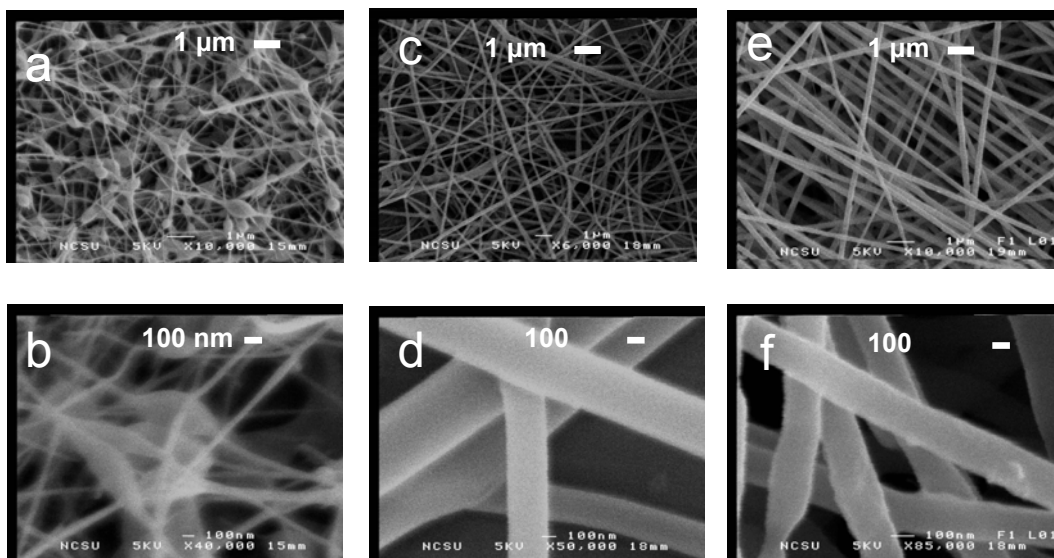


Figure 4.3: SEM of aligned and random nanofibers (1 wt % MWNT in 4 wt % PEO). Images were captured at 10,000X. The scale bar is 1 μm .

The polymer concentration can be viewed as a critical component that controls the morphology of the fibers produced. It was determined that less than 4 wt% PEO without MWNT produced beaded nanofibers. These structures exhibit poor mechanical properties due to their heterogeneous nature. By increasing the wt % of our polymer to 4 wt%, fibers were produced without any bead formation. Figure 4 illustrates the difference in morphologies for differing weight % concentrations. Incorporating the MWNT in a solution of 4 wt% PEO allows fabrication of uniform fibers with similar diameters. In contrast, spinning on the glass substrate of the interdigitated electrodes resulted in slightly beaded nanofibers for all MWNT concentrations. This can be attributed to the microelectrode not being completely grounded due to inadequate connection between the collector plate and the microelectrode front surface of the glass substrate. As beading in the nanofiber might be expected to decrease the conductance and increase the critical weight percentage, the electric conductance results can be considered upper and lower limits, respectively, on these quantities.



Figures 4.4a-f: SEM images of electrospun nanocomposites. 4.4a-b images of 3 wt% PEO, 4.4c-d images of 4 wt% PEO, 4.4e-f images of 4 wt% PEO with 1 wt% MWNT. By increasing the polymer concentration by 1%, we were able to produce uniform nanofibers. Images a, c, and e have scale bars of 1 μm , where images b, d, and f have scale bars of 100 nm.

In order to quantify that the produced fibers did contain oriented MWNT, TEM was utilized to view the alignment and orientation of MWNT within the nanofibers produced. The arrangement of the nanotubes within the fibers is able to influence the behavior of the composite when testing for conductivity and mechanical properties. If the MWNT have a high orientation within the fibers, then the apparent properties of the nanotubes should become superimposed within the electrospun fibers. Figure 4.5 confirms that the MWNT are aligned along the fiber axis via the flow and electric field direction. In some instances it can be seen that more than one MWNT was encapsulated within the produced nanofibers.

When more than one MWNT was encapsulated, a misshaped (or branched) nanofiber was produced as shown in Figure 4.5b. However, these fibers show numerous MWNT all dispersed and oriented along the axis of numerous fibers bonded together. Bonding of the fibers could have taken place due to the solvent evaporating too slowly, connecting the fibers together.

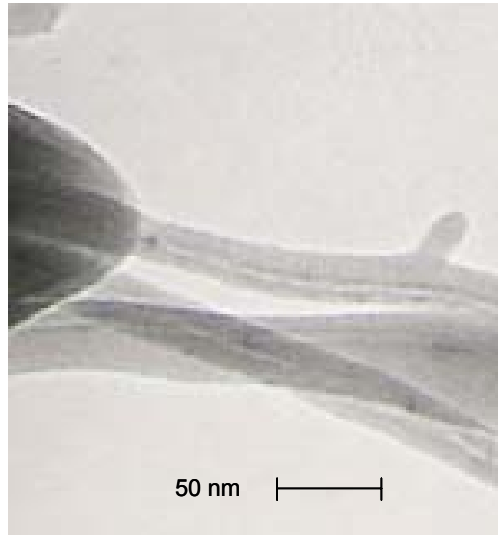


Figure 4.5a: TEM image of 2 wt % MWNT in 4 wt% PEO nanofibers showing dispersion and alignment along the axis of the fiber.

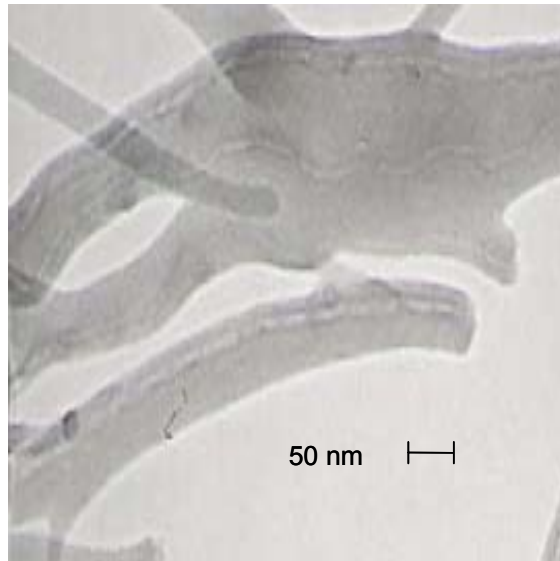


Figure 4.5b: TEM image of 2 wt% MWNT in 4 wt% PEO sample. This image captures four multi-walled carbon nanotubes within several nanofibers bonded together.

For composite systems composed of a conducting filler (MWNT) embedded in an insulating matrix (PEO), classical percolation theory is often invoked.³⁷ In short, the system is described as randomly orientated and positioned conducting rods in an insulating background. As the concentration of the conducting element is increased, conduction occurs when the density of MWNT is sufficient to create a single percolating path across the sample.³⁷ Below this critical concentration, any conductance is due to the polymer matrix and independent of MWNT concentration. As the density of filler further increases above the threshold value, the conductivity dramatically increases as more and more paths contribute to the current. Once current is flowing throughout the full geometrical volume of the sample, further increase in MWNT concentration has little effect and the conductance plateaus with only a slight dependence on nanotube density.³⁷ It is important to note that several of the assumptions implicit in classical percolation theory are not maintained in the

electrospun MWNT/PEO system.³⁸⁻⁴⁰ As shown above, the embedded nanotubes are generally aligned along the fiber axis, rather than being randomly oriented.⁴¹⁻⁴⁵ In addition, because the polymer and nanotubes are innately entangled, it is unlikely that true percolating paths, where all MWNT along the path are in physical contact, are formed and more likely that tunneling or hopping between MWNT plays a role in conduction.^{38, 46, 47} Percolation theory has been extensively and successfully used to describe nanocomposite conductivity and, as shown below, our results also indicate a percolation effect.

In this research the composite is formed of three elements: conducting nanotubes, polymer (non-conducting), and open space or voids. The morphological characteristics of both the fiber and the resulting mat may strongly influence the nature of the percolation process and the ultimate conductance of the material. For instance, significant MWNT alignment is observed in these fibers under SEM imaging, which may alter the critical weight percentage from that of an isotropic distribution.⁴² If such alignment is a function of fiber diameter, changing the fiber size may affect the percolation threshold of the system. When combining the fibers into the technologically important structure of a mat, additional variables such as mat density (the fraction of void space), the number of fiber intersections, and the character of these fiber-fiber contacts come into play. For instance, even if MWNT density is below that needed to carry current along long lengths of fiber, a mat may produce a percolating path consisting of short sections of several different fibers if there is a sufficiently high density of fiber-fiber connections. This would lead to a lower percolation threshold in the mat than for the fiber alone. In contrast, if fiber-fiber intersections are weak (leading to poor contacts between nanotubes) or if the fibers are aligned in the mat and rarely cross, the current may be

carried predominantly along individual fibers. Here the percolation threshold of the mat might be similar to that of the fiber.

Thus rather than generating universal values for the critical doping of MWNT in PEO nanofibers, we expect that our results are specific to the degree of nanotube alignment, the interface between the polymer and nanotube, the fiber size, the morphology of the mat, and the contact between fibers therein. This research represents a specific example of a conducting mat and an attempt to begin understanding the relative importance of these morphological factors.

We point out that an alternative model for this system can be obtained from work on doping polymer blends where the dopant resides primarily in one polymer type and a second material (in our case void space) takes up the remaining volume.⁴⁸⁻⁵¹ In these polymer-blend studies, a so-called double percolation process (reflecting the dependence on both doping density and percentage of volume-excluding polymer) is predicted. As discussed below, in this work, we do not alter the fraction of void space in our mats and observe percolation as a function of doping at this one value.

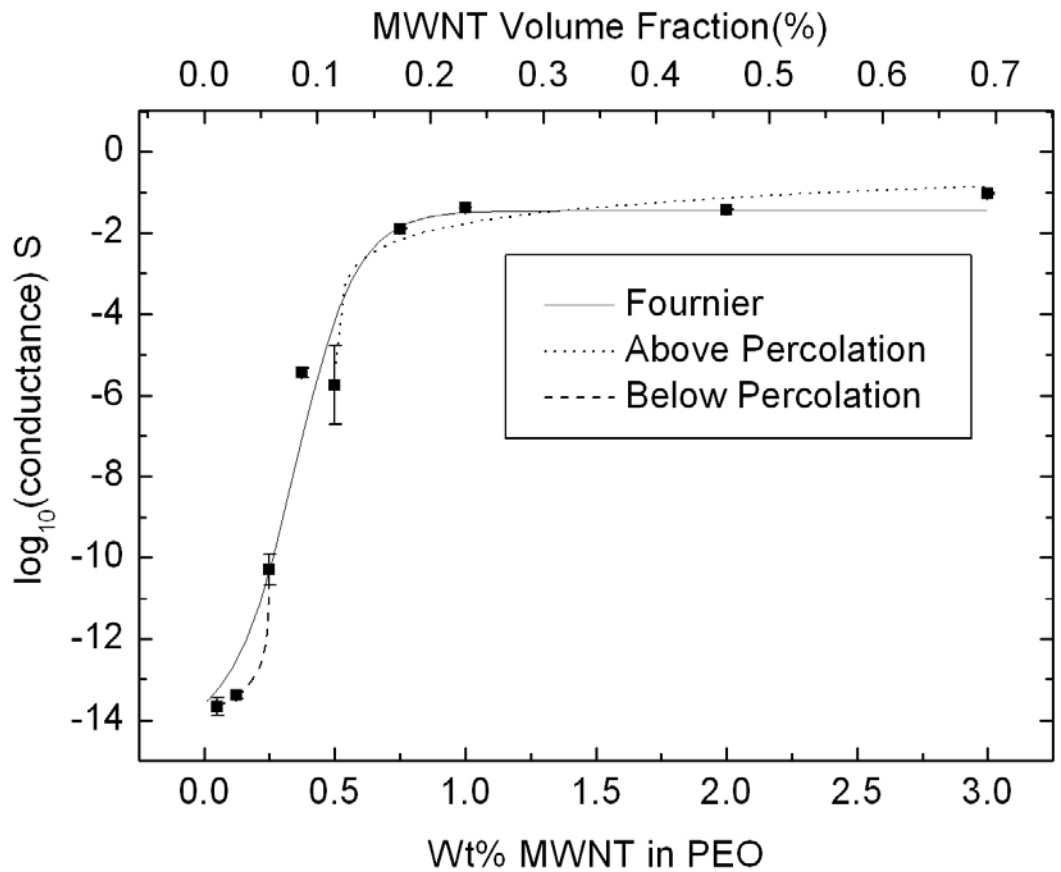


Figure 4.6: Electrical conductance vs. MWNT concentration in 4 wt% PEO or alternatively, versus the measured volume fraction of MWNT. With increasing MWNT concentration, the conductance demonstrates a percolation threshold for the random mats. The three fits are described in the text, with fit parameters presented in Table 1.

Using the techniques previously described, current-voltage characteristics of PEO with varying MWNT concentrations were recorded. A background, the current-voltage characteristic of each bare electrode, was taken before all depositions. All blank electrodes showed similar curves with a measured conductance of 6.3×10^{-15} S, which serves as the

lower limit of our measurement range. With the addition of MWNT to the PEO solution, the conductance versus MWNT concentration curve showed a dramatic increase consistent with a percolating behavior as seen in Figure 4.6. Figure 4.6 shows the conductance data plotted against two axes: the variable controlled in the experiment (the wt% of MWNT in the PEO solution) or alternatively, the experimentally observed volume fraction of MWNT. In the latter approach, the top layer of an SEM image of mats at 0 and 1 wt % MWNT was analyzed to determine the fraction of fiber and void space. Taking an average of four measurements for each image, the void space represented $74.79 \pm 2\%$ and $74.85 \pm 2\%$ for pure PEO and 1 wt% MWNT, respectively. Based upon these measurements, we conclude that the void space is constant over the nanotube doping range used in this work. Because the void and polymer are both insulating, the system is modeled as conducting MWNT embedded in this combined matrix. Based on the known doping, the fraction of MWNT to total volume is calculated. We observed that small variations in sample preparation, including dispersion of the MWNT in solution, can introduce significant changes in the resulting conductance. This can account for the 0.5 wt% sample having a slightly lower conductance than the 0.35 wt%. The placement of these points did not affect our overall results.

Figure 4.6 generates two alternative two-component systems to study. A model that ignores the void space and focuses on the density of MWNT in the PEO, minimizes the effect of the mat morphology and assumes that most conduction is along the fibers. Alternatively, modeling the nanotube density in the entire volume (voids + polymer), assumes the system is similar to randomly doped, homogeneous film of the combined matrix (voids + polymer). Clearly, the true physical situation is between these two extremes.

We characterize the conductance versus MWNT concentration curves with three alternative fits. Here we focus on the experimentally-controlled variable, the MWNT wt%; equivalent volume fraction values can be obtained by scaling according to Figure 6. The data is best represented by the Fournier model: $\log(\sigma) = \log(\sigma_n) + \frac{[\log(\sigma_m) - \log(\sigma_n)]}{(1 + \exp[b(p - p_c)])}$ which fits points above, below and throughout the percolation threshold region.^{52, 53} Here, σ , σ_n and σ_m are the composite, nanotube and polymer conductivity, respectively. MWNT concentration is represented by p , with p_c the critical weight percentage to obtain percolation. The empirical parameter b directs the change in conductance across the threshold. Data above the percolation threshold were also fit with $\sigma = a(p - p_c)^t$ from classical percolation theory. Data below the threshold can be fit with a similar functional form: $\sigma = c(p_c - p)^s$.⁴⁷ In these cases, a , c , s , and t are fit parameters. Because conductance $G \propto \sigma$, with a proportionality constant that depends only on the geometry of the sample, p_c , b , t and s should be unaffected by fitting conductance (rather than conductivity) data.

The fits and parameters can be seen in Figure 4.6 and Table 4.1. While the Fournier form yields the best fit to the data, all three fits give similar percolation thresholds of 0.35 +/- 0.04, 0.50 +/- 0.01, and 0.25 +/- 0.04 wt% MWNT, respectively. These values are higher than the percolation threshold of < 0.05 MWNT wt% observed for a single composite fiber of larger diameter (diameter 200 nm - 6 μ m) from poly-methylmethacrylate.³³ We find an exponent value of 1.32 +/- 0.6 for t , which is slightly lower than the standard values of 1.7 - 2.0 for 3-D systems⁵⁴ and consistent with the expected value (1.3) for 2-D arrays^{55, 56}. Work on other carbon-filled three-dimensional systems, has reported a wide range of t values including

similar low exponents^{47, 54, 57-59} Nevertheless, the observation of an exponent with reduced dimensionality may reflect the influence of the fiber geometry on the percolation⁶⁰; in particular polymer-blend systems where the dopant is constrained to the interface between the polymers have shown similar results.^{57, 61, 62} We find a value of $s = 1.39 \pm 0.7$ which is greater than the expected value of $\sim 0.7-0.9$ in 3-D and consistent with $s = 1.3$ in 2-D.^{47, 61, 63} Finally, recent studies linked composite systems with $t > 2$ to tunneling between conductive elements due to an intermediate insulating layer (poor constant between doping elements).^{54,}
⁶⁴ Our value of t indicates no evidence of this effect.

Table 4.1: Parameters for the three conductance models. * G_m was held at the conductance limit of our system. G_n , G_m , a' and c' are the conductance equivalents of the conductivity quantities given the text.

Fournier		Above Percolation		Below Percolation	
G_n	0.036 ± 0.04 S	a'	0.043 ± 0.02 S	c'	$2.3e-15 \pm 4e-15$ S
G_m	$6.3e-15$ S *	t	1.3 ± 0.6	s	1.4 ± 0.7
B	8.5 ± 1.8	p_c	0.45 ± 0.01	p_c	0.25 ± 0.04
p_c	0.35 ± 0.04				

To determine any changes in mechanical properties due to MWNT concentrations, tensile tests were performed on MWNT loading levels of 0, 1 and 3 wt%. For each sample measured, the thickness was determined by the mean of 10 measurements per sample. Each sample was collected from the plate collector and removed from the aluminum foil. The samples analyzed included a pure 4 wt% PEO sample, 1 wt% MWNT/ 4 wt% PEO, and 3 wt% MWNT/ 4 wt% PEO. The results are shown in Table 4.2. The stress calculation

accounts for the void volume fraction (75%), which was determined to be independent of MWNT concentration (as discussed earlier). With the addition of MWNT, both the 1 and 3 % samples demonstrated a statistically significant reduction in elongation. The 1 wt% MWNT/PEO sample maintained the same tensile stress yet had a statistically significant increase in modulus when compared to the pure PEO sample. However, the 3 wt% MWNT/PEO sample demonstrated a reduction in tensile stress with no change in modulus as compared to the pure PEO sample. This can be attributed to agglomeration of MWNT at the higher concentration, which could act as stress concentrations, leading to premature breaking.

Table 4.2: Modulus and tensile strength as a function of nanotube concentration.

Sample	Modulus (MPa)	Tensile Strength (MPa)
0% MWNT	12.28 ± 1.54	9.96 ± .20
1% MWNT	37.68 ± 2.14	9.40 ± 0.36
3% MWNT	23.56 ± 1.67	5.04 ± 0.25

4.5 Conclusions

This work demonstrates the fabrication, determination of optimal process parameters, and mechanical and electrical characterization of 100-200 nm PEO nanofibers with dispersed, encapsulated MWNT. Rheology measurements confirmed that the nanotubes were well-dispersed and integrated within the polymer solution used for electrospinning and that the viscosity, and thus flow curve of the polymer, was not significantly altered by the addition of low concentration of MWNT. This indicates that the electrospinning parameters are robust in this concentration regime. Randomly oriented, isotropic mats of the nanofibers were generated by utilizing a plate collector. A 4% or greater PEO solution in deionized water

was required for the formation of uniform diameter fibers. Conductance measurements on random mats showed a percolation threshold at ~ 0.35 wt% MWNT, depending on the model used for fitting. Above, about 1 wt%, the conductivity was maximized. Mechanical testing of the random mats showed an optimal Young's modulus also at the value of 1 wt % MWNT, indicating that this loading value is optimal for maximizing both mechanical and electrical properties.

4.6 Acknowledgements

This work was funded by the Nanotechnology Initiative at NC State University. W.A.R. acknowledges an Undergraduate Research Award from NC State. We especially thank Alfred Inman and Dr. Nancy Monteiro-Riviere for their time and assistance with electron microscopy. We also thank Dr. Wendy Krause for use of her rheometer and Rebecca Klossner, and Kelly Stano for their technical assistance.

4.7 References

1. Andrews, R.; Weisenberger, M. C. *Current Opinion in Solid State and Materials Science* **2004**, 8, 31-37.
2. Harris, P. J. F. *International Materials Review* **2004**, 49, (1), 31-43.
3. Hussain, F.; Hojjati, M.; Okamoto, M.; Gorgan, R. E. *Journal of Composite Materials* **2006**, 40, (17), 1511-1575.
4. Moniruzzaman, M.; Winey, K. I. *Macromolecules* **2006**, 39, (16), 5194-5205.
5. Iijima, S. *Science* **1991**, 354, (6348), 56-58.
6. Iijima, S.; Ichihashi, T. *Nature* **1993**, 363, (6430), 603-605.

7. Schadler, L. S.; Giannaris, S. C.; Ajayan, P. M. *Applied Physics Letters* **1998**, *73*, (26), 3842-3844.
8. Haggenueller, R.; Gommans, H. H.; Rinzler, A. G.; Fischer, J. E.; Winey, K. I. *Chem. Phys. Lett.* **2000**, *330*, (3,4), 219-225.
9. Qian, D.; Dickey, E. C.; Andrews, R.; Rantell, T. *Applied Physics Letters* **2000**, *76*, (20), 2868-2870.
10. Lozano, K.; Bonilla-Rios, J.; Barrera, E. V. *Journal of Applied Polymer Science* **2001**, *80*, (8), 1162-1172.
11. Lozano, K.; Barrera, E. V. *Journal of Applied Polymer Science* **2000**, *79*, (1), 125-133.
12. Jin, L.; Bower, C.; Zhou, O. *Applied Physics Letters* **1998**, *73*, (9), 1197-1199.
13. Jia, Z.; Wang, Z.; Xu, C.; Liang, J.; We, B.; Wu, D.; Zhu, S. *Materials Science and Engineering A* **1999**, (271), 395-400.
14. Gong, X.; Liu, J.; Baskaran, S.; Voise, R. D.; Young, J. S. *Chemistry Of Materials* **2000**, *12*, (4), 1049-1052.
15. Jin, Z.; Pramoda, K. P.; Xu, G.; Goh, S. H. *Chem. Phys. Lett.* **2001**, *337*, (1), 43-47.
16. Safadi, B.; Andrews, R.; Grulke, E. A. *Journal of Applied Polymer Science* **2002**, *84*, (14), 2660-2669.
17. Kearns, J. C.; Shambaugh, R. L. *Journal of Applied Polymer Science* **2002**, *86*, (8), 2079-2084.
18. Cooper, C. A.; Ravich, D.; Lips, D.; Mayer, J.; Wagner, H. D. *Composites Science and Technology* **2002**, *62*, (7-8), 1105-1112.

19. Bower, C.; Rosen, R.; Jin, L.; Han, J.; Zhou, O. *Applied Physics Letters* **1999**, *74*, (22), 3317-3319.
20. Pötschke, P.; Fornes, T. D.; Paul, D. R. *Polymer* **2002**, *43*, (11), 3247-3255.
21. Dondero, W. E.; Gorga, R. E. *Journal Of Polymer Science Part B-Polymer Physics* **2006**, *44*, (5), 864-878.
22. Gorga, R. E.; Cohen, R. E. *Journal Of Polymer Science Part B-Polymer Physics* **2004**, *42*, (14), 2690-2702.
23. Ponomarenko, A. T.; Shevchenko, V. G.; Enikolopyan, N. S. *Advances in Polymer Science* **1990**, *96*, 125-145.
24. Hooper, J. B.; Schweizer, K. S. *Macromolecules* **2006**, *39*, (15), 5133-5142.
25. Formhals, A. Process and Apparatus for Preparing Artificial Threads, 1,975,504. 1934.
26. Li, D.; Xia, Y. *Advanced Materials* **2004**, *16*, (14), 1151-1170.
27. Matthews, J. A.; Boland, E. D.; Wnek, G. E.; Simpson, D. G.; Bowlin, G. L. *Journal Of Bioactive And Compatible Polymers* **2003**, *18*, (2), 125-134.
28. Buttafoco, L.; Kolkman, N. G.; Poot, A. A.; Dijkstra, P. J.; Vermes, I.; Feijen, J. *Journal Of Controlled Release* **2005**, *101*, (1-3), 322-324.
29. Dror, Y.; Salalha, W.; Khalfin, R. L.; Cohen, Y.; Yarin, A. L.; Zussman, E. *Langmuir* **2003**, *19*, 7012-7020.
30. Ayutsede, J.; Gandhi, M.; Sukigara, S.; Ye, H. H.; Hsu, C. M.; Gogotsi, Y.; Ko, F. *Biomacromolecules* **2006**, *7*, (1), 208-214.
31. Ko, F.; Gogotsi, Y.; Ali, A.; Naguib, N.; Ye, H. H.; Yang, G. L.; Li, C.; Willis, P. *Advanced Materials* **2003**, *15*, (14), 1161-1164.

32. Mack, J. J.; Viculis, L. M.; Ali, A.; Luoh, R.; Yang, G. L.; Hahn, H. T.; Ko, F. K.; Kaner, R. B. *Advanced Materials* **2005**, 17, (1), 77-80.
33. Sundaray, B.; Subramanian, V.; Natarajan, T. S.; Krishnamurthy, K. *Applied Physics Letters* **2006**, 88, (143114).
34. Ren, Z. F.; Huang, Z. P.; Xu, J. W.; Wang, J. K.; Bush, P.; Siegel, M. P.; Provencio, P. *Science* **1998**, 282, 1105-1107.
35. Van Gerwen, P.; Laureyn, W.; Laureys, W.; Huyberegts, G.; Op De Beeck, M.; Baert, K.; Suls, J.; Sansen, W.; Jacobs, P.; Hermans, L.; Mertens, R. *Sensor Actuators B* **1998**, 49, 73-80.
36. Brydson, J., *Flow Properties of Polymer Melts*. 1st ed.; Van Nostrand Reinhold Company: London, 1970.
37. Stauffer, D.; Aharony, A., *Introduction to Percolation Theory*. 2nd ed.; Taylor & Francis: Washington DC, 1992.
38. Cheah, K.; Simon, G. P.; Forsyth, M. *Polymer Int.* **2001**, 50, 27-36.
39. Mamunya, E. P.; Davidenko, V. V.; Lebedev, E. V. *Polymer Composites* **1995**, 16, 319-324.
40. Rahatekar, S. S.; Hamm, M.; Shaffer, M. S. P.; Elliott, J. A. *J. Chem. Phys.* **2005**, 123, 134702.
41. Balberg, I.; Binenbaum, N.; Wagner, N. *Physical Review Letters* **1984**, 52, 1465-1468.
42. Du, F.; Fischer, J. E.; Winey, K. I. *Phys. Rev. B* **2005**, 72, 121404(R).
43. Grujicic, M.; Cao, G.; Roy, W. N. *Journal of Materials Science* **2004**, 39, (14), 4441-4449.

44. Natsuki, T.; Endo, M.; Takahashi, T. *Physica A* **2005**, 352, 498-508.
45. Ueda, N.; Taya, M. *Journal of Applied Physics* **1986**, 60, 459-461.
46. Hobbie, E. K.; Obrzut, J.; Kharchenko, S. B.; Grulke, E. A. *J. Chem. Phys.* **2006**, 125, 044712.
47. McLachlan, D. S. *Journal of Electroceramics* **2000**, 5, (2), 93-110.
48. Cheah, K.; Forsyth, M.; Simon, G. P. *J. Poly. Sci B: Poly. Phys.* **2000**, 38, 3106-3119.
49. Huang, J.-C. *Advances in Polymer Technology* **2002**, 21, 299-313.
50. Thongruang, W.; Balik, C. M.; Spontak, R. J. *J. Poly. Sci B: Poly. Phys.* **2002**, 40, 1013-1023.
51. Thongruang, W.; Spontak, R. J.; Balik, C. M. *Polymer* **2002**, 43, 3717-3725.
52. Fournier, J.; Boiteux, G.; Seytre, G.; Marichy, G. *Synthetic Metals* **1997**, 84, 839-840.
53. Coleman, J. N.; Curran, S.; Dalton, A. B.; Davey, A. P.; McCarthy, B.; Blau, W.; Barklie, R. C. *Phys. Rev. B* **1998**, 58, (12), R7492-7495.
54. Vionnet-Menot, S.; Grimaldi, C.; Maeder, T.; Strässler, S.; Ryser, P. *Phys. Rev. B* **2005**, 71, 064201.
55. Frank, D. J.; Lobb, C. J., *Phys. Rev. B* **1988**, 37, 302-307.
56. Smith, L. N.; Lobb, C. J. *Phys. Rev. B* **1979**, 20, 3653-3658.
57. Gubbels, F.; Jeromé, R.; Teyssié, P.; Vanlathem, E.; Deltour, R.; Calderone, A.; Parenta, V.; Brédas, J. L. *Macromolecules* **1994**, 27, 1972-1974.
58. Kilbride, B. E.; Coleman, J. N.; Fraysse, J.; Fournet, P.; Cadek, M.; Drury, A.; Hutzler, S.; Roth, S.; Blau, W. J. *Journal of Applied Physics* **2002**, 92, 4024-30.
59. Barrau, S.; Demont, P.; Peigney, A.; Laurent, C.; C., L. *Macromolecules* **2003**, 36, 5187-5194.

60. McLachlan, D. S.; Chiteme, C.; Park, C.; Wise, K. E.; Lowther, S. E.; Lillehei, P. T.; Siochi, E. J.; Harrison, J. S. *J. Poly. Sci B: Poly. Phys.* **2005**, 43, 3273-3287.
61. Calberg, C.; Blacher, S.; Gubbels, F.; Brouers, F.; Deltour, R.; Jérôme, R. *J. Phys. D: Appl. Phys.* **1999**, 32, 1517-1525.
62. Wan, Y.; Fang, Y.; Hu, Z.; Wu, Q. *Macromolecular Rapid Communications* **2006**, 27, 948-954.
63. The small number of points below threshold lend less reliability to the s value compared with our estimate of t .
64. Dalmas, F.; Dendievel, R.; Chazeau, L.; Cavaillé, J.-Y.; Gauthier, C. *Acta Materialia* **2006**, 54, 2923-2931.

Chapter 5

Development of electrospun poly (L-D-lactic acid) fibers containing multi-walled carbon nanotubes for tissue engineering scaffolds and optimization of fiber morphology

A paper submitted for publication to the Journal of Applied Polymer Science

Seth D. McCullen¹, Kelly L. Stano², and Russell E. Gorga³

5.1 Abstract

Electrospinning of poly (L-D-lactic acid) (PLDLA) was investigated with the addition of multi-walled carbon nanotubes (MWNTs) for development of a scaffold for bone tissue engineering. Through this experiment, it was determined that the optimal concentration of PLDLA with weight average molecular weight (M_w) 250,000 g/mol is approximately 20 wt% as indicated by scanning electron microscopy. This concentration produces fibers with no beading or film formation. The preferred solvent system is a combination of chloroform and dimethyl formamide (DMF) to alleviate the volatile action of chloroform. The optimum processing parameters for PLDLA are an electric field of 1 kV/cm which was determined by a surface response plot to minimize fiber diameter based on the applied voltage, working distance, and addition of MWNTs. Fourier Transform Infrared Spectroscopy (FTIR) has indicated that there is a slight residue of DMF on the electrospun samples but chloroform is not present. With the addition of 1 wt% MWNTs, the fiber diameter is drastically reduced by 70% to form fibers with a mean diameter of 700 nm. This is believed to be due to an

¹: Primary researcher and author, Department of Textile Engineering, Chemistry, and Science, NCSU; Joint Department of Biomedical Engineering at NCSU and UNC-CH

²: Undergraduate student who assisted with sample collection, Department of Textile Engineering, Chemistry, and Science, NCSU

³: Author for correspondence, Department of Textile Engineering, Chemistry, and Science, NCSU

increased surface charge density for the MWNT / polymer solution. Transmission electron microscopy (TEM) has validated the alignment of the MWNTs within the fibers. Future reports will focus on characterization and implementation in tissue engineering scenarios.

5.2 Introduction

The objective of this research is the development and characterization of electrospun nanocomposites for tissue engineering scaffolds incorporating carbon nanotubes. Carbon nanotubes have tremendous mechanical and electrical properties and have been reported to enhance the properties of polymeric matrices when they are adequately dispersed and oriented.^{1, 2} This work focuses on optimizing the processing parameters for electrospun nanofibers of poly (L-D-lactic acid) (PLDLA) and the incorporation of a low mass fraction of multi-walled carbon nanotubes (MWNTs) into electrospun scaffolds.

Carbon nanotubes are graphitic sheets rolled into seamless tubes (*i.e.* arrangements of carbon hexagons into tube-like fullerenes) and have diameters ranging from a nanometer to tens of nanometers with lengths up to centimeters. Nanotubes have received much attention due to their interesting properties (high modulus and electrical/thermal conductivity) since their discovery by Iijima in 1991.^{3, 4} Since then, significant effort has gone into fabricating polymer/nanotube composites for improved strength and conductivity.⁵⁻¹⁸

Electrospinning provides a means to construct a three dimensional matrix by creating fibers with diameters on the nano to micro scale. The fibers are created by electrostatic repulsion and the coulombic forces due to an external electric field applied to a polymer solution.^{19, 20}

By applying a critical voltage between the metallic needle of a syringe filled with polymer solution and a grounded collector, a polymer jet is generated which creates fibers that can be collected at the grounded plate.^{19, 21, 22} The end result is a randomly oriented mat of fibers with a high porosity due to the high ratio of surface area to volume. This aspect of electrospinning is advantageous for use as a means of production for scaffolds for tissue engineering, by producing a highly porous material with interconnected pores and tremendous surface area that is similar to the scale of the extra-cellular matrix.²³

Poly (lactic acid) (PLA) is linear aliphatic polyester that is biocompatible and biodegradable, and has three stereoisomeric forms, poly (L-lactic acid) (PLLA), poly (D-lactic acid) (PDLA), and poly (L-D-lactic acid) (PLDLA). PLA is known to be one of the more utilized biomaterials, due to its degradation by hydrolysis and well-characterized mechanical properties, as well as its biocompatibility. Numerous researchers have experimented with the use of electrospun PLA as a tissue scaffold by electrospinning.²⁴⁻³² In order to make PLA soluble, multiple organic solvents have been investigated including methylene chloride, dimethyl formamide, chloroform, and pyridine.^{24, 27, 30-32} It has been noted that drastic morphological changes are based on the concentration of the polymer.^{26, 32} In one study it was not possible to collect continuous fibers at concentration below 20 wt% and above 40 wt% due to the viscosity of the solution. The researchers hypothesized that fibers produced from 20-30 wt% had an apparent wetness when deposited on the collector, enabling a solidification process due to the surface tension and relaxation process by the viscoelastic property of the wet fibers.³² The electrospun nanofibers produced were non-crystalline, but the researchers were able to yield a high orientation by collecting the nanofibers on a rotating

drum.³² Overall the PLA at higher concentrations in solution produced uniform nanofibers at lower electrical fields. Thus, when choosing the specific polymer system it is imperative to understand the role of molecular weight and concentration and how these variables influence the number of entanglements of polymer chains in solution, ultimately dictating the viscosity. This was reported by Tan where the most prolific processing variables for minimizing fiber diameter were the weight average molecular weight (M_w) and concentration, as well as the conductivity of the solvent system.²⁷

The goal of our work is to produce composite nanofibers by the addition of MWNTs. Work by Zang demonstrated that drugs could be loaded into nanofibers by suspending them within the polymer solution.³⁰ With the addition of any particle, anionic, cationic, or nonionic, the diameter size and distribution of the electrospun fibers can be significantly reduced.³⁰ This has been hypothesized by the particle addition maintaining a more uniform charge density within the whipping instability created during electrospinning. A more recent work that incorporated silver particles within the electrospun fibers, noted an increase in overall fiber diameter, and attributed this to a phase separation between the PLA and the embedded silver particles which was hypothesized to be due to a strong interaction between the molecular chains and silver particles.²⁸ The silver particles in this study were spherical with an average diameter of 30 nm, and in order to produce a continuous contact of silver particles within the fibers, loading of 8, 16, and 32 weight % (wt %) with respect to the polymer concentration were necessary. Composite nanofibers containing hydroxyapatite (HAP) and growth factors, have also been investigated.²³ The researchers were able to encapsulate HAP crystals with a diameter of 50 nm inside electrospun silk. This composite fibers demonstrated a positive

impact on cell studies with mesenchymal stem cells by resembling the natural milieu of bone and was able to support mineralized tissue formation.²³

When choosing the filler material for a composite system, the most important parameter besides the apparent physical properties of the material is the geometric shape. For composite systems it is more advantageous to utilize fillers with an aspect ratio (length/diameter) greater than 1.³³ Cylindrical materials such as carbon nanotubes exhibit such characteristics with a large aspect ratio, in the range of thousands, which can reduce the amount of filler needed to obtain large increases in physical properties. Gorga has been able to show that through dispersion and orientation of carbon nanotubes, improved physical properties including Young's Modulus, toughness, and tensile strength can be achieved in polymeric matrices including poly(methyl methacrylate) and polypropylene.^{1, 2} It was determined that the most prolific increases in mechanical properties occurred at MWNTs loading equal to or less than 1 wt%. Therefore, carbon nanotubes are ideal candidates for nanocomposite applications and have demonstrated large increases in physical properties with relatively low mass fractions. By producing scaffolds with MWNTs, increased conductance can also be attained due to the percolation behavior of MWNTs in electrospun fibers as we have previously reported.³⁴

For bone tissue engineering scaffolds, it is essential to good mechanical strength within a three-dimensional porous structure. This combination allows for the physical integrity of the scaffold to be maintained while allowing the needed space for tissue growth into the scaffold, and provides an interconnected pore structure for the diffusion of nutrients and removal of

wastes.³⁵ Through the incorporation of low mass fractions of carbon nanotubes into electrospun fibers, we will be able to develop a composite material with improved modulus and electrical conductivity. By incorporating carbon nanotubes into the polymeric matrix, the scaffolds could have improved physical properties by taking advantage of the properties of the carbon nanotubes within a biocompatible matrix provided by PLDLA. This work will show the optimum process parameters for electrospinning MWNT/PLDLA nanofibers and highlights the effect MWNTs have on the fiber morphology.

5.3 Materials and Methods

5.31. Fabrication

The electrospinning apparatus includes a programmable syringe pump obtained from New Era Pump Systems Model NE 500. The high voltage power supply was obtained from Glassman High Voltage Model # FC60R2 with a positive polarity. The pump operated at a flow rate of 0.5-2 mL/min. The operating voltage was from 10-20 kV with an electric field of .5-2 kV/cm. The solutions were loaded into 10 mL syringes with luer-lock connections and used in conjunction with a 4 inch 20 gauge blunt tip needle. The design of the electrospinning set-up was based on a point-plate configuration.

5.32 Materials

Poly(L-D-lactic acid) was obtained from Sigma-Aldrich with a weight average molecular weight (M_w) of 250,000 g/mol and a number average molecular number (M_n) of 100,000 g/mol. PLDLA was solubilized in Chloroform and dimethyl formamide (DMF) (Sigma-Aldrich) at a ratio of 1:0 and 3:1 respectively. Multi-walled carbon nanotubes were supplied

by Nano-Lab. The MWNTs were produced by plasma enhanced chemical vapor deposition using acetylene and ammonia with an iron catalyst and grown on a mesoporous silica substrate.³⁶ The MWNTs used had a diameter of 15 +/- 5 nm and length of 5- 20 μm at 95% purity. Multi-walled carbon nanotubes were sonicated using an Ultrasonic Model 2000U generator and needle probe, operating at 25 Hz in DMF at a concentration of 0.1 mg/ 1 ml to produce a stock solution for MWNTs incorporation into the solubilized PLDLA. The MWNTs were sonicated for approximately 4 hours to produce a homogeneous suspension within the DMF. A 0 wt% MWNTs / 5, 10, and 20 wt% PLDLA and a 1 wt% MWNTs / 20 wt% PLDLA solution were produced and electrospun.

5.33 Characterization

5.33.1 Scanning Electron Microscopy

For scanning electron microscopy (SEM) a JEOL JSM-6400 FE w/ EDS, operating at 5 kV, was used to determine fiber morphology of the electrospun samples. The electrospun samples were coated with Au/Pd approximately 100 Å thick to reduce charging and produce a conductive surface. Digital images were captured at 500X, 5000X, and 10000X and analyzed using Scion ImageTM software for fiber diameter measurements.

5.33.2 Transmission Electron Microscopy

Transmission electron microscopy (TEM) was performed on a JEOL 100S operating at 80 kV, with samples spun directly on a Cu 400 mesh grid coated with holey thin carbon film. Micrographs were developed, digitally scanned, and were not further modified.

5.33.3 Fourier Transform Infrared Spectroscopy

To determine the presence of the organic solvents a Nicolet Nexus 470 Fourier Transform InfraRed Spectrophotometer (FTIR) was used. Accessories include a single bounce attenuated reflectance device (OMNI Sampler™ with Ge crystal) for identification of contaminants and small particles/fibers. Transmission and reflectance measurements were performed for qualitative analyses of unknowns. Spectral searches to identify the unknown compound can be performed using commercially available libraries from Sigma.

5.33.4 Statistical Analysis

For statistical analysis, the SAS (Cary, NC) software package JMP version 6.0 was used for data interpretation and graphic image design. Response surface methodology (RSM) was used for modeling and analysis for the variables of the electrospinning process investigated in this work. Surface response diagrams allow the outline of specific parameters of the operating system and display the optimum set of parameters for the response. Thus the process yield is a function of the levels of interest where $y = f(x_1 + x_2) + \varepsilon$, where y is the process yield, x_1 and x_2 are the factors at the level of interest, ε is the error observed in the response. By denoting $E(y) = f(x_1 + x_2) = \eta$, then this surface represented by $\eta = f(x_1 + x_2)$.³⁷ Generally the second-order model is used for RSM where $y = \beta_0 + \sum \beta_i x_i + \sum \beta_{ii} x_i^2 + \sum \sum \beta_{ij} x_i x_j + \varepsilon$ when $i = 1$ to k and $i < j$, where β are the coefficients, x_i are the variables of interest, k is the level of factors, and ε is the observed error in the response, y .³⁷ The parameters and values for each parameter are shown in Table 5.1.

Table 5.1: Design of Experiment for electrospinning of PLDLA with MWNTs.

Flow Rate (mL/min)	0.5	1	2
Working Distance (cm)	10	15	20
Applied Voltage (kV)	10	15	20
Solvent System	Chloroform	Chloroform:DMF (3:1)	
MWNTs (wt%)	0	1	

5.4 Results and Discussion

5.4.1 Effect of Polymer Concentration

Electrospinning proves to be a very complex process dependent on numerous variables. The initial investigation was pertinent to determine the appropriate polymer concentration in order to obtain highly uniform electrospun fibers before the addition of MWNTs. PLDLA weight percentages of 5, 10, and 20 were investigated with favorable results for the higher concentrations of PLDLA in chloroform. Figure 5.1 shows the PLDLA morphology as a function of concentration.

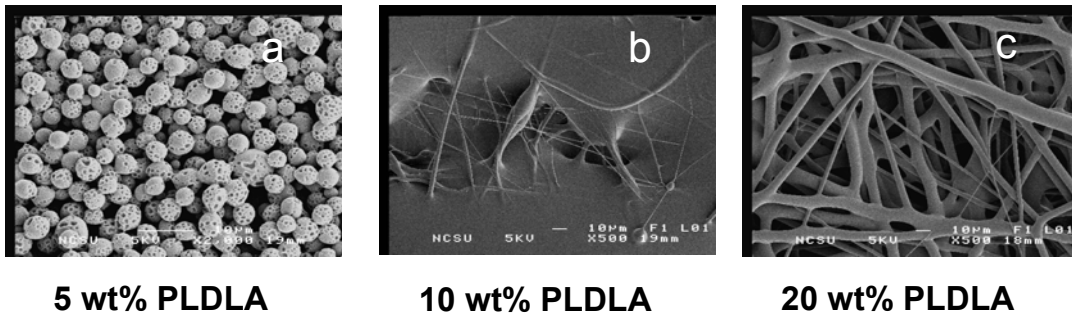


Figure 5.1(a-c): SEM Images of electrospun PLDLA at varying concentrations.

At 5 wt% PLDLA porous beads were produced, because the concentration of the polymer was too low to allow chain entanglements to occur. At 10 wt% PLDLA, inconsistent fibers were produced, which was followed up by the electrospinning of 20 wt% PLDLA. This concentration produced homogeneous nanofibers with a distribution of fiber diameters. Shenoy was able to determine the role of chain entanglements on fiber formation for electrospinning by characterizing the number of entanglements per chain (n_e).²⁶ For a polymer solution, $(n_e)_{\text{soln}} = M_w / (M_e)_{\text{soln}} = (\phi_p * M_w) / (M_e)_{\text{soln}}$, where M_w is the molecular weight of the polymer, M_e is the entanglement molecular weight, and ϕ_p is the volume fraction or concentration of polymer, is greater than or equal to 3.5 for complete stable fiber formation.²⁶ The M_e of PLA has been reported to be 8,000 g/mol, and represents the average molecular weight between chain entanglements.³⁸ Shenoy was able to compile estimations and experimental observations for entanglements concentration of the polymer in solution for PDLA and PLLA (M_w of 109,000 g/mol and 670,000 g/mol, respectively). For the PDLA, the estimated concentration for fiber formation without beading is 32 wt%. This estimation was valid by fiber formation for PDLA being in the range of 30-35 wt%. The PLLA entanglement concentration estimation ranged from 3.4 – 4 and was validated experimentally. In this study, the PLDLA has a M_w of 250,000 g/mol and as seen in Figure 1, we were able to produce fibers at 20 wt%. For our system, the minimum PLDLA concentration needed to spin continuous fibers is 11.2 wt % ($n_e=3.5$). When calculating n_e as seen in Table 5.2, n_e is 1.56 for a weight fraction of 5% which agrees with Shenoy's model for bead formation and with our morphology as shown in Figure 5.1a. When the weight fraction was raised to 10%, we obtained an n_e of 2.82 and were unable to produce uniform fully developed fibers as seen in Figure 5.1b as the theory predicts.

Table 5.2: Estimated chain entanglements per chain based on weight average molecular weight, entanglement molecular weight, and polymer concentration.

Molecular Weight (g/mol)	Entanglement Molecular Weight (g/mol)	Weight %	Volume Fraction (ϕ_p)	Estimated Chain Entanglements / Chain (n_e)
250,000	8000	5%	5%	1.56
250,000	8000	10%	9%	2.81
250,000	8000	20%	17%	5.2

To overcome this, we increased the weight fraction of polymer to 20% where n_e is 5.0, and were able to produce uniform fibers with no beading. Though this entanglement concentration seems high and produced micron sized fibers, we believe that we can minimize the fiber diameter and maximize the surface area for the electrospun scaffolds by optimizing the processing parameters including flow rate (mL/min), applied voltage (kV), and working distance (cm).

5.42 Effect of Flow Rate

After determining the concentration of polymer at 20 wt%, the flow rate or metering of the polymer solution was evaluated. It was observed that at flow rates below 1 mL/min the solvent system would evaporate quickly and tend to clog the syringe needle. Flow rates above 1 mL/min led to an unstable jet because the Taylor cone did not form properly due to the volume of polymer solution being too large and the viscosity being too low. Thus it was determined that the optimum flow rate for PLDLA was 1 mL/min to generate a continuous stream with minimal clogging.

5.43 Effects of Voltage

In this section, a concentration of 20 wt%, flow rate of 1 mL/min and voltages of 10, 15 and 20 kV were investigated in order to find the optimum electric-field concentration for use in electrospinning. We were unable to generate continuous fibers below 10 kV. Figure 5.2 shows the morphological changes as a function of the applied voltage. At 10 kV, fibers with a mean diameter of $1.98 \pm 1.10 \mu\text{m}$ were produced but with beads and films apparent. At 15 kV, fibers with a mean diameter of $2.11 \pm 2.17 \mu\text{m}$ were consistently formed, with a reduction in films and beads. At 20 kV, it was determined that a higher average density of fibers over the sample area was produced through SEM analysis. Past work by Zong examined the effects of voltages above 20 kV and determined that with increasing intervals of 5 kV, beaded fibers are produced as a result of the Taylor cone being unstable which can result in non-uniform fibers³². Thus 15 and 20 kV served as the optimum voltage range for further testing when analyzing the effect of the working distance.

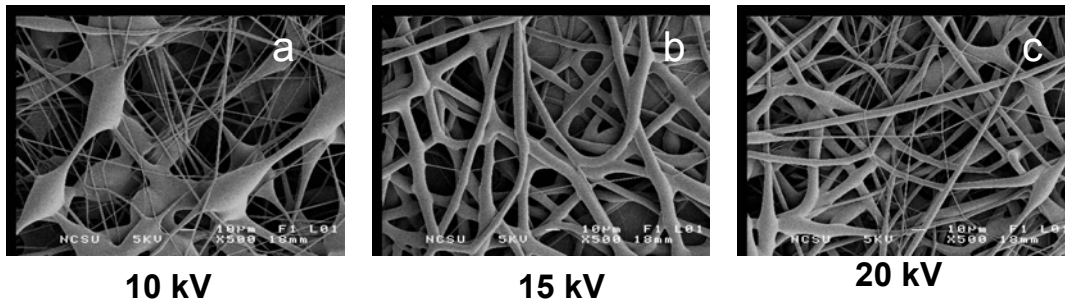


Figure 5.2(a-c): SEM images of electrospun 20 wt% PLDLA at varying voltages.

5.44 Effect of Working Distance

After determining an optimum spinning voltage, the distance from the syringe tip to the collector plate was investigated at measurements of 10, 15, and 20 cm maintaining a polymer concentration of 20 wt% and flow rate of 1 mL/min. Distances below 10 cm yielded no nanofibers and only thick films, while distances of 20 cm proved to be inefficient in collecting the charged jets of fibers. As the working distance increased from 10 to 15 cm smaller fibers were produced by extending the whipping distance of the polymer jet. Hence, it was determined that 15 cm provided the optimal spacing for the electrospinning of PLDLA to achieve the smallest fiber diameter and to maximize the surface area of the scaffold.

5.45 Effect of Solvent System

Until this point, chloroform was the solvent used. In preparation for the addition of MWNTs, the effects of two different solvent systems were investigated. Using the aforementioned processing parameters, the pure PLDLA and chloroform solution created fibers with a mean diameter of $2.51 \pm 2.13 \mu\text{m}$ for all processing conditions. With the addition of DMF, the fiber diameter was reduced dramatically as can be viewed in Figure 5.3.

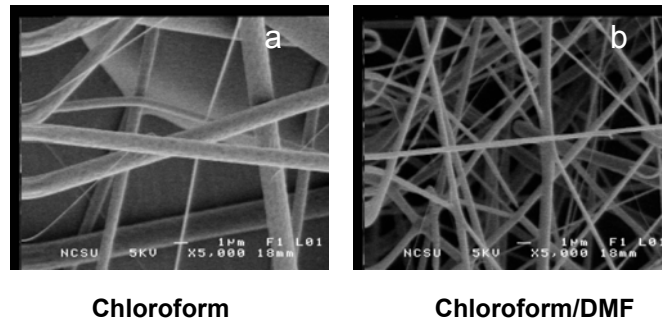


Figure 5.3(a-b): SEM images of electrospun 20 wt% PLDLA with different solvent systems.

This is attributed to the addition of another solvent, where the volatile properties of chloroform at room temperature are abated. By adding DMF to chloroform, the syringe needle experienced less clogging and was able to maintain a more stable jet without intervention. With the Chloroform/DMF solvent system at a ratio of 3:1, fibers with smaller diameters were produced by DMF enabling stable jets from the needle to the collector. We confirm that it is needed in the spinning solution which agrees with previous studies³².

5.46 Effect of MWNT Addition

Based on a previous study for mechanical and electrical properties of electrospun mats, 1 wt% MWNTs appears to be an optimal concentration.³⁴ Therefore we will focus on the morphology of 1 wt% MWNT/PLDLA fibers. By incorporating the MWNTs into the polymer solution, the solution behaved somewhat differently when compared to the PLDLA polymer solution for the same processing parameters. The MWNT/PLDLA solution appeared to produce fibers much more rapidly as seen by visual inspection. This can be attributed to the conductivity of the MWNTs, which can increase the conductivity of the

solution, or maintain a more uniform charge density on the fiber surface as hypothesized by Zang.³⁰ It can be postulated that there is a significant interaction between the MWNTs and the PLDLA during electrospinning as the Taylor cone forms. The addition of MWNTs is not only able to increase the conductance of the spinning solution, but also allow the fibers to crystallize around them when collected, as hypothesized by Zang.³⁰ In Figure 5.4, the SEM images of electrospun PLDLA show the dramatic decrease in fiber diameter with the addition of MWNTs.

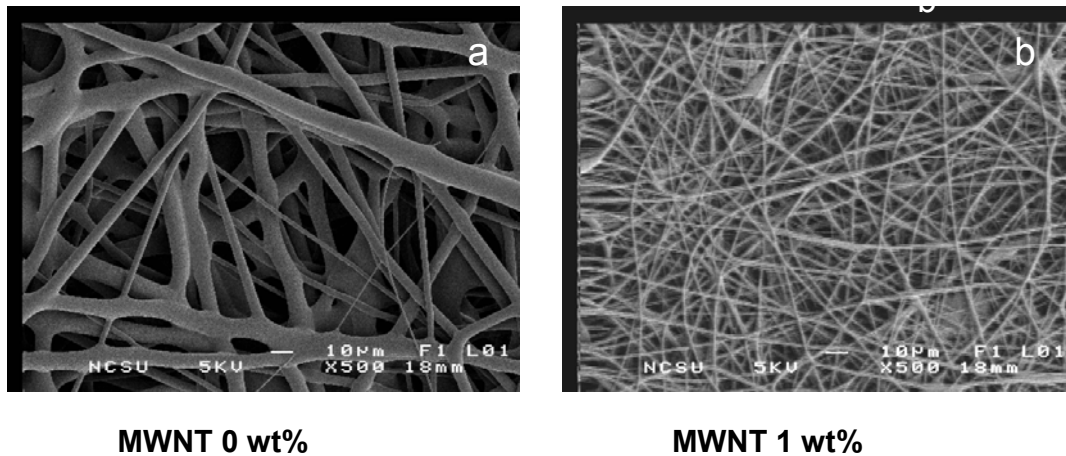


Figure 5.4(a-b): SEM images of a) electrospun 20 wt% PLDLA and b) 1wt% MWNT/ 20% PLDLA.

For each SEM image, fiber diameters were calculated using the Scion ImageTM software. Approximately 20 measurements were taken per image. In Table 5.3, the processing variables and resulting fiber diameters are compiled.

Table 5.3: Electrospinning parameters and fiber diameters for PLDLA and MWNT/PLDLA nanofibers. All solutions were in the solvent system of Chloroform and DMF at a ratio of 3:1 respectively and at a flow rate of 1 mL/min.

MWNT (wt%)	Working Distance (cm)	Applied Voltage (kV)	Mean Fiber Diameter (μm)	Standard Deviation (μm)	Standard Err Mean (μm)
0	10	10	1.98	1.1	0.2
0	10	15	2.77	2.28	0.19
0	10	20	2.96	2.2	0.21
0	15	15	0.55	0.38	0.05
0	15	20	0.79	0.42	0.09
1	10	15	0.79	0.34	0.08
1	10	20	0.96	0.29	0.06
1	15	15	0.56	0.29	0.05
1	15	20	0.55	0.23	0.05
1	20	15	0.65	0.42	0.09
1	20	20	0.86	0.52	0.12

When analyzing the SEM images of the MWNTs/PLDLA fibers, the fibers appear to form a more densely interconnected network and produce significantly smaller fibers by a reduction of approximately 70%. Histogram charts were developed using the data obtained from Scion ImageTM software, and inputted directly into the JMP 6.0 software for statistical analysis. Figures 5.5 and 5.6 confirm the fiber diameter distributions where 67.9% of the PLDLA fibers are greater than 1 μm in diameter (Figure 5.5), where 82.9% of the MWNTs/PLDLA fibers are less than 1 μm in diameter (Figure 5.6). Both data sets have skewed data and do not fit a normal distribution.

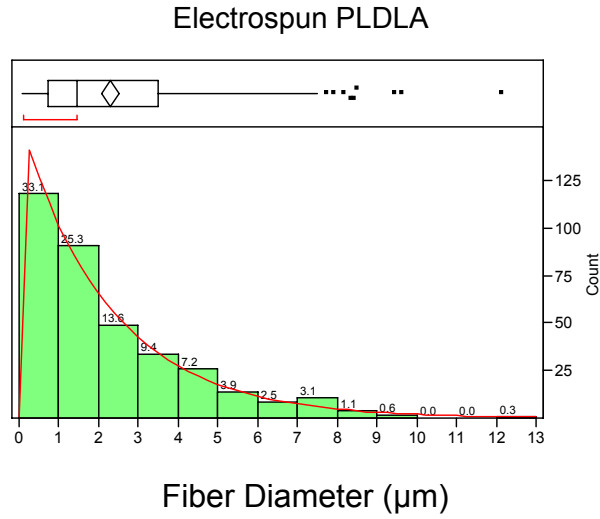


Figure 5.5: Distribution of fiber diameters for electrospun PLDLA.

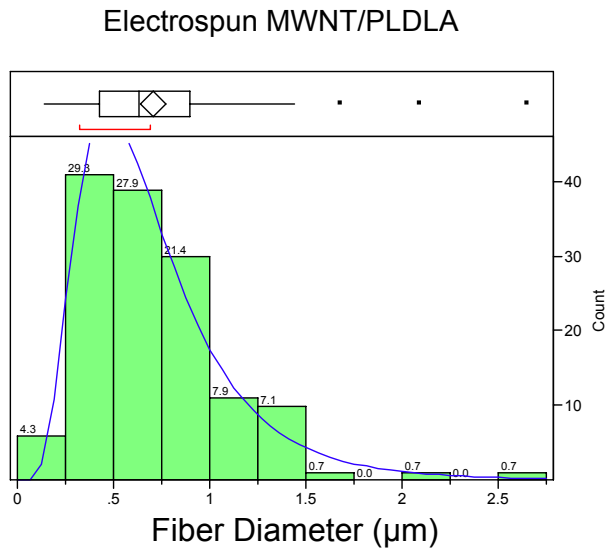


Figure 5.6: Distribution of fiber diameters for electrospun MWNT/PLDLA.

When analyzing the electrospun PLDLA fiber histogram, it should be noted that the data can be fitted with an exponential distribution, retaining a p-value of 0.0743 which meets H_0 or the null hypothesis that the data set qualifies as an exponential fit. The electrospun

MWNT/PLDLA fiber diameter histogram can be fitted with a log normal distribution, retaining a p-value of 0.15 which also meets the H_0 or the null hypothesis that the data set qualifies as a log normal distribution. With the addition of the MWNTs we are able to increase the charge density and produce a more uniform fiber distribution. In order to qualify that there is a statistical difference between the two data sets, a Wilcoxon / Kruskal-Wallis Test was performed because the data are nonparametric. Because the data is nonparametric and distributed differently, the test analyzes the median values of each set, not the mean. This measure of analysis returned a p-value of 0.0001 which designates the data is statistically different and that the addition of MWNTs is able to produce fibers consistently smaller than pure PLDLA. The bivariate plot is shown in Figure 5.7. In Figure 5.7, the line is representative of the statistical difference between the 0 and 1 wt% MWNTs. The medians are represented inside the whiskers of the data plot.

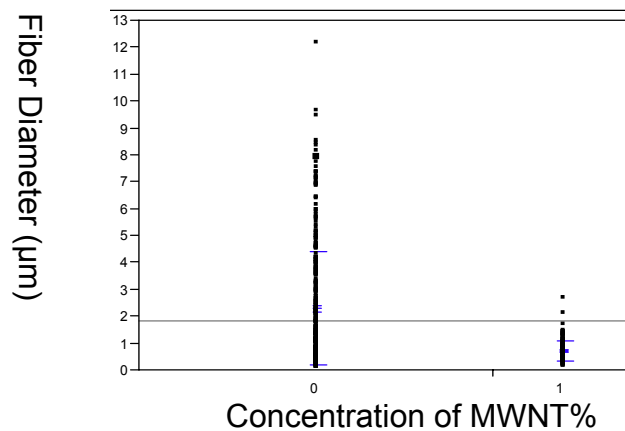


Figure 5.7: Bivariate plot of electrospun PLDLA fiber diameter by MWNT concentration.

High-resolution TEM images were taken to determine the orientation of the MWNTs within the electrospun fibers. The fibers for PLDLA and MWNT/PLDLA were deposited on individual TEM grids during the electrospinning process. The MWNTs were oriented along the axis of the fibers, and are shown in Figure 8. When viewing Figure 5.8, we can see that the MWNT is completely dispersed and aligned within the fiber and that no agglomeration is taking place.

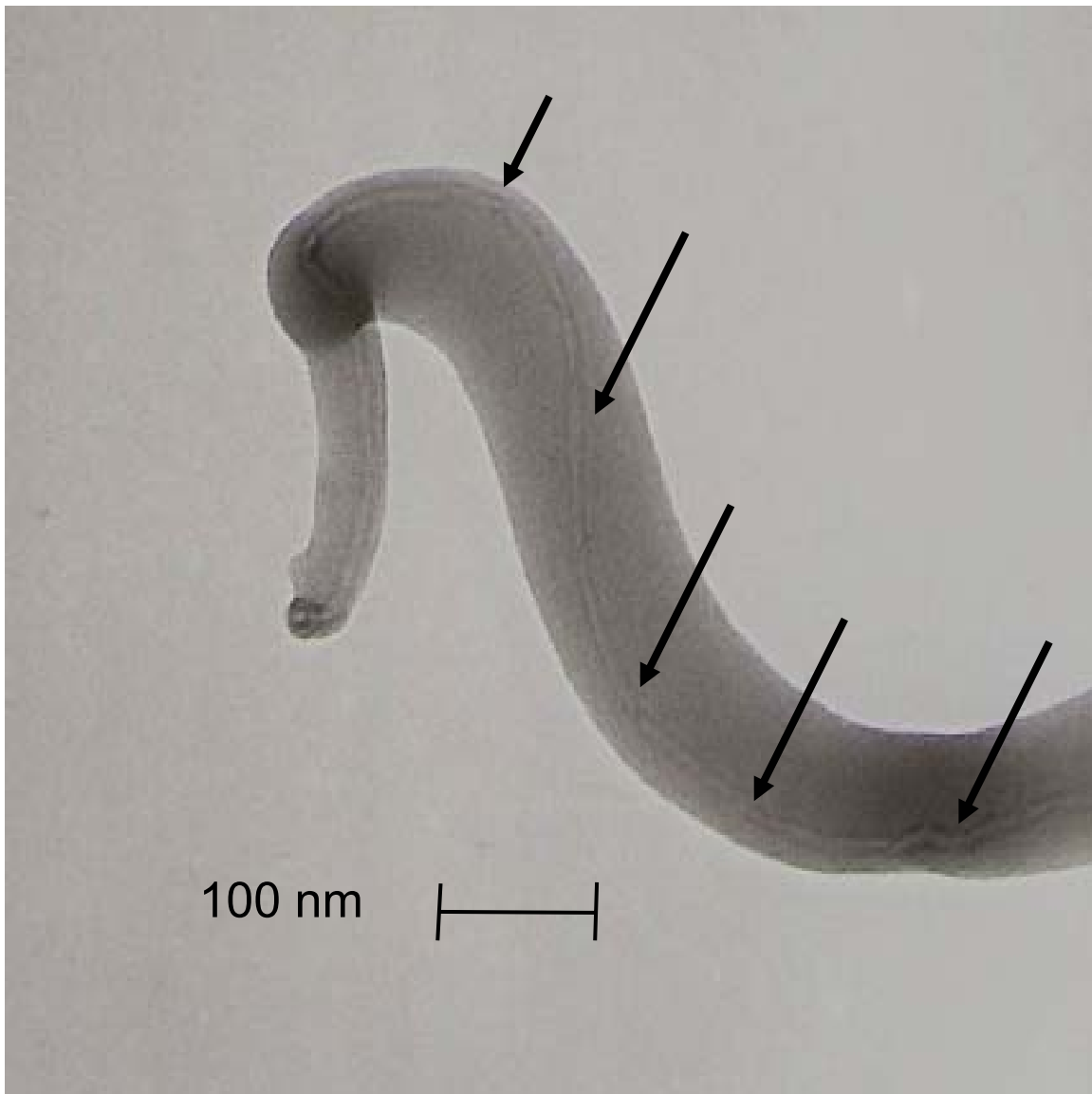


Figure 5.8: TEM image of electrospun MWNT/PLDLA. The arrows indicate the MWNT.

Response surface methodology (RSM) is a useful technique for examine the response of interest for a specific system. By analyzing the effects of the electric field, E (kV/cm) and presence of MWNTS, a surface response diagram and contour plot can be produced. This type of analysis provides a means to take into account the combined effects of multiple variables and determine a response. Surface response diagrams allow the user to outline specific parameters of the operating system and display the optimum set of parameters for the response. The surface response diagram or contour plot of the predicted fiber diameter can be developed based on the data set obtained and will provide contour curves to illustrate where significant changes take place in the production of electrospun PLDLA fibers. In Figure 5.9, for pure PLDLA, applied voltage and working distance are plotted to illustrate their apparent effect on fiber diameter.

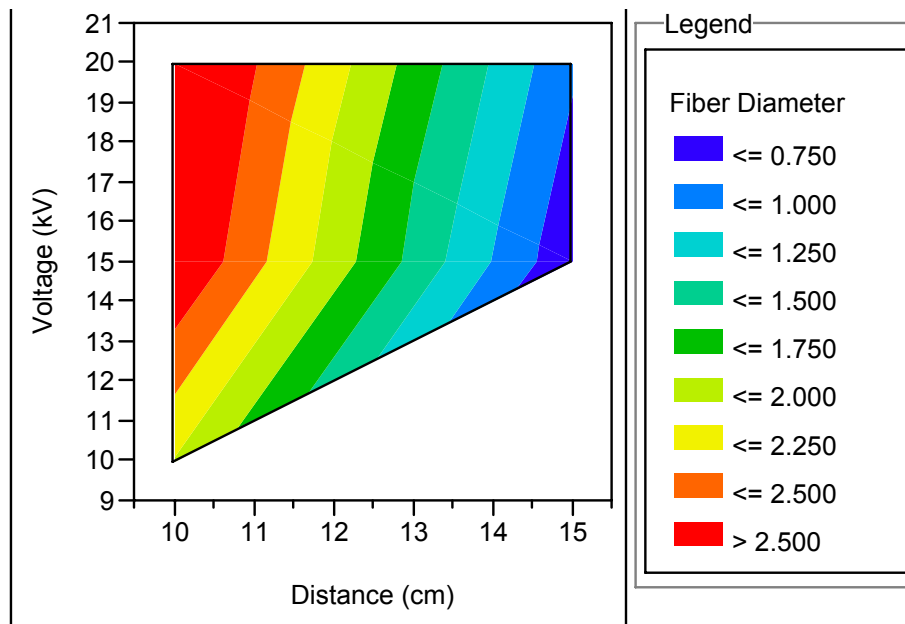


Figure 5.9: Contour Plot for Electrospun PLDLA fiber diameters.

Fiber diameter is strongly affected by both the applied voltage and working distance, decreasing when both of the variables are increased. In MWNT/PLDLA nanofibers it can be seen that with a minimum working distance of 13 cm and an applied voltage equal to or greater than 15 kV, fibers can be produced with diameters equal to or less than 700 nm (as shown in Figure 5.10). Therefore, this contour plot indicates a wide processing range for the production of sub-micron fibers.

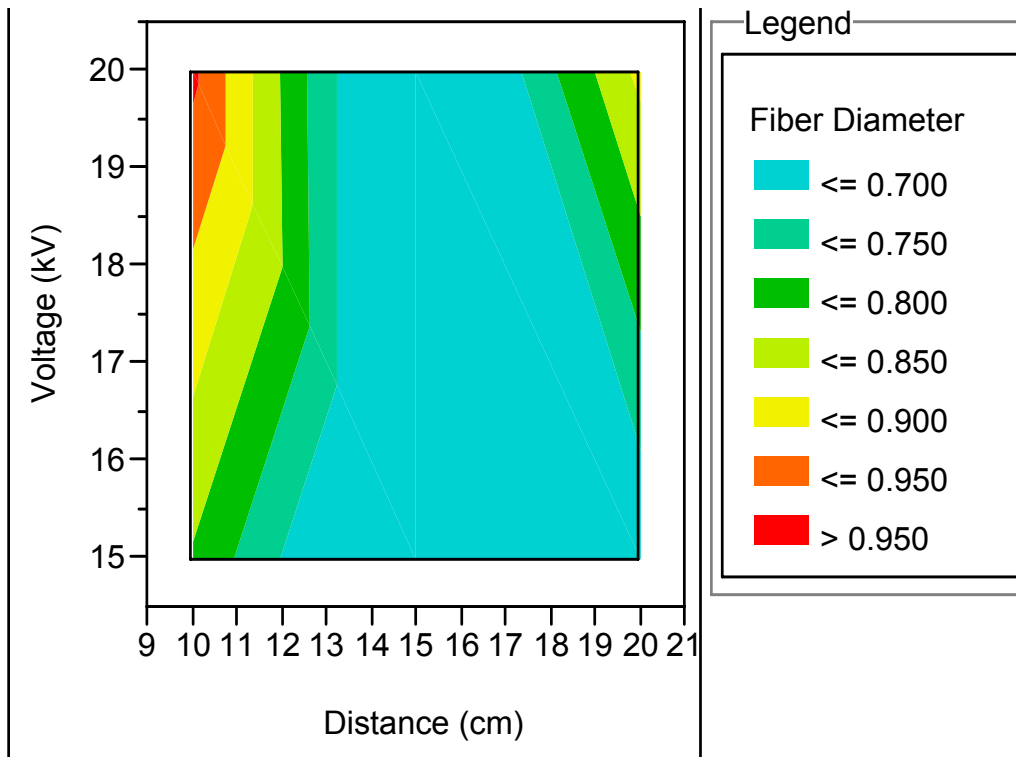


Figure 5.10: Contour plot for Electrospun MWNT/PLDLA fiber diameters.

5.47 Fourier Transform Infrared Spectroscopy

FTIR was employed to determine if there were any residual solvents within the electrospun samples. The samples were not further processed after electrospinning.

Figure 5.11 shows an FTIR spectrum for a control sample of as-received PLDLA (represented by the blue absorbance plot).

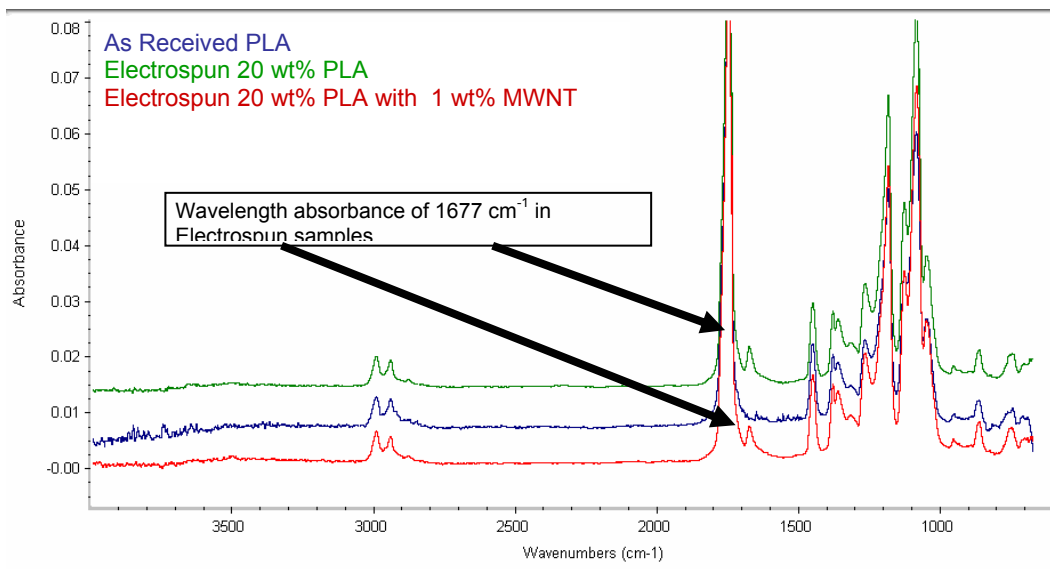


Figure 5.11: Absorbance spectrum for PLDLA from FTIR.

The electrospun PLDLA with and without MWNTs are indicated by the green and red absorbance plots, respectively. The electrospun samples have the same absorbance as the control PLDLA with the addition of a small perturbation at 1677 cm^{-1} indicated by the arrows. When comparing the electrospun samples to the absorbance spectrums of the solvents chloroform and N-N-DMF, it is apparent that there is no residue of chloroform retained in the sample as seen in Figure 5.11. However, there appears to be a residue of N-N-DMF which is indicated by the 1677 cm^{-1} and can be seen in Figure 5.12.

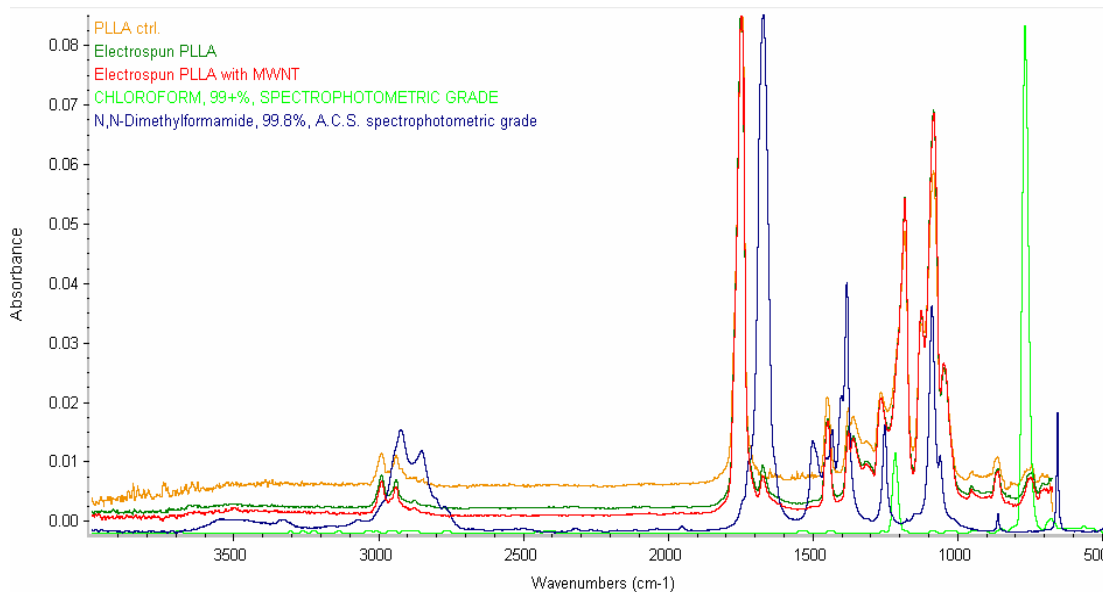


Figure 5.12: Absorbance spectrum for PLDLA and the individual solvents (chloroform and DMF) from FTIR.

For this absorbance, it could be either indicative of a carbonyl group or a primary amine. The molecular structure of DMF is an amide compound. Thus, the absorbance at the wavelength is due to a slight presence of the DMF left in the electrospun samples. This could pose a biocompatibility issue if this material is to be used as a tissue scaffold. Conversely, DMF is a solvent that is miscible in water and ethanol and could conceivably be removed by washing prior to use in cell culture applications.

5.5 Conclusions

From this investigation it has been determined that the optimal concentration of PLDLA with M_w 250,000 g/mol is approximately 20 wt% producing a chain entanglement value (n_e) of 5.20 for proper fiber formation. This concentration produces fibers with no beading or film formation. Also, the optimum processing parameters for this concentration are an applied

voltage of 15 kV and a working distance of 15 cm. The preferred solvent system is a combination of chloroform and DMF to reduce the volatile action of chloroform. FTIR has indicated that there is a residual of DMF on the electrospun samples but chloroform is not present. With the addition of 1 wt% MWNTS, the fiber diameter is drastically reduced by 70% to form fibers with a mean diameter of 700 nm in the processing range between 13-18 cm and a voltage of 15-20 kV. TEM has validated the alignment of the MWNTS within the fibers which has been hypothesized to the fabrication of fibers on the nano-scale.

5.6 Acknowledgements

This work was supported by the Nanotechnology Initiative Grant at North Carolina State University. We thank Birgitt Anderson, Alfred Inman, Nancy Monteiro-Riviere, and Dale Batchelor for their assistance.

5.7 References

1. Dondero, W. E.; Gorga, R. E. *Journal Of Polymer Science Part B-Polymer Physics* **2006**, 44, (5), 864-878.
2. Gorga, R. E.; Cohen, R. E. *Journal Of Polymer Science Part B-Polymer Physics* **2004**, 42, (14), 2690-2702.
3. Iijima, S. *Nature (London, United Kingdom)* **1991**, 354, (6348), 56-8.
4. Iijima, S.; Ichihashi, T. *Nature (London, United Kingdom)* **1993**, 363, (6430), 603-5.
5. Schadler, L. S.; Giannaris, S. C.; Ajayan, P. M. *Applied Physics Letters* **1998**, 73, (26), 3842-3844.
6. Haggenueller, R.; Gommans, H. H.; Rinzler, A. G.; Fischer, J. E.; Winey, K. I. *Chemical Physics Letters* **2000**, 330, (3,4), 219-225.

7. Qian, D.; Dickey, E. C.; Andrews, R.; Rantell, T. *Applied Physics Letters* **2000**, 76, (20), 2868-2870.
8. Lozano, K.; Bonilla-Rios, J.; Barrera, E. V. *Journal of Applied Polymer Science* **2001**, 80, (8), 1162-1172.
9. Lozano, K.; Barrera, E. V. *Journal of Applied Polymer Science* **2000**, 79, (1), 125-133.
10. Jin, L.; Bower, C.; Zhou, O. *Applied Physics Letters* **1998**, 73, (9), 1197-9.
11. Jia, Z.; Wang, Z.; Xu, C.; Liang, J.; We, B.; Wu, D.; Zhu, S. *Materials Science and Engineering A* **1999**, A271, 395-400.
12. Gong, X.; Liu, J.; Baskaran, S.; Voise, R. D.; Young, J. S. *Chemistry of Materials* **2000**, 12, (4), 1049-1052.
13. Jin, Z.; Pramoda, K. P.; Xu, G.; Goh, S. H. *Chemical Physics Letters* **2001**, 337, (1,2,3), 43-47.
14. Safadi, B.; Andrews, R.; Grulke, E. A. *Journal of Applied Polymer Science* **2002**, 84, (14), 2660-2669.
15. Kearns, J. C.; Shambaugh, R. L. *Journal of Applied Polymer Science* **2002**, 86, (8), 2079-2084.
16. Cooper, C. A.; Ravich, D.; Lips, D.; Mayer, J.; Wagner, H. D. *Composites Science and Technology* **2002**, 62, (7-8), 1105-1112.
17. Bower, C.; Rosen, R.; Jin, L.; Han, J.; Zhou, O. *Applied Physics Letters* **1999**, 74, (22), 3317-3319.
18. Potschke, P.; Fornes, T. D.; Paul, D. R. *Polymer* **2002**, 43, (11), 3247-3255.
19. Formhals, A. Process and Apparatus for Preparing Artificial Threads, 1,975,504. (1934).
20. Li, D.; Xia, Y. *Advanced Materials* **2004**, 16, (14), 1151-1170.
21. Matthews, J. A.; Boland, E. D.; Wnek, G. E.; Simpson, D. G.; Bowlin, G. L. *Journal Of Bioactive And Compatible Polymers* **2003**, 18, (2), 125-134.

22. Buttafoco, L.; Kolkman, N. G.; Poot, A. A.; Dijkstra, P. J.; Vermes, I.; Feijen, J. *Journal Of Controlled Release* **2005**, 101, (1-3), 322-324.
23. Li, C.; Vepari, C.; Jin, H.-J.; Kim, H. J.; Kaplan, D. *Biomaterials* **2006**, 27, 3115-3124.
24. Inai, R.; Kotaki, M.; Ramakrishna, S. *Nanotechnology* **2005**, 16, 208-213.
25. Pham, Q. P.; Sharma, U.; Mikos, A. G. *Tissue Engineering* **2006**, 12, (5), 1197-1211.
26. Shenoy, S. L.; Bates, W. D.; Frisch, H. L.; Wnek, G. E. *Polymer* **2005**, 46, (10), 3372-3384.
27. Tan, S.-H.; Inai, R.; Kotak, i. M.; Ramakrishna, S. *Polymer* **2005**, 6128-6134.
28. Xu Xiaoyi; Yang Qingbiao; Wang Yongzhi; Yu Haijun; Chen Xuesi; Xiabin, J. *European Polymer Journal* **2006**, In Press.
29. Yoshimoto, H.; Shin, Y. M.; Terai, H.; Vacanti, J. P. *Biomaterials* **2003**, 24, (2077-2082).
30. Zang, J.; Xu, X.; Chen, X.; Liang, Q.; Jing, X.; Yang, L.; Bian, X. *Journal of Controlled Release* **2003**, 92, 227-231.
31. Zong, I.; Chung, C.-Y.; Yin, L.; Fang, D.; Hsiao, B.; Chu, B.; Emilia, E.; Bien, H. *Biomaterials* **2005**, 26, 5330-5338.
32. Zong, X.; Kim, K.; Fang, D.; Ran, S.; Hsiao, B.; Chu, B. *Polymer* **2002**, 43, 4403-4412.
33. Ponomarenko, A. T.; Shevchenko, V. G.; Enikolopyan, N. S. *Advances in Polymer Science* **1990**, 96, 125-145.
34. McCullen, S. D.; Stevens, D. R.; Roberts, W. A.; Ojha, S. S.; Clarke, L. I.; Gorga, R. E. *Macromolecules* **2006**, Submitted.
35. Hutmacher. *Biomaterials* **2000**, 21, 2529-2543.
36. Ren, Z. F.; Huang, Z. P.; Xu, J. W.; Wang, J. K.; Bush, P.; Siegel, M. P.; Provencio, P. *Science* **1998**, 282, 1105-1107.

37. Montgomery, D. C., *Design and Analysis of Experiments*. 6th ed.; John Wiley & Sons: Hoboken, 2005; 'Vol.' p.
38. Cooper-White, J.; Mackay, M. *Journal Of Polymer Science Part B-Polymer Physics* **1999**, 37, 1803-1814.

Chapter 6

Electrospun conductive nanocomposites with adipose-derived human mesenchymal stem cells for tissue engineering applications

A paper submitted for publication to the International Journal of Nanomedicine

Seth D. McCullen¹, Derrick R. Stevens², Wesley A. Roberts³, Laura I. Clarke⁴, Susan H.

Bernacki⁵, Russell E. Gorga⁶, and Elizabeth G. Lobo⁷

6.1 Abstract

Electrospun nanocomposites were fabricated by encapsulating multi-walled carbon nanotubes (MWNTs) in poly (lactic acid) (PLA) nanofibers. Scanning electron microscopy (SEM) confirmed the fabrication of nanofibers, and transmission electron microscopy identified the alignment and dispersion of MWNTs along the axis of the fibers. Tensile testing showed an increase in the tensile modulus for a MWNT loading of 0.25 wt% compared to electrospun nanofibrous mats without MWNT reinforcement. Conductivity measurements indicated that the reduced dimensionality of the fibrous system requires only minute doping to obtain significant enhancements at 0.32 wt%. Adipose-derived human mesenchymal stem cells (hMSCs) were seeded on electrospun scaffolds containing 1 wt%

¹: Primary researcher and author, Department of Textile Engineering, Chemistry, and Science, NCSU; Joint Department of Biomedical Engineering at NCSU and UNC-CH

²: Graduate student who contributed conductivity data, Department of Physics, NCSU

³: Undergraduate student who contributed conductivity data, Department of Physics, NCSU

⁴: Provided conductivity systems measurement and expertise, Department of Physics, NCSU

⁵: Developed DNA assay and cell culture training, Joint Department of Biomedical Engineering at NCSU and UNC-CH

⁶: Provided nanocomposite expertise and funding for work, Department of Textile Engineering, Chemistry, and Science,

⁷: Author for correspondence, Joint Department of Biomedical Engineering at NCSU and UNC-CH

MWNTs and 0 wt% MWNTs, to determine the efficacy of the scaffolds for cell growth, and the effect of MWNTs on hMSC viability and proliferation over two weeks in culture. Staining for live and dead cells and DNA quantification indicated that the hMSCs were alive and proliferating through day 14. SEM images of cells at 14 days showed morphological differences, with cells on PLA well spread and cells on PLA with 1% MWNTs closely packed and longitudinally aligned.

6.1 Introduction

Mesenchymal stem cells play a significant role in the advancement of regenerative medicine for tissue and organ replacement¹⁻³. These cells are found in adult tissues including bone and adipose tissue, as reservoirs of reparative cells, ready to populate an area and differentiate in response to signaling from wounds or diseases^{4,5}. At present, mesenchymal stem cells are on the forefront of tissue engineering research due to their availability from different source tissues and their multilineage potential⁴. One critical research focus is the development of scaffolds with properties and functionality that mimic the natural extracellular matrix.

Scaffold materials play an important role in directing tissue growth and offer opportunities to manipulate and control stem cell behavior⁶. Tissue engineering scaffolds have been evolving through creation of preferred morphologies and specifically tailored physical properties. For example, scaffold materials for bone tissue engineering demand an internal structural design that is highly porous in nature and exhibits a large surface to volume ratio^{7,8}. These characteristics support the adhesion of cells, promote cellular ingrowth, and help regulate delivery of nutrients and removal of wastes. Scaffolds for tissue repair should have good

biocompatibility, be biodegradable, and be capable of interacting with the cells of interest ⁹. Polymeric matrices are of relevance because they are able to meet these requirements for tissue scaffolds; however, they are not able to provide the specific cues needed for cellular growth and differentiation ¹⁰. Thus, composite scaffolds have gained more interest due to their enhanced physical properties and biocompatibility ¹¹⁻¹⁹. In particular, doping the polymer with a conducting material provides electrical conductivity to the scaffold, which may be important for facilitating cell migration, proliferation, and differentiation via electrical stimulation ²⁰⁻²². Incorporating a conductive scaffold with an applied electric field has shown increases in cellular proliferation, calcium deposition, and gene expression for osteogenesis ²². Thus, this work will highlight the specific conductance obtained by doping a polymeric system with fractional weight percentages of multi-walled carbon nanotubes in a three dimensional matrix and the efficacy of this scaffold in culture with adipose-derived hMSCs.

In order to create scaffolds for tissue engineering, researchers have revisited the method of electrospinning ²³. Electrospinning is a process that yields a highly porous scaffold by producing fibers on the sub-micron scale ²⁴, similar to the natural features of the extracellular matrix ¹¹. During the electrospinning process, a polymer solution is fed through a capillary at a metered rate while an electric potential is applied. When this potential overcomes the surface tension of the polymer solution, a whipping instability is created that produces extremely small fibers that are collected on a grounded collector. Fiber formation occurs when the intrinsic properties of the solution and the processing parameters are optimized ^{23,25}. Electrospinning is an advantageous process because it can produce three-

dimensional scaffolds from various polymer systems using essentially the same method and technique. Numerous investigators have experimented with the use of electrospun poly (lactic acid) (PLA) as a tissue scaffold and biocompatible membrane due to it being approved for use *in vivo* and its mechanical and degradation properties being well understood²⁶⁻³⁰.

To produce composite scaffolds using this fabrication method, nanomaterials can be encapsulated in nanofibers during electrospinning. Zang et al (2003) demonstrated that drugs could be loaded into nanofibers by suspending them within a polymer solution. With the addition of any particle: anionic, cationic, or nonionic, the diameter size, and distribution of the electrospun fibers can be significantly reduced, enabling a modification of the fiber diameter for specific applications. A more recent study by Xu (2006) incorporated silver particles within the electrospun fibers, and noted an increase in overall fiber diameter. Composite nanofibers containing hydroxyapatite (HAP) and growth factors have also been investigated¹¹. That study involved encapsulation of HAP crystals with a diameter of 50 nm inside electrospun silk. The composite nanofibers had a positive impact by promoting osteogenic differentiation of bone marrow derived mesenchymal stem cells, as evidenced by mineralized tissue formation.

Recent studies have investigated the combination of MWNTs with PLA^{31,32}. Carbon nanotubes, discovered by Iijima (1991), possess tremendous properties by having a very large aspect ratio³³. Carbon nanotubes have a tensile strength approaching 1 TPa and electrical conductivity of 100 S/cm³⁴. Chen et. al (2005) was able to graft oligomers of PLA to the surface of MWNTs; however, the grafting was not uniform and left much of the

MWNT surface bare³¹. Zhang et al (2006) prepared nanocomposite PLA/MWNTs scaffolds by solution casting. This fabrication method left MWNTs exposed on the surface but created uniform films with increased conductance. As these studies and others show, carbon nanotubes can provide three specific enhancements to fibrous tissue scaffolds: modified fiber size, electrical conductivity, and increased material properties (strength) in a lightweight material.

Though carbon nanotubes have such promising physical properties, their use in biomedical applications, specifically tissue engineering, has been limited due to concerns of cytotoxicity. This issue has been investigated by various researchers with differing results depending on the purity of the carbon nanotubes and the method of production³⁵. A collaborative study by Smart et al (2006), noted that the main causes for possible toxicity were due to the surface area / volume ratio, retention time of carbon nanotubes within a tissue, and residues of chemical within the carbon nanotube³⁵. They also noted that the main deterrents for a comparative standard for carbon nanotube toxicity is due to the dosage, size scale of the carbon nanotubes, and how well the carbon nanotubes are dispersed³⁵.

For this investigation, the primary goal is to encapsulate a high percentage of MWNTs inside polymeric PLA nanofibers to increase the conductance to produce a conductive scaffold. Dispersion and alignment of carbon nanotubes in electrospun nanofibers has been shown in other polymer systems including poly(ethylene oxide) and poly(acrylonitrile); however, the level of interaction between the MWNTs and polymer has not been investigated for biocompatibility or use as a tissue scaffold³⁶⁻³⁹. In a previous study, we identified

processing parameters for the creation of electrospun nanocomposites with MWNTs and validated the integration of MWNTs into polymer nanofibers ⁴⁰. In this investigation our focus is on determining the efficacy of electrospun MWNTs/PLA composite nanofibers as a tissue scaffold with adipose-derived hMSCs and evaluating their effects on viability and proliferation on this electrospun scaffold.

6.3 Materials and Methods

6.31 Materials

Poly(L-D-lactic acid; PLA) with a molecular weight (M_w) of 250,000 g/mol was obtained from Sigma-Aldrich (St. Louis, MO). PLA was solubilized in chloroform and dimethyl formamide (DMF) (Sigma-Aldrich). Multi-walled carbon nanotubes with a diameter of 15 +/- 5 nm and length of 5-20 μ m at 95% purity were obtained from Nano-Lab (Brighton, MA). They were produced by plasma enhanced chemical vapor deposition using acetylene and ammonia with an iron catalyst and grown on a mesoporous silica substrate ⁴¹.

6.32 Electrospinning Solution Preparation

Multi-walled carbon nanotubes were sonicated at a concentration of 0.1 mg/ml in DMF with 1% Pluronic F127 (BASF, Florham Park, NJ) using an Ultrasonic Model 2000U generator and needle probe at 25 Hz for 4 hours ^{42,43}. This produced a stock solution for MWNTs incorporation into the solubilized PLA. 20 wt% PLA was solubilized in 3:1 chloroform and dimethyl formamide. Electrospun nanocomposites containing 0-2 wt % MWNTs were produced for physical property analysis and 0 and 1 wt% MWNTs to test cell growth and viability.

6.33 Electrospinning Apparatus

The electrospinning apparatus included a programmable syringe pump obtained from New Era Pump Systems (Model NE 500) (Farmingdale, NY). The high voltage power supply was obtained from Glassman High Voltage Model # FC60R2 with a positive polarity (High Bridge, NJ). The pump operated at a flow rate of 1 mL/min with an electric field of 1 kV/cm. Solutions were loaded into 10 mL syringes with luer-lock connections and used in conjunction with a 4 inch 20 gauge blunt tip needle. The design of the electrospinning set-up was based on a point-plate configuration (Figure 1).

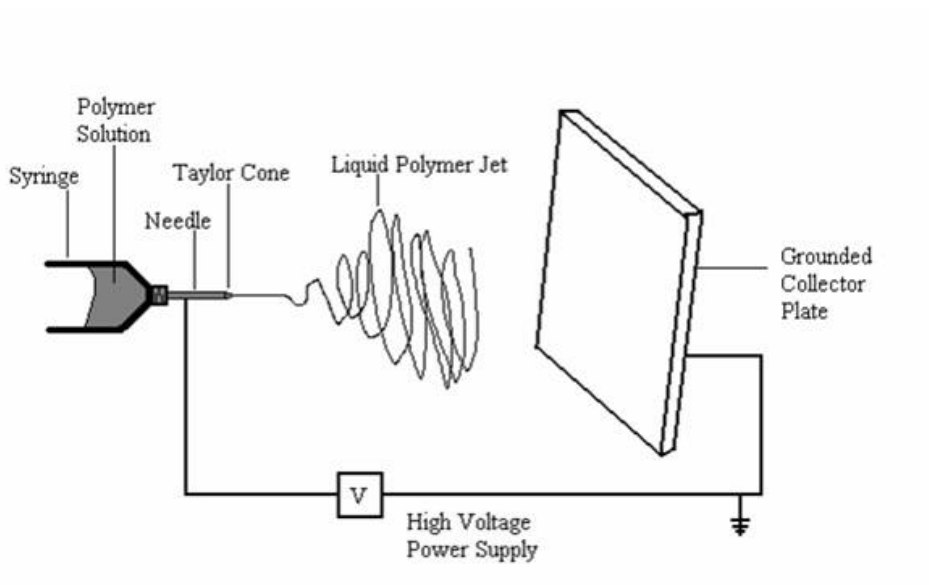


Figure 6.1: Labeled schematic of the electrospinning apparatus used to produce the nanocomposite samples.

Scaffolds for mechanical testing were deposited directly on the collector plate, while for cell culture, scaffolds were deposited on polystyrene wafers that had been placed on the plate. The electrospun scaffolds for cell culture were soaked in phosphate buffered saline (PBS) for 12 hrs to remove any residual solvent, sterilized in 70% ethanol for 1 hr, and rinsed again with PBS before seeding with hMSCs.

6.34 Electrospun Scaffold Characterization

Fiber morphology of the electrospun samples was determined via scanning electron microscopy (SEM) (JEOL JSM-6400 FE) operating at 5 kV. The electrospun samples were coated with Au-Pd at a thickness of 100 Å to reduce charging and produce a conductive surface and digital images were captured. Transmission electron microscopy (TEM) (JEOL 100S) was performed with samples spun directly on a Cu 400 mesh grid coated with holey thin carbon film. Micrographs were developed and digitally scanned.

Tensile tests on electrospun nanocomposites were performed with an Instron Model 5544 using the Bluehill™ Version 1.00 software on samples of 0-2 wt% MWNTs at a crosshead speed of 2.00 mm/min. Scaffold thickness was approximated by averaging 5 measurements for each sample.

To determine the electrical characteristics of the scaffold material, thin (~1 µm) films were electrospun directly onto flat, interdigitated electrodes on glass (fabricated by standard uv-lithography). Interdigitated electrodes create an electric field parallel to the surface and allow conductance measurements of films grown between and above the digits. The electrodes had twenty-six finger pairs, with each digit 1 mm long, equal digit width and spacing (10 µm), and digit height of approximately 1200 Å (125 Å chromium/ 1100 Å gold). External wires were connected to the electrode at two contact pads with conductive silver epoxy. Home-made triaxial cables connected the sample, which rested on a copper stage in a vacuum of $\sim 1 \times 10^{-7}$ torr, to a Keithley Model 6430 sub-femto amp remote source meter. Standard current-voltage sweeps before and after deposition were conducted (-10 V to 10 V in 0.1 V steps, 15

second delay after voltage changes) and the low-voltage linear region was fit to determine the conductance. All blank electrodes showed similar curves with a measured conductance of $\sim 1 \times 10^{-15}$ S, which serves as the lower limit of our measurement range.

6.35 Human Mesenchymal Stem Cell Isolation and Expansion

All protocols involving human tissue were approved by the Institutional Review Boards of the University of North Carolina at Chapel Hill and North Carolina State University. Excess adipose tissue from elective plastic surgery procedures was obtained with donor consent. The hMSC isolation method was modified from Gabbay *et al.*⁴⁴. Approximately 50 grams of adipose tissue from a 50 year old Caucasian female was rinsed in phosphate buffered saline (PBS), minced with a scalpel, combined with 50 ml of 0.075% collagenase I (Worthington Biochemical Corp., Lakewood, NJ), 100 I.U. penicillin / 100 μ g/mL streptomycin (Mediatech, Inc., Herndon, VA) in alpha-modified minimal essential medium (α -MEM with L-glutamine, Invitrogen, Carlsbad CA), and incubated at 37°C on a rotator for 30 minutes. 50 ml of hMSC growth medium (alpha-modified minimal essential medium (α -MEM with L-glutamine, Invitrogen), 10% fetal bovine serum (Premium Select, Atlanta Biologicals, Lawrenceville, GA), 100 I.U. penicillin /100 μ g streptomycin per mL, 200 mM L-glutamine (Mediatech, Inc.) was added, and the suspension was centrifuged for 10 minutes at 10,000 x g. The supernatant was discarded, and the hMSC-rich cell pellet suspended in 160 mM NH_4Cl for 10 minutes to lyse red blood cells. Unlysed cells were pelleted by centrifugation for 10 minutes at 10,000 x g, and seeded in tissue culture flasks (one 75 cm^2 flask per 5 grams initial tissue) in hMSC growth medium . After 24 hours, cultures were washed with PBS to remove non-adherent cells and supplied with fresh growth medium. Cultures were

passaged or cryopreserved at 80% confluency. Re-seeding density was 100,000 cells per 75 cm² flask. Cells for this study were used at the third passage following isolation.

6.36 Cell Seeding

Third passage cells were grown to 80% confluency, trypsinized, and resuspended in growth medium. Circular electrospun scaffolds (approximately 1.76 cm diameter) were prewet with PBS and placed in multi-well tissue culture plates. 50,000 cells in a volume of 100 microliters were seeded onto each scaffold. The seeded scaffolds were incubated at 37°C for 30 minutes to allow the cells to adhere, then covered with 2 mL growth medium. Medium was replaced every 3 days. At 1, 3, 7 and 14 days post seeding, scaffolds were removed for viability and proliferation analysis. Viability was determined using a Live/Dead Assay Viability Cytotoxicity kit (calcein AM, ethidium homodimer-1) for Mammalian Cells (Molecular Probes, Eugene, OR) as per manufacturer's instructions. Live and dead cells were imaged on the scaffolds using fluorescent microscopy. Proliferation was determined by quantitating DNA using the DNA binding dye Hoechst 33258 (Molecular Probes) in a microplate based format. For each time point, scaffolds with attached cells were digested overnight at 60°C in 2.5 units/ml papain from papaya latex in PBS with 5 mM EDTA and 5 mM cysteine HCl (all reagents from Sigma, St. Louis, MO), then assayed with Hoescht 33258 according to manufacturer's instructions.

For SEM, scaffolds were fixed with Trump's fixative and stored at 4°C. After all time points had been collected, scaffolds were dehydrated in increasing concentrations of ethanol of 50%, 70%, 95%, and 100% for 15 minutes each, then critical point dried (CPD) with CO₂.

After CPD, samples were sputter-coated with 200 Å Au-Pd then imaged with a JEOL JSM-6360 at 5 kV in secondary electron imaging mode.

6.4 Results

6.41 Scaffold Characterization

SEM images of electrospun PLA with and without MWNTs are shown in Figure 6.2. Nanocomposite fibers had a markedly smaller average diameter when compared to PLA without MWNTs, 700 nm versus approximately 5-8 μm. Both scaffolds featured an interconnected porous network with an average porosity of 75%, advantageous for cellular growth.

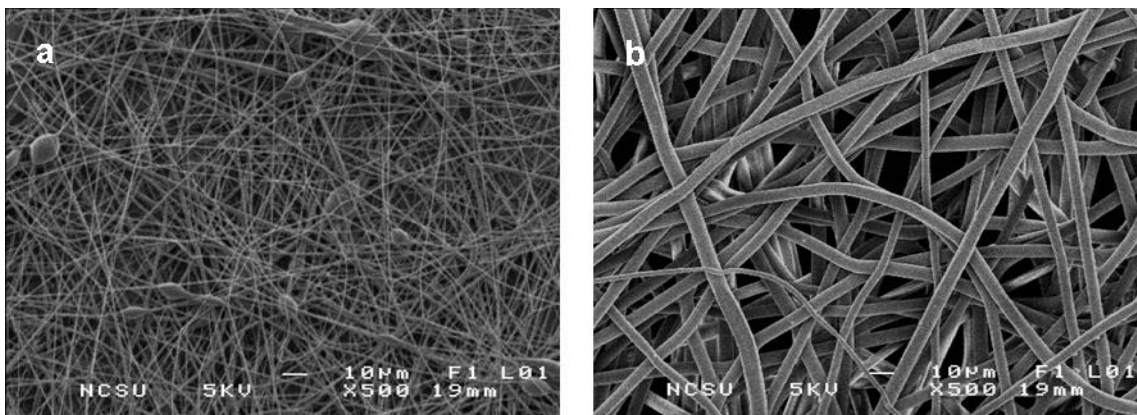


Figure 6.2: SEM image of electrospun PLA, containing a) 1 wt% MWNTs and b) 0 wt% MWNTs.

TEM was used to visualize interaction of the MWNTs with PLA. Figure 6.3a shows a fiber with an individual MWNT aligned with the long axis, and encapsulated by the PLA.

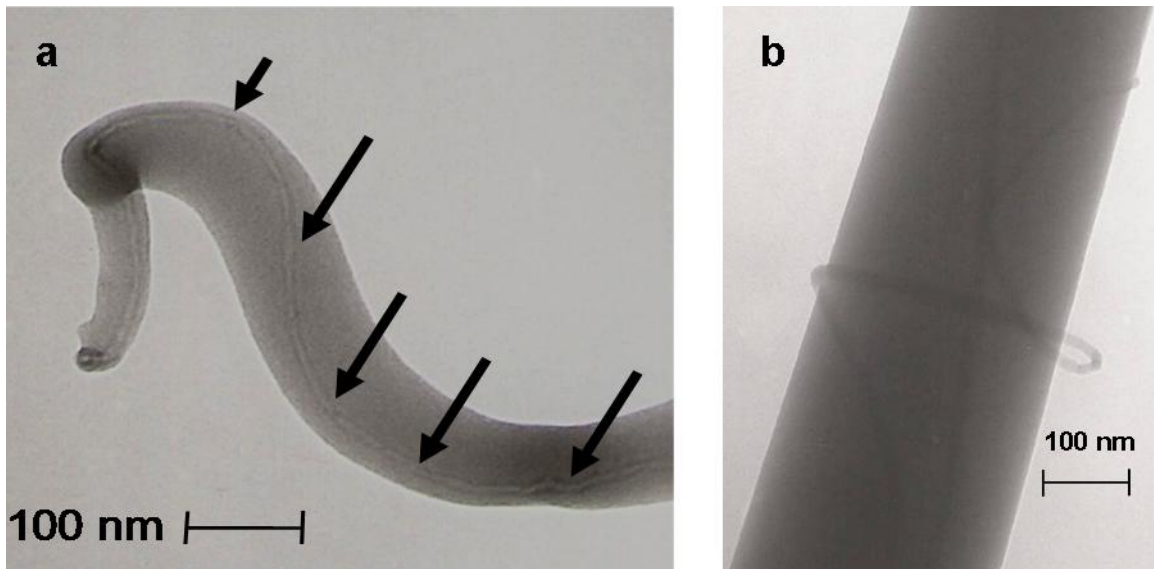


Figure 6.3: TEM images of electrospun nanocomposite, a: showing MWNT alignment along fiber axis and b: showing MWNT aggregation.

Occasional fibers with the MWNT incompletely encapsulated were also observed (Figure 6.3b). The fibers shown are smaller than average to best visualize the MWNTs.

Young's moduli of scaffolds with different wt% of MWNTs was determined (n=10; Figure 6.4). Young's modulus was low for all samples, however, inclusion of MWNTs slightly increased the modulus. 0.25 wt% MWNTS gave the largest increase, from approximately 15 MPa to 55 MPa.

Young's Modulus of PLA Nanofibers vs. MWNT wt%

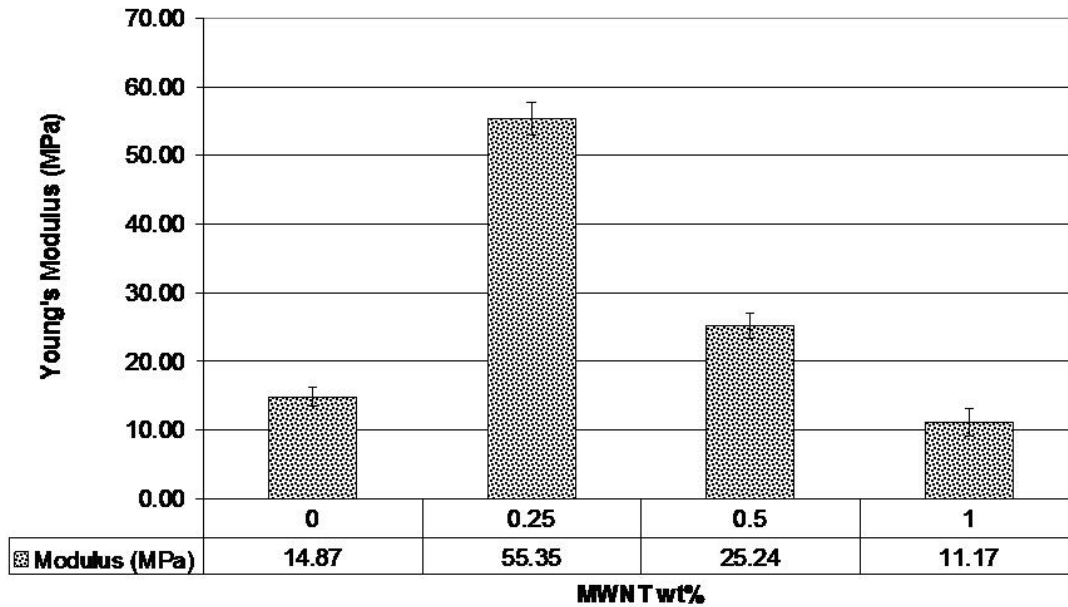


Figure 6.4: Plot of the Young's modulus of the electrospun fibrous mats by MWNT wt %; (n = 10), Error Bars = Std Error Mean.

Electrical conductance versus MWNT wt% for an approximately 1 μm thick sample with area of approximately 0.5 mm^2 is shown in Figure 6.5. By fitting the data after Fournier we obtain a percolation threshold of 0.32%⁴⁵. An estimate of the conductivity above threshold based on the geometry of the system and an assumed value of 75% void space (25% fiber) within the mat yielded a maximum conductivity on the order of 1E-3 S/cm.

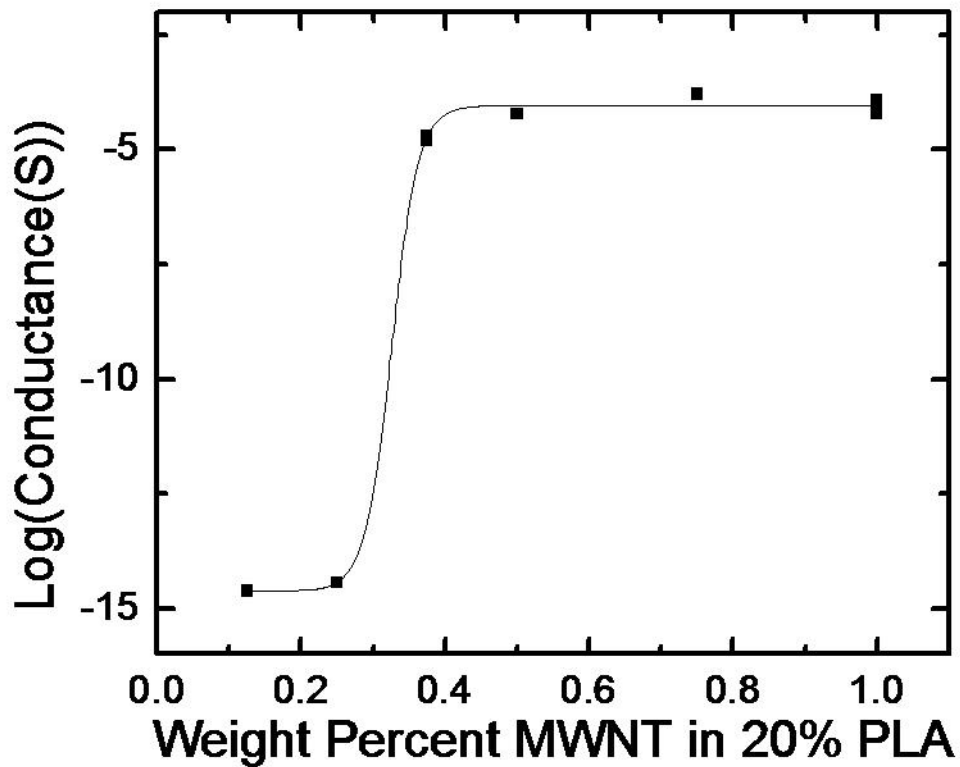


Figure 6.5: Conductance plot for mats spun from varying MWNT wt% in 20 wt% PLA solution. The error on each point is exceeded by the point size. At both 0.375 and 1 wt% two samples are represented. The mat conductance, G , is fit after (Fournier 1997) with $\log(G) = \log(G_f) + [\log(G_m) - \log(G_f)]/z$ where G_m and G_f are the matrix (polymer) and final composite (maximum) conductance, p is the wt%, and p_c the critical weight percentage for conductance. The parameter b determines the slope of the curve across the percolation threshold. We find $G_m = 2 \times 10^{-15}$ S (indistinguishable from the limit of conductance in our system), $G_f = 9 \times 10^{-5}$ S, $b = 53$, and $p_c = 0.32\%$.

6.42 Cell/Scaffold Interaction

Fluorescent dyes were used to visualize live and dead cells on the scaffolds. Calcein AM stains the cytoplasm of live cells green, whereas ethidium homodimer-1 stains the nuclei of dead cells red. hMSCs were viable on PLA scaffolds both with and without MWNTs throughout the culture period (14 days). Three scaffolds were examined at each time point, 1, 3, 7 and 14 days. A maximum of 10 dead cells was observed in any field of view (ten fields viewed per scaffold). Representative images from cultures at days 1 and 14 are shown in Figure 6.6. Individual viable cells are visible in the images from day 1. Day 14 images show confluent patches of viable cells. Similar patches were visible throughout the scaffolds.

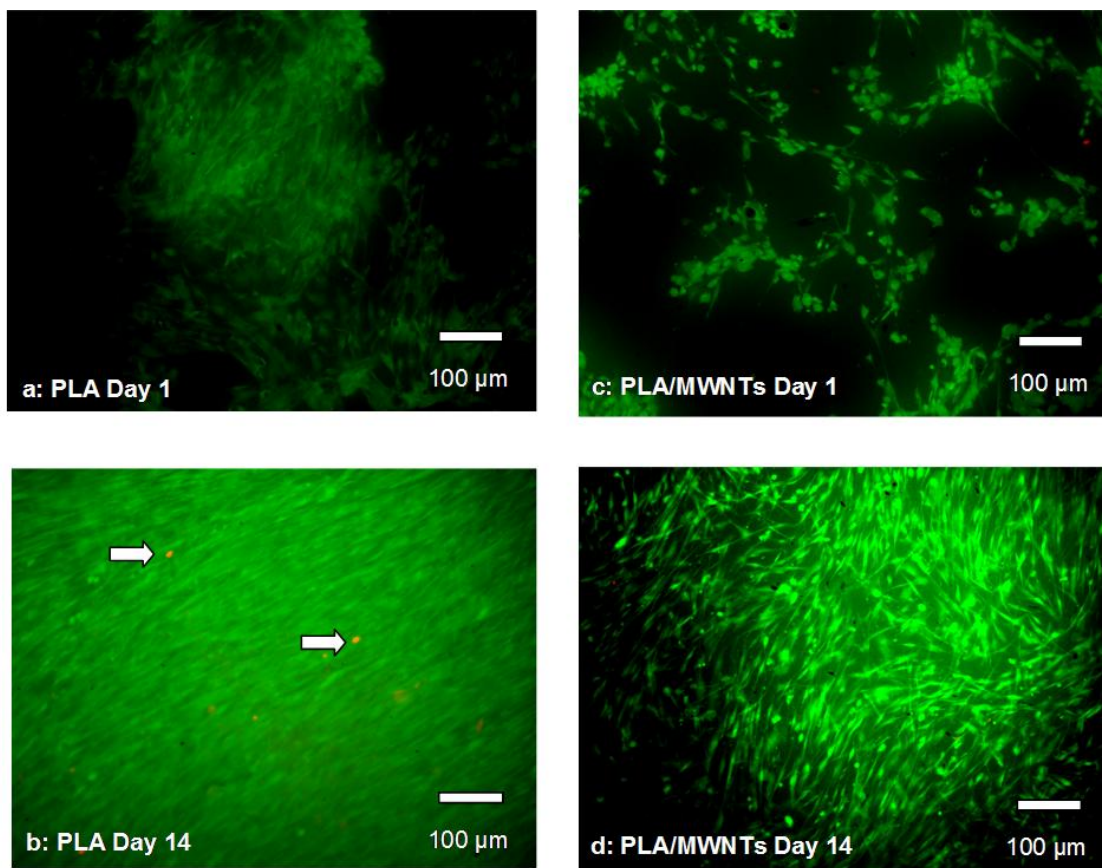


Figure 6.6: Live/Dead images of hMSCs on electrospun PLA without MWNTs (a,b) and with MWNTs (1 wt %) (c,d) where green = live and red = dead (indicated by arrows).

DNA was extracted from three scaffolds at each time point and quantitated (Figure 6/7), using triplicate samples for each scaffold. hMSCs proliferated during the entire culture period on both types of scaffold. The large increase in DNA from 7-14 days is consistent with exponential growth of the cells. A significant difference was observed between scaffolds with and without MWNTs 1 wt% on day 14.

hMSC DNA Content

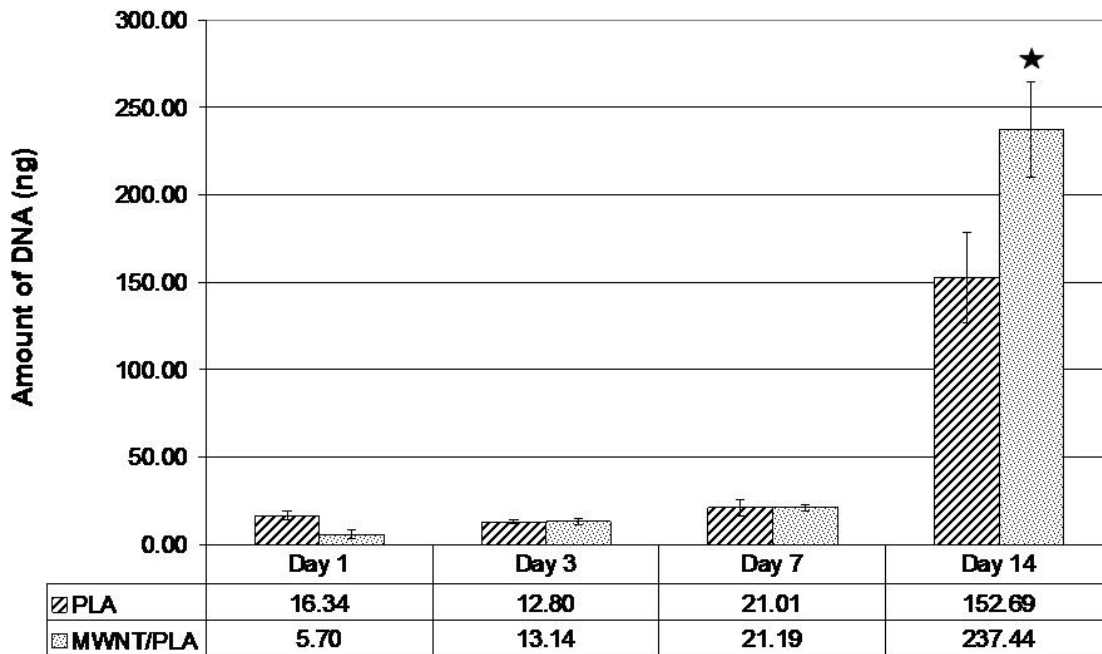


Figure 6.7: Number of hMSCs present throughout the course of the experiment on the electrospun tissue scaffolds with and without MWNTs. (n = 3, three scaffolds / time point, three samples / scaffold) (Error bars = Standard Error Mean), where star indicates significance p-value < 0.05.

SEM showed that the hMSCs adhered and spread extensively within 1 day of seeding (Figure 6.8). Human MSCs on PLA without MWNTs appeared to have more small processes than those on PLA with MWNTs.

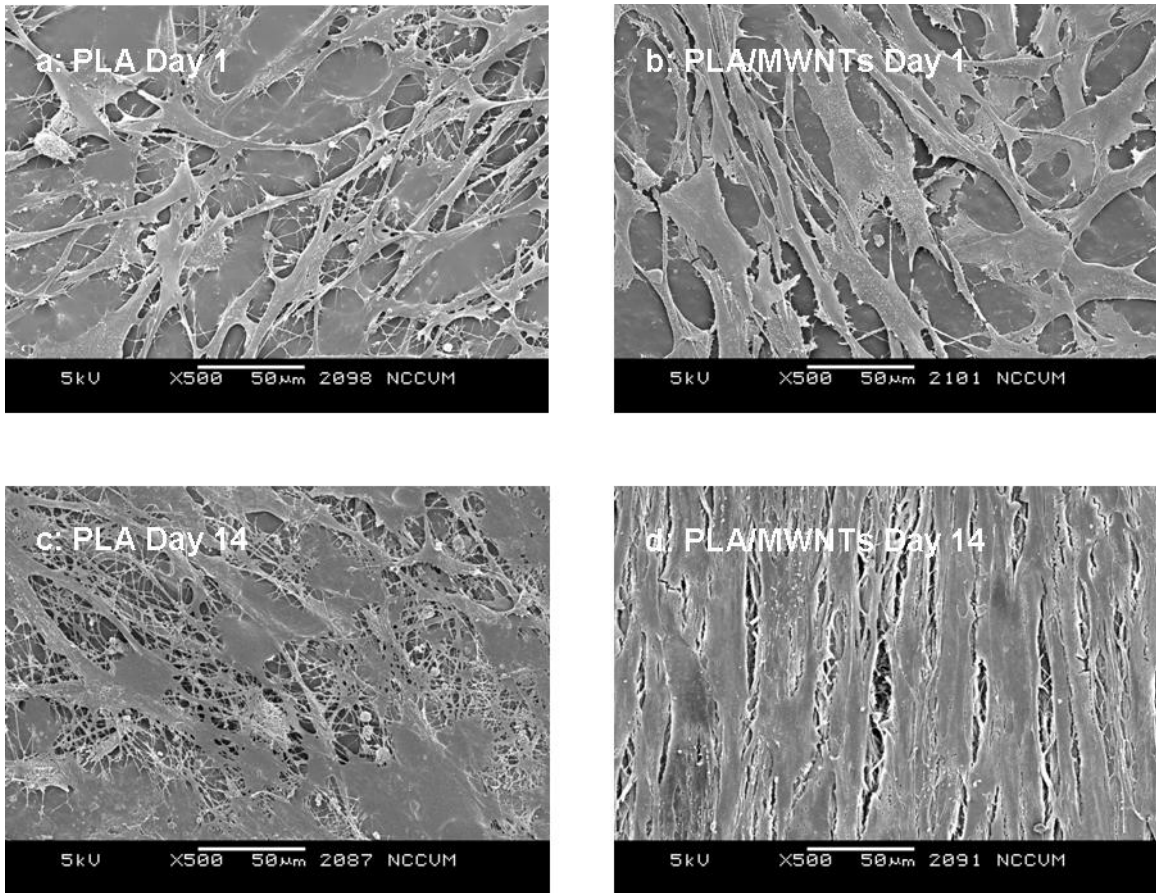


Figure 6.8: SEM image of hMSCs at Day 14, completely confluent on the surface of the electrospun PLA with MWNTs.

At 14 days, cells were confluent on both types of scaffold. Cells on scaffolds with MWNTs were aligned (Figure 6.9), whereas cells on PLA alone appeared to have a random orientation.

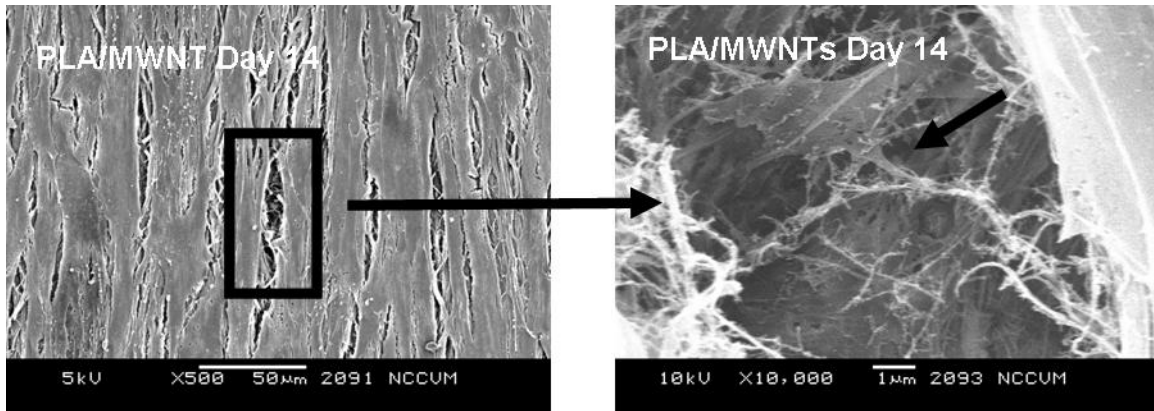


Figure 6.9: SEM image at Day 14 of hMSCs integration into the electrospun nanocomposite scaffold. Arrows indicate hMSC with processes into scaffold.

6.5 Discussion

In this study, we demonstrated that adipose derived hMSCs adhered to and proliferated on nanocomposite scaffolds of electrospun PLA with 1% MWNTs, which possessed enhanced conductive properties.

6.51 Scaffold Characterization

Electrospinning allows for the creation of unique structures with preferred morphologies on the nano-submicron scale. During electrospinning, fiber formation must occur by identifying a critical concentration for the polymer solution that allows for chain entanglements to occur for each molecular chain. This has been reported by Shenoy et. al (2005) and we have affirmed this concentration at 20 wt% PLA²⁵. As shown in Figure 6.2, we are able to detail the porous nonwoven architecture, which has been reported to be similar to the fibrillar nature of the extracellular matrix found *in vivo*¹¹. With the addition of MWNTs we

observed that there was a tremendous decrease in fiber diameter, possibly due to an increase in the charge density on the Taylor cone during electrospinning.

By incorporating the MWNTs into the polymer solution, the solution behaved somewhat differently when compared to the PLDLA polymer solution for the same processing parameters. The MWNT/PLDLA solution appeared to produce fibers much more rapidly as seen by visual inspection. This can be attributed to the conductivity of the MWNTs, which can increase the conductivity of the solution, or maintain a more uniform charge density on the fiber surface as hypothesized by Zang.²⁸ It can be postulated that there is a significant interaction between the MWNTs and the PLDLA during electrospinning as the Taylor cone forms. The addition of MWNTs is not only able to increase the conductance of the spinning solution, but also allow the fibers to crystallize around them when collected, as hypothesized by Zang.²⁸ In Figure 4, the SEM images of electrospun PLDLA show the dramatic decrease in fiber diameter with the addition of MWNTs. For each SEM image, fiber diameters were calculated using the Scion ImageTM software. Approximately 20 measurements were taken per image.

Transmission electron microscopy showed that the MWNTs were dispersed within the nanofibers and oriented along the axis of the fiber (Figure 6.3). This incorporation has been theorized by others as a result of the induced electric charge on the fluidic polymer jet⁴⁶. Figure 6.3a shows that the carbon nanotubes are dispersed and aligned. However, in Figure 6.3b, the MWNTs appear to be aggregating; this could be due to the interaction with different segments via van der Waals forces. Also, this aggregation could be attributed to the length

scale of the carbon nanotubes; as the carbon nanotube gets longer, it becomes more difficult to disperse due to a larger increase in the surface area. In general, the aggregation shown in Figure 6.3b occurred much less frequently than the aligned fiber orientation shown in Figure 6.3a.

Mechanical properties were determined with tensile testing. The tensile strain at break of all samples was low, commonly between 2-4% strain. The fibers in the breaking zone showed very little alignment before breaking, demonstrating their highly brittle nature. Previous work has shown that the fracture behavior of electrospun fibrous mats with carbon nanotubes undergoes similar crazing and rupture, and that during this transformation, the carbon nanotubes become aligned along the axis of the fiber⁴⁷. The large differences appear to be from the carbon nanotubes not being completely dispersed in the polymer matrix, leading to stress concentrations for crazing. This behavior has been detected in unaligned and aligned electrospun nanocomposites⁴⁸. A loading level of 0.25 wt% MWNTs seemed to have the greatest effect on the nanocomposites.

Composites made of an insulating matrix doped with an electrically-conductive filler often display percolation behavior as a function of dopant density⁴⁹. Below a certain threshold the filler particles are isolated and thus no current flows. At threshold doping, a single percolating path of dopant (MWNTs) is formed and the sample exhibits a dramatically increased conductance. As the filler density further increases, additional paths contribute to the current until the majority of the sample volume is conducting. Above this saturation value, no further increase in conductance as a function of doping is observed. As can be seen

in Figure 6.5, the PLA/MWNT scaffold system exhibited a dramatic percolation behavior accompanied by an increase in conductance of ten orders of magnitude. The critical weight percentage for percolation (0.3%) is much lower than the previous result (13.5%) for MWNTs in PLA spin-coated films³². This reflects the reduced dimensionality of the fibrous system which may require only minute doping to obtain significant conductivity (Sundaray, 2006), thus minimizing carbon residue in scaffold applications.

6.52 Human MSC/Scaffold Interaction

Scaffolds containing 0 wt% and 1 wt% MWNTs were electrospun, seeded with hMSCs and incubated for two weeks. Live/Dead staining was performed at 1, 3, 7, and 14 days throughout the experiment. Microscopy showed that hMSCs were able to grow and remain viable on the scaffolds up to 14 days (Figure 6.6). The hMSCs showed an increase in number at day 14. However when viewing the number of cells throughout the course of the experiment, it should be noted that there was approximately the equivalent number of hMSCs until day 7. Between day 7 and 14, the hMSCs numbers increased dramatically (Figure 6.7). By quantifying the amount of DNA present in each scaffold, we were able to determine a significant difference at day 14 between the PLA scaffolds with MWNTs compared to PLA scaffolds alone (Figure 6.7). This difference could be attributed to the increased surface area due to the fibers being considerably smaller (Figure 6.2). SEM images of cells at 14 days showed confluent layers of cells with fibroblastic morphology (Figure 6.8). By viewing between two cells on this scaffold (Figure 6.9), we capture the interaction between the hMSCs and the nanofibers. The cells appeared to be completely integrated into the structure of the scaffold, extending cellular processes into and around the nanofibers. This interaction

shows that the cells are able to not only become aligned on the scaffold, but that due to the difference in fiber size, hMSCs are able to fully proliferate on electrospun nanocomposite fibers. Further, a pronounced difference in cell morphology is apparent on the two different scaffolds: hMSCs were spread unoriented on PLA alone, while they were aligned on PLA with encapsulated MWNTs.

6.6 Conclusions

In this study, we have produced electrospun nanocomposites by encapsulating MWNTs inside PLA nanofibers with fiber diameters on the average of 700 nm. The porous structure was validated by SEM. Integration of the MWNTs into the nanofibers was confirmed by TEM. With only minute doping of MWNTs, the conductivity of the scaffold increased by approximately ten orders of magnitude. Fluorescence microscopy indicated adipose-derived hMSCs were viable in and on the scaffolds for up to two weeks in culture, and that they proliferated on day 14. The hMSCs formed a confluent three-dimensional construct. With the addition of MWNTs in the PLA scaffold, SEM revealed a preferential alignment and orientation of the cells on the scaffold. In conclusion, this work has shown that with the addition of MWNTs to electrospun PLA fibers, we are able to reduce the fiber diameter, increase the conductivity of the scaffold, and potentially provide a functional composite for tissue engineering.

6.7 Acknowledgements

This work was funded by the Nanotechnology Initiative at North Carolina State. We would like to thank Alan Kinlaw, Kelly Stano for technical assistance, the Center for Chemical

Toxicology Research and Pharmacokinetics (CCTRP) and the Laboratory for Advanced Electron and Light Optical Microscopy (LAELOM) at North Carolina State for scaffold image analysis, and the entire Cell Mechanics Laboratory (CML) at North Carolina State.

6.8 References

1. P. Andrews and N. Benvenisty, *Current Opinion Biotechnology*, **16**, 485-486 (2005).
2. M. Pittenger and e. al., *Science*, **284**, 143-147 (1999).
3. M. Pittenger, A. Mackay, S. Beck, R. Jaiswal, R. Douglas, J. Mosca, M. Moorman, D. Simonetti, S. Craig and D. Marshak, *Science*, **284**, 143-147 (1999).
4. N. Habib, M. Gordon, N. Levicar, L. Jiao and G. Thomas-Black, *Stem Cell Repair and Regeneration*, Imperial College Press, London, UK, 2005.
5. A. Battler and J. Leor, *Stem Cell and Gene-Based Therapy*, Springer, London, UK, 2006.
6. J. Elisseeff, A. Ferran, S. Hwang, S. Varghese and Z. Zhang, *Stem Cells and Development*, **15**, 295-303 (2006).
7. C. Laurencin, *Bone Graft Substitutes*, ASTM International, Bridgeport, 2003.
8. F. G. Lieberman Jay, *Bone Regeneration and Repair: Biology and Clinical Applications*, Humana Press, Totowa, 2005.
9. L. Hench and J. Polak, *Science*, **295**, 1014-1017 (2002).
10. Hutmacher, *Biomaterials*, **21**, 2529-2543 (2000).
11. C. Li, C. Vepari, H.-J. Jin, H. J. Kim and D. Kaplan, *Biomaterials*, **27**, 3115-3124 (2006).
12. P. Ma, *Materials Today*, 30-40 (2004).

13. R. MacDonald, *Wiley InterScience*, 489-496 (2005).
14. B. Sharma and J. Elisseeff, *Annals of Biomedical Engineering*, **32**, 148-159 (2004).
15. Xu Xiaoyi, Yang Qingbiao, Wang Yongzhi, Yu Haijun, Chen Xuesi and J. Xiabin, *European Polymer Journal*, **In Press**(2006).
16. B. Zhao, H. Hu, S. K. Mandal and R. C. Haddon, *Chemistry Of Materials*, **17**, 3235-3241 (2005).
17. J. H. Lee, T. G. Park, H. S. Park, D. S. Lee, Y. K. Lee, S. C. Yoon and J.-D. Nam, *Biomaterials*, **24**, 2773-2778 (2003).
18. I. Firkowska, Olek, M, *Langmuir*, **22**, 5427-5434 (2006).
19. M. Li, Guo, Y., *Biomaterials*, **27**, 2705-2715 (2006).
20. A. a. S. Kotwal, C. E., *Biomaterials*, **22**, 1055-1064 (2001).
21. D. M. K. Pedrotty, J., *Am. J. Physiol Heart Circ. Physiol.*, **288**, 1620-1626 (2005).
22. P. R. Supronowicz, P. M. Ajayan, K. R. Ullmann, B. P. Arulanandam, D. W. Metzger and R. Bizios, *Journal Of Biomedical Materials Research*, **59**, 499-506 (2002).
23. Q. P. Pham, U. Sharma and A. G. Mikos, *Tissue Engineering*, **12**, 1197-1211 (2006).
24. A. Formhals. USA, (1934).
25. S. L. Shenoy, W. D. Bates, H. L. Frisch and G. E. Wnek, *Polymer*, **46**, 3372-3384 (2005).
26. R. Inai, M. Kotaki and S. Ramakrishna, *Nanotechnology*, **16**, 208-213 (2005).
27. S.-H. Tan, R. Inai, i. M. Kotak and S. Ramakrishna, *Polymer*, 6128-6134 (2005).
28. J. Zang, X. Xu, X. Chen, Q. Liang, X. Jing, L. Yang and X. Bian, *Journal of Controlled Release*, **92**, 227-231 (2003).

29. I. Zong, C.-Y. Chung, L. Yin, D. Fang, B. Hsiao, B. Chu, E. Emiliaand H. Bien, *Biomaterials*, **26**, 5330-5338 (2005).
30. X. Zong, K. Kim, D. Fang, S. Ran, B. Hsiaoand B. Chu, *Polymer*, **43**, 4403-4412 (2002).
31. G.-X. Chen, H.-S. Kim, B. H. Parkand J.-S. Yoon, *Journal of Physical Chemistry B*, **109**, 22237-22243 (2005).
32. D. Zhang, M. A. Kandadai, J. Cech, S. Rothand S. Curran, *Journal of Physical Chemistry B*, **110**, 12910-12915 (2006).
33. S. Iijima, *Science*, **354**, 56-58 (1991).
34. P. Poncharal, Z. L. Wang, D. Ugarteand W. A. de Heer, *Science*, **283**, 1513-1517 (1999).
35. S. K. Smart, A. I. Cassady, G. Q. Luand D. J. Martin, *Carbon*, **44**, 1034-1047 (2006).
36. C. T. Yavuz, C. M. Sayes, P. E. Laibinisand V. L. Colvin, *Abstracts Of Papers Of The American Chemical Society*, **227**, U1552-U1552 (2004).
37. Dror Yael, Salalha Wael, Khalfin Rafail, Cohen Yachin, Yarin Alexanderand Z. Eyal, *Langmuir*, **19**, 7012-7020 (2003).
38. H. J. Gong, X. P. Yang, G. Q. Chen, T. Q. Liu, S. M. Zhang, X. L. Dengand X. Y. Hu, *Acta Polymerica Sinica*, 297-300 (2005).
39. J. Ayutsede, M. Gandhi, S. Sukigara, H. H. Ye, C. M. Hsu, Y. Gogotsiand F. Ko, *Biomacromolecules*, **7**, 208-214 (2006).
40. S. D. McCullen, K. L. Stanoand R. E. Gorga, *Journal of Applied Polymer Science*, **Submitted**(2006).

41. Z. F. Ren, Z. P. Huang, J. W. Xu, J. K. Wang, P. Bush, M. P. Siegel and P. Provencio, *Science*, **282**, 1105-1107 (1998).
42. N. Monteiro-Riviere, A. Inman, Y. Wang and R. Nemanich, *Nanomedicine: Nanotechnology, Biology, and Medicine* **1**, 293-299 (2005).
43. V. C. Moore, M. S. Strano, E. H. Haroz, R. H. Hauge and R. E. Smalley, *Nano Letters*, **3**, 1379-1382 (2003).
44. J. S. Gabbay, S. C. Mitchell, J. B. Heller, P. A. Zuk, C. M. O'Hara, P. Benhaim and J. P. Bradley, *Journal Of The American College Of Surgeons*, **201**, S49-S49 (2005).
45. J. Fournier, G. Boiteux, G. Seytre and G. Marichy, *Synthetic Metals*, **84**, 839-840 (1997).
46. F. Ko, Y. Gogotsi, A. Ali, N. Naguib, H. H. Ye, G. L. Yang, C. Li and P. Willis, *Advanced Materials*, **15**, 1161-1164 (2003).
47. H. H. Ye, H. Lam, N. Titchenal, Y. Gogotsi and F. Ko, *Applied Physics Letters*, **85**, 1775-1777 (2004).
48. J. Ayutsede, M. Gandhi, S. Sukigara, M. Micklus, H. E. Chen and F. Ko, *Polymer*, **46**, 1625-1634 (2005).
49. D. Stauffer and A. Aharony, *Introduction to Percolation Theory*, Taylor & Francis, Washington DC, 1992.

Chapter 7

Conclusions

7.1 Conclusions

The research presented in this thesis has been able to contribute to the developing fields of nanocomposites and tissue engineering. This study implemented electrospun polymeric matrices doped with multi-walled carbon nanotubes. Microscopy identified multi-walled carbon nanotubes dispersed and aligned in two polymer systems, poly ethylene oxide and poly (lactic acid). The electrospinning of PLA underwent a full factorial design of experiment and was able to capture the morphological features of the different operating levels. Through the use of microelectrodes we were able to model the percolative behavior of multi-walled carbon nanotubes in electrospun mats associated with increases in conductivity with rudimentary percolation equations and more specifically, the Fournier model. Enhancements in physical properties were determined to occur before percolation in the conductivity samples.

The electrospun nanocomposites of PLA/MWNTs were implemented into tissue engineering scenarios with adipose-derived human mesenchymal stem cells. Viability was confirmed by Live/Dead staining through fluorescence microscopy, and proliferation was measured via DNA quantification. SEM indicated that the hMSC's possessed a fibroblastic morphology and grew confluent on the nanocomposite scaffold becoming aligned after 14 days in culture. Overall, this research has developed a fundamental understanding of electrospinning nanocomposites and their application as a scaffold for tissue engineering.

Chapter 8

Future Work

8.1 Future Directions

This research has been able to develop fundamental research in both the development of nanocomposites and tissue engineering scaffolds. However, this work only focused on one specific dopant for the nanocomposite. Future work should branch out and investigate different materials, of similar size scale to compare the possible enhancements in physical properties. Furthermore, this research was initiated for development of a scaffold for a bone graft substitute. This goal is more evident than ever, but requires additional work, in the implementation of this novel composite system with multiple cell lines, to fully understand the nature by which osteogenic differentiation can take place. This research was hypothesized to utilize a conductive matrix with an applied electric field. Thus far, it has been demonstrated that with the addition of multi-walled carbon nanotubes, increases in conductance can be obtained, yet the electric field applied to the scaffold is only one potential avenue. Countless other electric fields remain to be attempted with the conductive scaffold, yet a full understanding of the transduction cascade, particularly voltage-gated ion channels, will play a critical role in the advancement of this knowledge. Future studies should implement direct electric fields applied through electrodes in contact with the substrate, and larger fields applied through indirect methods, such as capacitor plates or inductive coupling.